ISSN 2587-1366

TUJE

TURKISH JOURNAL OF ENGINEERING

VOLUME 4 ISSUE 2 APRIL 2020

Dr. Ghazi DROUBI
Robert Gordon University Engineering Faculty
Scotland, UK

JOURNAL SECRETARY

Nida DEMİRTAŞ
nidademirtas@mersin.edu.tr

TURKISH JOURNAL OF ENGINEERING (TUJE)

Turkish Journal of Engineering (TUJE) is a multi-disciplinary journal. The Turkish Journal of Engineering (TUJE) publishes the articles in English and is being published 4 times (January, April, July and October) a year. The Journal is a multidisciplinary journal and covers all fields of basic science and engineering. It is the main purpose of the Journal that to convey the latest development on the science and technology towards the related scientists and to the readers. The Journal is also involved in both experimental and theoretical studies on the subject area of basic science and engineering. Submission of an article implies that the work described has not been published previously and it is not under consideration for publication elsewhere. The copyright release form must be signed by the corresponding author on behalf of all authors. All the responsibilities for the article belongs to the authors. The publications of papers are selected through double peer reviewed to ensure originality, relevance and readability.

AIM AND SCOPE

The Journal publishes both experimental and theoretical studies which are reviewed by at least two scientists and researchers for the subject area of basic science and engineering in the fields listed below:

Aerospace Engineering
Environmental Engineering
Civil Engineering
Geomatic Engineering
Mechanical Engineering
Geology Science and Engineering
Mining Engineering
Chemical Engineering
Metallurgical and Materials Engineering
Electrical and Electronics Engineering
Mathematical Applications in Engineering
Computer Engineering
Food Engineering

PEER REVIEW PROCESS

All submissions will be scanned by iThenticate® to prevent plagiarism. Author(s) of the present study and the article about the ethical responsibilities that fit PUBLICATION ETHICS agree. Each author is responsible for the content of the article. Articles submitted for publication are priorly controlled via iThenticate ® (Professional Plagiarism Prevention) program. If articles that are controlled by iThenticate® program identified as plagiarism or self-plagiarism with more than 25% manuscript will return to the author for appropriate citation and correction. All submitted manuscripts are read by the editorial staff. To save time for authors and peer-reviewers, only those papers that seem most likely to meet our editorial criteria are sent for formal review. Reviewer selection is critical to the publication process, and we base our choice on many factors, including expertise, reputation, specific recommendations and our own previous experience of a reviewer's characteristics. For instance, we avoid using people who are slow, careless or do not provide reasoning for their views, whether harsh or lenient. All submissions will be double blind peer reviewed. All papers are expected to have original content. They should not have been previously published and it should not be under review. Prior to the sending out to referees, editors check that the paper aim and scope of the journal. The journal seeks minimum three independent referees. All submissions are subject to a double blind peer review; if two of referees gives a negative feedback on a paper, the paper is being rejected. If two of referees gives a positive feedback on a paper and one referee negative, the editor can decide whether accept or reject. All submitted papers and referee reports are archived by journal Submissions whether they are published or not are not returned. Authors who want to give up publishing their paper in TUJE after the submission have to apply to the editorial board in written. Authors are responsible from the writing quality of their papers. TUJE journal will not pay any copyright fee to authors. A signed Copyright Assignment Form has to be submitted together with the paper.

PUBLICATION ETHICS

Our publication ethics and publication malpractice statement is mainly based on the Code of Conduct and Best-Practice Guidelines for Journal Editors. Committee on Publication Ethics (COPE). (2011, March 7). Code of Conduct and Best-Practice Guidelines for Journal Editors. Retrieved from http://publicationethics.org/files/Code%20of%20Conduct_2.pdf

PUBLICATION FREQUENCY

The TUJE accepts the articles in English and is being published 4 times (January, April, July and October) a year.

CORRESPONDENCE ADDRESS

Journal Contact: tuje@mersin.edu.tr

CONTENTS

Volume 4 – Issue 2

ARTICLES

Turkish Journal of Engineering

Turkish Journal of Engineering (TUJE)
Vol. 4, Issue 2, pp. 57-61, April 2020
ISSN 2587-1366, Turkey
DOI: 10.31127/tuje.572457
Research Article

THE USE OF HORIZONTAL GEOMAGNETIC FIELD COMPONENTS FOR ESTIMATION OF GEOMAGNETICALLY INDUCED CURRENT OVER TURKEY DURING SPACE WEATHER EVENTS

Erdinç Timoçin *[1] and Selma Erat [1,2]

[1] Mersin University, Vocational School of Technical Sciences, Department of Medical Services and Techniques, Mersin, Turkey
ORCID ID 0000 – 0002 – 3648 – 2035
erdinctimocin@mersin.edu.tr

[2] Mersin University, Advanced Technology, Research and Application Center, Mersin, Turkey
ORCID ID 0000 – 0001 – 7187 – 7668
selmaerat33@gmail.com

*Corresponding Author
Received: 31/05/2019 Accepted: 15/10/2019

ABSTRACT
In this study, the time derivatives of the horizontal geomagnetic field components were computed to estimate the geomagnetically induced current (GIC) over Turkey during space weather events and the results were compared with the geomagnetic activity indices. The interplanetary magnetic field (IMF) index, disturbance storm time (D_{st}) index, global geomagnetic activity indices (a_p and K_p) were used as indicator of space weather events. The changes because of solar flares and coronal mass ejections in the space environment between the Sun and Earth are defined as space weather events. Such events' effects on the Earth's magnetosphere are called geomagnetic storms. In this study, two different space weather events that occurred on 20-26 June 2015 and 06-10 September 2017 are analyzed. The data of the horizontal magnetic field components used in the analysis are obtained from İznik magnetic observatory (40.5°N, 29.7°E). During space weather event on 20-26 June 2015, the maximum (max.) value of time derivative of (dX/dt and dH/dt) X and H horizontal magnetic field components were calculated as 72,22 nT/min. and 74,40 nT/min., respectively, while during space weather event on 06-10 September 2017, the max. value of the time derivative of the X and H horizontal magnetic field components are calculated and the results are 36,90 nT/min. and 38,12 nT/min., respectively. Also, it was observed that the strength of the local geomagnetic disturbance and amplitude of dX/dt and dH/dt at the observatory station depend strongly on the characteristics of geomagnetic activity indices during the space weather events. The southward IMF B_z component induces larger amplitude of dX/dt and dH/dt. The results indicate that the possibility of GIC occurrence over Turkey is quite high. Therefore, we strongly believe that further research and experiment on GIC for Turkey is important.

Keywords: *Space Weather Events, Horizontal Components of Magnetic Field, Geomagnetically Induced Current, Magnetometer*

1. INTRODUCTION

The coronal mass ejections and solar flares, occurring as a result of the changes in solar activity, cause space weather events. During such events, an interaction occurs between space weather and the magnetic field of Earth. This interaction causes to sudden and dramatic changes in the components of Earth's magnetic field (Prölss, 2004; Schunk and Nagy, 2000; Timoçin *et al*., 2018; Timoçin, 2019). The changes in Earth's magnetic field caused by space weather events induce an electrical current that flow on the technological conductor systems, for instance electric power transmission networks, telecommunication cables, railway equipment, oil and gas pipelines. These currents are called geomagnetically induced currents (GIC) that flow on the technological conductor systems can cause great damages in the system attached to that conductor (Boteler *et al*., 1998; Pirjola *et al*., 2000; Pirjola, 2007; Schrijver *et al.*, 2014).

Large GICs are usually observed at high latitudes in or near the auroral regions where strong auroral electrojet currents that are one of the principal causes of the geomagnetic disturbances leading to GICs occur. (Pirjola, 2005; Wik *et al*., 2009; Eroshenko *et al*., 2010; Falayi and Beloff, 2012; Stauning, 2013; Myllys *et al*., 2014). It was believed that mid- and low-latitude regions are not affected by GICs. However, numerous GIC studies that were performed in mid- and low- latitude regions proved that strong space weather events can induce intense GICs also at mid- and low-latitudes (Kappenman, 2003; Trivedi *et al*., 2007; Liu *et al*., 2009; Watari *et al*., 2009; Caraballo *et al*., 2013; Liu*et al*., 2014; Viljanen *et al*., 2014; Doumbia *et al*., 2017; Tozzi *et al*., 2018).

During the last decades, the increasing dependence on technology of society has increased the interest in the investigation of the mechanisms of GICs that cause great damages on the man-made infrastructures. To the best of our knowledge, there are no studies about the geomagnetically induced currents and their effects on power systems in Turkey.

In this study, the horizontal magnetic field components measured over İznik/Turkey magnetic observatory were examined to the estimate the GIC over Turkey during two space weather events that occurred on 20-26 June 2015 and 06-10 September 2017. This study can be pioneer and basic research about estimating the geomagnetic induced currents over Turkey.

The results can provide important contributes to expand awareness about GICs over Turkey and to efforts to understanding GIC activity. Also, the results can encourage researchers to do further investigation and experimentation on GIC activity over Turkey.

2. DATA AND ANALYSIS METHOD

In this study, the data of the horizontal magnetic field components were examined to the estimate the GICs over Turkey during two space weather events that occurred on 20-26 June 2015 and 06-10 September 2017. The data of the horizontal magnetic field components were obtained from İznik magnetic observatory (40.5°N, 29.7°E). The time derivatives of the horizontal magnetic field components were computed to estimate the GICs over Turkey during two space weather events.

Several methods are used in the GICs research, such as calculation of the magnetospheric, ionospheric parameters, and technological conductor parameters. The most widely used of these methods is the method that calculates the horizontal components of the Earth's magnetic field with respect to time. Since the rate of change at the horizontal component of the Earth's magnetic field cause the GICs, the time derivative of the horizontal magnetic field components is directly related to the GICs (Pirjola *et al*., 2000; Pirjola, 2007;Trivedi *et al*., 2007; Watari *et al*., 2009; Wik *et al*., 2009; Eroshenko *et al*., 2010; Caraballo *et al*., 2013; Stauning, 2013; Myllys *et al*., 2014; Liu*et al*., 2014; Viljanen *et al*., 2014; Doumbia *et al*., 2017; Kalafatoğlu and Kaymaz, 2017; Tozzi *et al*., 2018). The electric field induced on the Earth's surface is determined using the rate of change of the Earth's magnetic field during geomagnetic storms using the following Eq. 1.

$$\nabla \times \mathbf{E} = -\frac{\partial \mathbf{B}}{\partial t} \tag{1}$$

It is obvious that the effects of GICs over the world particularly on the technological systems can be observed once the derivative of horizontal magnetic field components with respect to 1 min. is higher than 30 nT/min. In other words, the value of derivative, dX/dt > 30nT/min. and dH/dt > 30nT/min. indicate the possibility of the GIC occurrence at Earth's surface particularly on the technological systems (Viljanen, 1997; Viljanen *et al*., 2001; Ngwira *et al*., 2011). In this study, we use the time derivatives of horizontal magnetic field components obtained from Eq.2 to prediction the GIC.

$$\frac{dH}{dt} = \sqrt{\left(\frac{dX}{dt}\right)^2 + \left(\frac{dY}{dt}\right)^2} \tag{2}$$

In addition to data of horizontal magnetic field components, interplanetary magnetic field (IMF) index, disturbance storm time (D_{st}) index, and global geomagnetic activity indices (a_p and K_p) were used as indicator of space weather events. The interplanetary magnetic field is the magnetic field of sun that is carried into space environment by the solar winds. This field has three components, B_x, B_y and B_z, of which B_z is responsible for energy input into the Earth's magnetosphere during space weather events. The D_{st} index is a measure of changes in the horizontal component of the Earth's magnetic field in the equatorial region during geomagnetic storms. This index is measured by magnetometer stations located in the equatorial region. Large negative values of the D_{st} index are indicative of a severe storm. K_p and a_p indices are obtained from changes in the horizontal component values of the Earth's magnetic field. These indices are used as a global indicator of the level of geomagnetic activity and are not dependent on local time, latitude and seasons. The time derivatives of horizontal magnetic field components were compared with these indices.

3. RESULTS AND DISCUSSION

The daily changes of dX/dt, dH/dt, IMF B_z, D_{st}, a_p, and K_p on 20-26 June 2015 are shown in Fig. 1a-1f, respectively. The IMF B_z presents three mainly rapid and severe southward turnings on 21-23 June 2015. Upon the first southward turning of IMF B_z, the D_{st} started to decrease slowly and the global geomagnetic indices (a_p and K_p) increase drastically and reach to the max. values.

Upon the second southward turning of IMF B_z, the value of the D_{st} reduces rapidly and finally reaches to the min. value. Next, the D_{st}, a_p, and K_p indices turn back to recovery phase. The first southward turning of IMF B_z disturb the regular pattern which is tend to about 0 nT/min. of the dX/dt and dH/dt values. The southward turning of IMF B_z results in the dX/dt and dH/dt values to reach the max. value of 72,22 nT/min. and 74,40 nT/min., respectively. That is, the first southward turning of IMF B_z has induced the highest dX/dt and dH/dt. It is easy to see in Fig. 1a-1f that the behaviors of geomagnetic activity indices are strongly related to dX/dt and dH/dt patterns.

Figures 2a-2f show the daily changes of dX/dt, dH/dt, IMF B_z, D_{st}, a_p, and K_p on 6-10 September 2017, respectively. The IMF B_z presents two mainly rapid and severe southward turnings on 7-8 June 2015. The first southward turning of IMF B_z cause a sudden decrease in the D_{st} and an increase in the global geomagnetic indices (a_p and K_p). With the intensification of the southward IMF B_z, the D_{st} reaches the min. value and the global geomagnetic indices experience first peaks. Next, the D_{st} turns back to recovery phase. The space weather event intensifies again due to the second large southward turning. The second southward turning of IMF B_z cause again a sudden decrease in the D_{st} and the global geomagnetic indices (a_p and K_p) reach the max. value. Then, the space weather event turns back to recovery phase.

The first southward turning of IMF B_z disturb the regular pattern which is tend to about 0 nT/min. of the dX/dt and dH/dt values. With southward turning of IMF B_z, the dX/dt and dH/dt values reach the max. value of 36,90 nT/min. and 38,12 nT/min., respectively. That is, the first southward turning of IMF B_z has induced the highest value dX/dt and dH/dt. As it is shown in Fig. 2a-2f, the behaviors of geomagnetic activity indices are strongly related to dX/dt and dH/dt patterns.

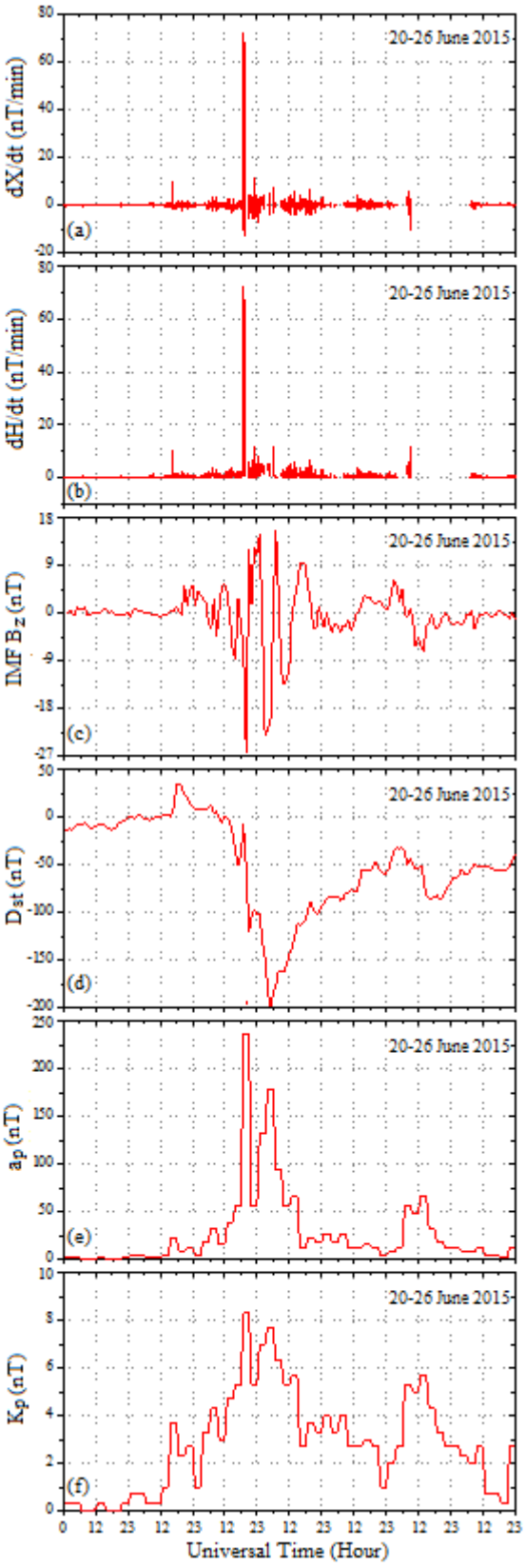

Fig. 1. The daily changes of (a) dX/dt, (b) dH/dt, (c) IMF B_z, (d) D_{st}, (e) a_p, (f) K_p, during 20-26 June 2015.

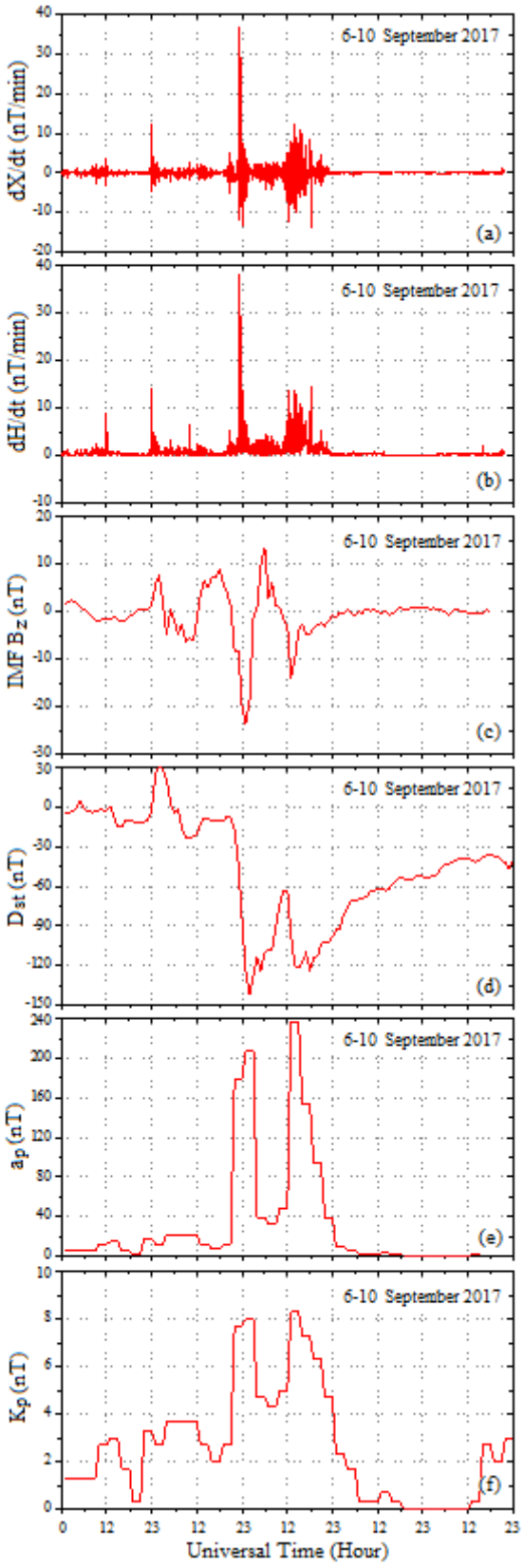

Fig. 2. The daily changes of (a) dX/dt, (b) dH/dt, (c) IMF B_z, (d) D_{st}, (e) a_p, (f) K_p, during 6-10 September 2017.

4. CONCLUSIONS

The results show that the effects of two space weather events cause large amplitude in the horizontal magnetic field components' time dependent derivatives measured at İznik magnetic observatory. For two different space weather events (20-26 June 2015 and 6-10 September 2017), the strength of the local geomagnetic disturbance and amplitude of dX/dt and dH/dt depend strongly on the characteristics of the IMF B_z component, disturbance storm time (D_{st}) index, and global geomagnetic activity indices (a_p and K_p). A strong correlation between the fluctuations in the dX/dt and dH/dt values and the geomagnetic indices is observed once the matching one to one is applied. We can conclude that it is possible that a large geomagnetic disturbance with dH/dt exceeding 30 nT/min. may occur.

The results indicate that the possibility of GIC occurrence over Turkey is quite high. Therefore, more detailed research for determination and experimentation about GIC event over Turkey is quite important. Further studies will be carried out about GIC event over Turkey.

ACKNOWLEDGEMENTS

The authors acknowledge with thanks the members of the İznik magnetic observatory for the data

REFERENCES

Baker, D. N., Balstad, R., Bodeau, J. M., Cameron, E., Fennell, J. F., Fısher, G. M., Forbes, K. F., Kıntner, P. M., Leffler, L. G., Lewıs, W. S., Reagan, J. B., Small, A. A., Stansell, T. A. and Strachan, L. (2008). *Severe Space Weather Events-Understanding Societal and Economic Impacts: A Workshop Report*, Space Studies Board, The National Academies Press, Washington, USA.

Baker, D. N., Li, X., Pulkkinen, A., Ngwira, C. M., Mays, M. L., Galvin, A. B. and Simunac, K. D. C. (2013). "A major solar eruptive event in July 2012: Defining extreme space weather scenarios." *Space Weather*, Vol. 11, No. 10, pp. 585-591.

Boteler, D. H., Pijola, R. J. and Nevanlinna, H. (1998). "The effects of geomagnetic disturbances on electrical systmes at the Earth's surface." *Advances in Space Research*, Vol. 22, No.1, pp. 17-27.

Caraballo, R., Bettucci, L. and Tancredi, S. G. (2013). "Geomagnetically induced currents in the Uruguayan high-voltage power grid." *Geophysical Journal International*, Vol.195, No. 2, pp. 844–853.

Doumbia, V., Boka, K., Kouassi, N., Grodji, O. D. F., Mazaudier, C. A. and Menvielle, M. (2017). "Induction effects of geomagnetic disturbances in the geo-electric field variations at low latitudes." *Annales Geophysicae*, Vol.35, No.1, pp. 39-51.

Eroshenko, E. A., Belov, A. V., Boteler, D., Gaidash, S. P., Lobkov, S. L., Pirjola, R. and Trichtchenko, L. (2010). "Effects of strong geomagnetic storms on Northern railways in Russia." *Advances in Space Research*, Vol. 46, No. 1, pp. 1102-1110.

Falayi, E. O. and Beloff, N. (2012). "Modelling of geomagnetically induced currents during geomagnetic storms using geoelectric fields and auroral electrojet indices." *Indian Journal of Physics*, Vol. 68, No. 6, pp. 423-429.

Kalafatoğlu, E. E. C. and Kaymaz, Z. (2017). "Magnetic and electric field variations during geomagnetically active days over Turkey." *Advances in Space Research*, Vol. 60, No. 9, pp. 1921-1948.

Kappenman, J. G. (2003). "Storm sudden commencement events and the associated geomagnetically induced current risks to ground-based systems at low-latitude and mid-latitude locations." *Space Weather*, Vol.1, No.3, pp. 1-16.

Liu, C. M., Liu, L. G., Pirjola, R. and Wang, Z. Z. (2009). "Calculation of geomagnetically induced currents in midto lowlatitude power grids based on the plane wave method: A preliminary case study." *Space Weather*, Vol. 7, No. 4, pp.1-9.

Liu, C, Li, Y. and Pirjola, R. (2014). "Observations and modeling of GIC in the Chinese large-scale high-voltage power networks." *Journal of Space Weather and Space Climate*, Vol. 4, No. A03, pp. 1-7.

Myllys, M., Viljanen, A. Rui, Ø. A. and Ohnstad, T. M. (2014). "Geomagnetically induced currents in Norway: the northernmosthigh-voltage power grid in the world." *Journal of Space Weather and Space Climate*, Vol. 4, No. A10, pp. 1-10.

Ngwira, C. M., McKinnell, L. A. and Cilliers, P. J. (2011). "Geomagnetic activity indicators for geomagnetically induced current studies in South Africa." *Advances in Space Research*, Vol. 48, No. 3, pp. 529-534.

Pirjola, R., Viljanen,A., Pulkkinen, A. and Amm, O. (2000). "Space Weather Risk in Power Systems and Pipelines." *Physics and Chemistry of the Earth, Part C: Solar, Terrestrial & Planetary Science*, Vol. 24, No. 4, pp. 333-337.

Pirjola, R. (2005). "Effects of space weather on high-latitude ground systems." *Advances in Space Research*, Vol. 36, No. 12, pp. 2231-2240.

Pirjola, R. (2007). "Calculation of geomagnetically induced currents (GIC) in a high-voltage electric power transmission system and estimation of effects of overhead shield wires on GIC modelling." *Journal of Atmospheric and Solar-Terrestrial Physics*, Vol.69, No.12, pp. 1305-1311.

Prölss, G. W. (2004). *Physics of the Earth's space environment*, Berlin-Heidelberg-New York Springer-Verlag Press, USA.

Schunk, R. W. and Nagy, A. F. (2000). *Ionospheres-physics, plasma physics, and chemistry*, Cambridge University Press, UK.

Schrijver, C. J., Dobbins, R., Murtagh, W. and Petrinec, S. M. (2014). "Assessing the impact of space weather on the electric power grid based on insurance claims for industrial electrical equipment." *Space Weather*, Vol.12, No. 7, pp. 487-498.

Stauning, P. (2013). "Power grid disturbances and polar cap index during geomagnetic storms." *Journal of Space Weather and Space Climate*, Vol. 3, No. A22, pp. 1-10.

Timoçin, E., Ünal, İ., Tulunay, Y. and Göker, Ü. D. (2018). "The effect of geomagnetic activity changes on the ionospheric critical frequencies (foF2) at magnetic conjugate points."*Advances in Space Research*, Vol. 62, No.4, pp. 821-828.

Timoçin, E. (2019). "The north and south symmetry of the ionospheric storms at magnetic conjugate points for low latitudes during the March 1976 severe geomagnetic storms and the relation between daily changes of the storms with geomagnetic activity indices." *Advances in Space Research*, Vol. 63, No.12, pp. 3965-3977.

Tozzi, R. Michelis, P. D., Coco, I. and Giannattasio, F. (2018). "A Preliminary Risk Assessment of Geomagnetically Induced Currents over the Italian Territory." *Space Weather*, Vol. 17, No. 1, pp. 46-58.

Trivedi, N. B. Vitorello, I´., Kabata, W., Dutra, S. L. G., Padilha, A. L., Bologna, M. S., Pa´dua, M. B., Soares A. P., Luz, G. S., Pinto, F. A.,Pirjola, R. and Viljanen, A. (2007). "Geomagnetically induced currents in an electric power transmission system at low latitudes in Brazil: A case study." *Space Weather*, Vol.5, No.4, pp. 1-10.

Viljanen, A. (1997). "The Relation Between Geomagnetic Variations and Their Time Derivatives and Implications for Estimation of Induction Risks." *Geophysical Research Letters*, Vol. 24, No. 6, pp. 631-634.

Viljanen, A., Nevanlinna, H., Pajunpaa, K. and Pulkkinen, A. (2001). "Time derivative of the horizontal geomagnetic field as an activityindicator." *Annales Geophysicae*, Vol. 19, No. 9, pp. 1107-1118.

Viljanen, A., Pirjola, R., Pracser, E., Katkalov, J. and Wik, M. (2014). " Geomagnetically induced currents in Europe. Modelled occurrence in a continent-wide power grid." *Journal of Space Weather and Space Climate*, Vol. 4, No. A09, pp. 1-9.

Watari, S., Kunitake, M., Kitamura, K., Hori, T. Kikuchi, T. Shiokawa, K. Nishitani, N. Kataoka, R. Kamide, Y. Aso, T. Watanabe, Y. and Tsuneta, Y. (2009). "Measurements of geomagnetically induced current in a power grid in Hokkaido, Japan." *Space Weather*, Vol. 7, No.3, pp. 1-11.

Wik, M., Pirjola, R., Lundstedt, H., Viljanen, A., Wintoft, P. and Pulkkinen, A. (2009). "Space weather events in July 1982 and October 2003 and the effects of geomagnetically induced currents on Swedish technical systems." *Annales Geophysicae*, Vol. 27, No. 4, pp. 1775-1787.

Turkish Journal of Engineering

Turkish Journal of Engineering (TUJE)
Vol. 4, Issue 2, pp. 62-69, April 2020
ISSN 2587-1366, Turkey
DOI: 10.31127/tuje.616960
Research Article

WASTE MINERAL OILS RE-REFINING WITH PHYSICOCHEMICAL METHODS

Ufuk Sancar Vural *[1]

[1] Seda Kauçuk, Plastik, Maden, Kimya, Enerji İhr.İth. San. Tic. Ltd. Şti., Afyonkarahisar, Turkey
ORCID ID 0000 – 0002 – 8510 – 9616
usvural@gmail.com

* Corresponding Author
Received: 08/09/2019 Accepted: 16/10/2019

ABSTRACT
Refining of waste mineral oils is usually done by distillation or acid/clay methods, or a combination of both. In this study, waste oil refining was carried out in order to obtain higher efficiency than acid /clay method by using more environmentally friendly physicochemical methods which could be an alternative to acid /clay method and distillation methods. For this purpose, demetalization and decolorization stages were applied in order. It was observed that the oils obtained had equivalent parameters to base oils.

Keywords: *Waste Mineral Oil, Recycling, Re-refining*

1. INTRODUCTION

Waste mineral oil is any industrial oil that has become unsuitable for the use to which it was initially assigned. These especially include used oils from combustion engines, transmission systems, turbines and hydraulic systems, the different sectors of the car industry and industrial shipping activities.

Mineral oils are petroleum origin and synthetic lubricants used in generators and other machines, especially in automotive engines. It is one of the most dangerous sources of pollution. Engine oil is not clean after draining from a motor because it collects dirt particles and other chemicals while the engine is running. Used, out-of-service lubricating oils are defined as waste oil, waste engine oil, waste lubricating oil or used lubricating oil depending on where it is used. The United States Environmental Protection Agency defines waste oils (used oils) as lubricating oils obtained from refinery or synthetic methods of crude oil contaminated with physical and chemical impurities (Zitte, 2016).

Used lube oil normally tends to have a high concentration of potentially harmful pollutant materials and heavy metals which could be dangerous to both living and non-living things on the earth. Used lube oil may cause damage to environment when dumped into ground or into water streams including sewers. This may result in ground water and soil contamination (Hopmans, 1974). Therefore, development of environmentally safe, sustainable and cost-effective solution is required for recycling of used lubricant (Stehlik, 2009). Nowadays due to different treatment and finishing methods, there are currently available many new Technologies (Bridjanian, 2006).

The direct effects that these types of oil can have on health include the following: Irritation of lung tissue due to the presence of gases that contain aldehydes, ketone, aromatic compounds, etc. The presence of chemical elements such as Cl (chlorine), NO_2 (nitrogen dioxide), H_2S (hydrogen sulphide), Sb (antimony), Cr (chrome), Ni (nickel), Cd (cadmium), and Cu (copper) that affect the upper respiratory tract and lung tissue. They produce asphyxiating effects that prevent oxygen transportation due to their content of carbon monoxide, halide solvents, hydrogen sulphide, etc. Carcinogenic effects on the prostate and lungs due to the presence of metals such as lead, cadmium, manganese, etc. (web 1). Direct effects on the environment that stand out include the following: The pollution of soils, rivers and the sea due to their low biodegradability. On coming into contact with water, they produce a film that prevents oxygen circulation. Uncontrolled combustion can lead to the emission of chlorine, lead and other gas elements into the atmosphere, with the corresponding effects (web 1).

It is also understood that used engine oil contains some components which mix with the oil when the engine is worn. These include iron, steel, copper, lead, zinc, barium, cadmium, sulfur, water and ash. Used waste engine oil contains hazardous pollutant chemicals, so it is more harmful to the environment than crude oil (Zitte, 2016), which can cause both short-term and long-term adverse environmental effects (Zitte, 2016). Only one ton of used waste oil makes one million tons of clean water unusable (US EPA, 1996). Even in sewage treatment, 50-100 ppm oil remains in water without disposal (US EPA, 1996). In general, it has been found that five liters of oil can cover a small lake (Zitte, 2016). The oil film formed on the water surface causes the BOD value to decrease and causes toxic effects. As a result, drinking water sources are polluted, dead plants and animals are observed (Zitte, 2016). Diran (1997) reported that oil in surface water seriously disrupts water's life support capacity. The oil prevents sunlight and oxygen from entering the water, making it difficult for fish to breathe and photosynthesis in aquatic plants. Thus, it kills plants and fish in aqueous environments. Toxic substances in used oil can also kill small organisms that support the rest of the food chain (Diran, 1997; Arner, 1992). Lubricant consumption is 5.3 million tons in Europe and 39 million tons in the world (Giovanna, 2003). The uses of oils are shown in Fig. 1 (Diphare, 2015).

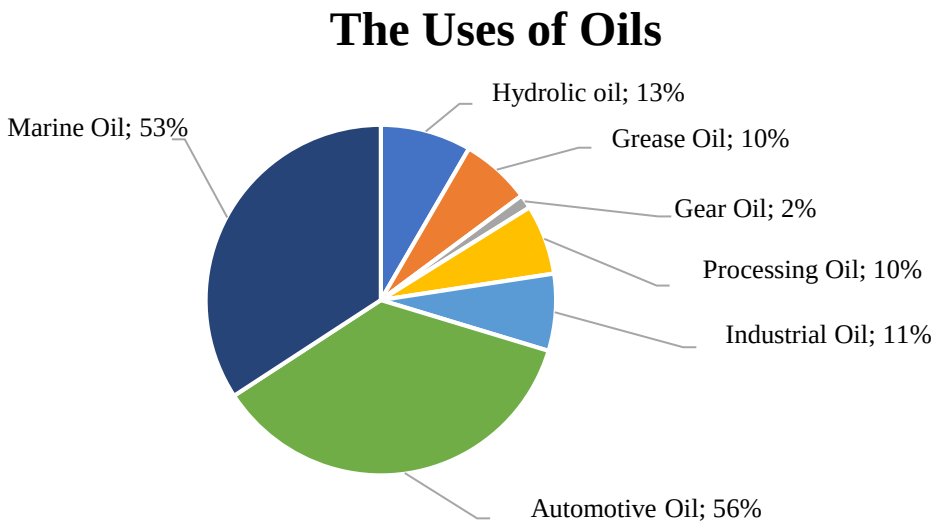

Fig. 1. Application areas of oils

After understanding the pollutant effects of waste oils, intensive studies have been carried out worldwide for the disposal and recovery of waste oils. The recovery and disposal of waste oils is possible by three methods (Fig. 2). These methods are reprocessing, re-refining or direct destruction (Diphare, 2015).

Reprocessing: It is the production of fuel by separating water and sediments in the waste oil. For this purpose, the water and contaminated components in the waste oils are removed by precipitation, adsorption and filtration; sometimes distillation and thermal cracking (pyrolysis) are applied before filtration.

Re-Refining: After some pretreatments, fractional distillation methods are applied to obtain base oil. Lubricating oils can be produced by adding additives to the base oils.

Disposal: Especially waste oils containing PCB (polychlorobenzenes) are disposed of directly by incineration without any pretreatment.

The refining of waste oils is possible by using highly advanced technology. In this study, by refining the waste oils with physicochemical methods, it is tried to determine the more economical alternative to distillation methods.

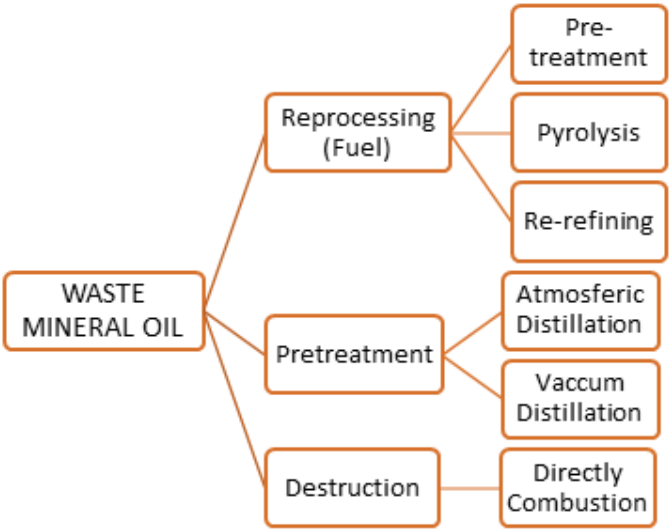

Fig. 2. Waste mine oil recovery and disposal methods

2. MATERYAL VE METOD

The waste oils used in the experiments were obtained from the auto services that change the oil. The viscosity measurements of waste oils and obtained oils were determined by Shanghai God NDJ-55 rotary viscometer, density measurements by Anton Paar DMA35 densimeter, flash point measurements by Teknosem Tan-400 device and color measurement by X-RITE SP 62 device. Metal measurements were determined by the Merlab GBC Avanta model atomic absorption device. Aluminum oxide (Al_2O_3), sodium silicate, tetraethylenepentamine (TEPA) used in the experiments were obtained from Merck.

Physicochemical refining stages of pre-analyzed waste mineral oils are as follows.

Pretreatment (Dewatering and Dematilization): It can be defined as dewatering step. To this end, 1 liter of waste oil was added to a 2 liter beaker, 10 mL of 20% diammonium phosphate solution was added and heated at 120°C for 120 minutes with careful stirring. The mixture was then allowed to cool. After 8 hours, a viscous mixture was formed as a precipitate at the bottom of beaker. The supernatant was carefully transferred to another beaker so that no precipitate was contaminated.

Chemical Refining: The supernatant transferred to another beaker was stirred with heating to 30°C. 1.5% ethylene glycol was added, stirring for 5 minutes to reduce the viscosity of the oil. Then 1% sodium silicate was added and stirred at 30°C for 10 minutes. Subsequently, 2% Al_2O_3 was added thereto and heating was continued with stirring to 50°C. 1% tetraethylenepentamine was added and stirred at constant temperature for 15 minutes. Subsequently, stirring was continued by careful addition of about 8-10% acid active bentonite to 160°C. Occasionally, the waste oil was sampled and dripped onto the filter paper to control the color. When the color was sufficiently lightened, the addition of bentonite was stopped and stirred for a further 10 minutes. The mixture was allowed to cool and filtered under vacuum at 60°C. The obtained oil was analyzed.

3. RESULT AND DISCUSSION

During the prolonged use of lubricating oils, black viscous structures are formed as a result of interactions between additives and metals in the oil, carbonation and polymerization reactions. Saturated hydrocarbons (30 to 70%), aromatic hydrocarbons polyaromatic (20 to 40%), polar compounds (5 to 25%) and asphalt based (0 to 10%). Waste oil also contains metal toxic metal pollutants (Pb, Hg, Zn, Cd, As and persistent organic pollutants PCB, PCT (Ouffoue, 2013; Boadu, 2019). In our country,

waste oils are recovered according to the Regulation on Control of Waste Oils published by the Ministry of Environment (Resmî gazete, 2008). Although it is aimed to produce base oils from waste oils according to the regulation criteria, due to high refining plant costs and lack of technical knowledge, many recycling companies use the reprocessing method to produce fuel in existing plants. In the recovery of oils by reprocessing, catalytic decomposition or direct thermal decomposition at high temperatures is generally employed to obtain low viscosity fuel-equivalent products. However, the production of lubricating oil by adding some chemical additives to the base oils obtained by refining of waste oils according to the purpose of use is extremely important both in terms of commercial and national economy.

The recycling regulation applied in our country prohibits the production of fuel from waste oils. Heavy fines and even imprisonment are often applied to firms that produce fuel through the reprocessing method. Therefore, it is clearly known that companies with little experience in recycling are looking for more economical and practical methods to produce base oil from waste oils instead of fuel. The most common recovery methods of waste oils are as follows (Secretariat of the Stockholm Convention on Persistent Organic Pollutants, 2007):

Acid / Clay Method: In this process, after dehydration and distillation of used lubricant oil, re-refining or reprocessing operation is done using sulfuric acid. Clay is used to remove certain impurities. The acid/clay process has minimal environmental safety. The main by-product of this process is the large amounts of acidic sludge. Based on the concentration of contaminants, the type of lubricant oil and the regenerated oil quality, this process can be as a reprocessing or regenerative method. These two methods are different in terms of the heating rate (distillation unit) and the generated by-products. this method has many disadvantages: It also produces large quantity of pollutants, is unable to treat modern multigrade oils and it's difficult to remove asphaltic impurities. To reduce these hazardous contaminants from this method, the acid treatment stage of the process can be done under the atmospheric pressure to remove the acidic products, oxidized polar compounds, suspended particles and additives (Rahman *et al.*, 2008; Hani *et al.*, 2011; Hamawand *et al.*, 2013; Udonne *et al.*, 2013; Abu-Elella *et al.*, 2015).

Vacuum Distillation: In this method, used lube oil collected is heated at a temperature of 120°C to remove the water added to the oil during combustion. Then the dehydrated oil is subjected to vacuum distilled at a temperature of 240°C and pressure 20 mmHg. This results the production of a light fuel oil (the light fuel oil can be used as fuel source for heating) and lubricating oil at 240°C. The advantages of vacuum distillation process over atmospheric pressure distillation are: Columns can be operated at lower temperatures; more economical to separate high boiling point components under vacuum distillation; avoid degradation of properties of some species at high temperatures therefore thermally sensitive substances can be processed easily. However, the remaining oil generated at this temperature (240°C) contains the dirt, degraded additives, metal wear parts and combustion products like carbon and is collected as residue. The residue is in the form similar to that of tar, which can be used as a construction material, for example, road and bitumen production. The disadvantage of this method is the high investment cost and/or the use of toxic materials such as sulphuric acid (Havemann, 1978; Puerto-Ferre *et al.*, 1994; Kanna *et al.*, 2014).

Hydrogenation: To avoid formation of harmful products and environmental issues based on above methods, some modern processes have been used and the best one is hydrotreating (Bridjanian, 2006). This method follows vacuum distillation. In this process, the distillate from vacuum distillation is hydrotreated at high pressure and temperature in the presence of catalyst for the purpose of removing chlorine, sulphur, nitrogen and organic components. The treated hydrocarbons resulted in products of improved odour, chemical properties and colour Another important aspect of this method is that, this process has many advantages: Produces of high Viscosity Index lube oil with well oxidation resistance and a good stable colour and yet having low or no discards. At the same time, it consumes bad quality feed. In addition to that, this method has advantage that all of its hydrocarbon products have good applications and product recovery is high with no (or very low) disposals. Other hydrocarbon products are: In oil refinery the light–cuts can be used as fuel in plant itself. Gas oil may be consumed after being mixed with heating gas oil and the distillation residue can be blended with bitumen and consumed as paving asphalt, because it upgrades a lot its rheological properties. Also, it can be used as a concentrated anti-corrosion liquid coating, for vehicles frames (Durrani, 2014). The disadvantage of this method is that the residue resulting from the process is of high boiling range of hydrocarbon product fractionated into neutral oil products with varying viscosities which can also be used to blend lube oil.

Solvent de-asphalting process: This method has replaced acid-clay treatment as preferred method for improving oxidative stability and viscosity as well as temperature characteristics of base oils. Base oils obtained from Solvent Extraction are of good quality and contains less amounts of contaminants. In contrast to acid-clay treatment, it operates at higher pressures, requires skilled operating system and qualified personnel. The solvent selectively dissolves the undesired aromatic components (the extract), leaving desired saturated components, especially alkanes, as a separate phase (the raffinate) (Rincon *et al.*, 2005). Different solvents types have been used for solvent extraction such as 2-propanol, 1-butanol, methyl ethyl ketone (MEK), ethanol, toluene, acetone, propane etc. used propane as solvent (Quang *et al.*, 1974; Rincon *et al.*, 2003). He found out that propane was capable of dissolving paraffinic or waxy material and intermediately dissolved oxygenated material. Asphaltenes which contain heavy condensed aromatic compounds and particulate matter are insoluble in liquid propane. These properties make propane ideal for recycling the used engine oil, but there are many other issues that have to be considered. Propane is hazardous and flammable therefore this process is regarded as hazardous method. In general, involves solvent losses and highly operating maintenance. Also, it occurs at pressures higher than 10 atm and requires high pressure sealing

systems which makes solvent extraction plants expensive to construct, operate and the method also produces remarkable amounts of hazardous by-products (Quang *et al.*, 1974; Rincon *et al.*, 2003; Rincon *et al.*, 2005; Hamawand *et al.*, 2013).

Modern Technologies for Used Oil Re-Refining: Pyrolytic distillation method, pyrolysis process, thin film evaporation (TFE), including combined TFE and clay finishing, TFE and solvent finishing, TFE and hydrofinishing, thermal de-asphalting and clay finishing or hydrofinishing etc. In addition, environmentally friendly and affordable solvent extraction and adsorbents are being developed as a means of removing contaminants in used lube oil. The thin film technique is an alternative to vacuum distillation process. (Kalnes, 1990, Hamed *et al.*, 2005).

Thin Film Evaporation (TFE) with hydro-finishing: These methods are utilized to segregate oil and foreign components via a TFE, and purify it through hydro-finishing to prevent the secondary pollution. First, the moisture and light oil contained in the used oil are eliminated and then vacuum distillation of free components is required to permit for continuous separation of a TFE. Finally, the oil is encountered to hydro-finishing to eliminate chlorine, nitrogen, oxygen, and sulfur compounds. There is a difference between these both methods, that clay is used for absorption (Kalnes, 1990).

TFE with solvent finishing: This method is used to segregate oil and foreign substances via a TFE, and request the solvent-finishing with the flow process analogous to TFE with hydro-finishing.

Solvent extraction hydro-finishing: This method combines solvent extraction and hydro-finishing by eliminating the foreign substances using the solvent and then fortifying oil quality by hydro-finishing. First, the moisture is eliminated and segregated the used oil. Then the mixture of solvent and used oil is encountered to hydro-finishing to eliminate sulfur, nitrogen and oxygen for purification purposes.

TDA with clay finishing and TDA with hydro-finishing: The dehydrated used oil is vacuum-heated at 360 ◦C. The ash remains at the bottom, and the oil is divided to 3 types, i.e. vacuum gas oil, base oil (as lubricant) and asphalt residues. Next, the base oil is encountered to hydro-finishing or clay-finishing under highpressure (107 Pa) for continuous utilization (Hamad *et al.*, 2005).

Pyrolysis of waste oil: From research conducted by Arpal (Arpal *et al.*, 2010), a fuel named as diesel-like fuel was produced by applying pyrolytic distillation method. Lam *et al.* (2012 and 2016), describe pyrolysis as a thermal process that heats and decomposes substance at high temperature (300-1000°C) in an inert environment without oxygen. Pyrolysis process is not yet widespread but it has been receiving much attentions nowadays due to its potential to produce energy-dense products from materials. Examples of pyrolysis process includes microwave pyrolysis process and conventional pyrolysis process (Oladimeji *et al.*, 2018).

Various process combinations can be formed by configuring atmospheric distillation, vacuum distillation, solvent extraction, hydrogenation, acid / clay methods in different ways. Generally the first stage in all processes is atmospheric distillation. The cost of the recycling processes consisting of combinations of atmospheric and vacuum distillation method, distillation and solvent extraction method is quite high. Advanced processes can be considered for high capacity plants. In the waste oil recycling regulations, Category III contaminated oils are allowed to be burned only in disposal plants such as cement factories, lime quarries and Category I and II waste oils are allowed to be recycled. (Resmi Gazete, 2008). Therefore, it is not possible for many licensed recycling plants to process high capacity waste oil. Due to high investment costs and high taxes, it is not feasible to establish small capacity processes.

In the oldest known acid / clay method in chemical refining, water and low boiling point components are first removed from the waste oil by atmospheric distillation. Subsequently, the waste oil is reacted with sulfuric acid at low temperature to remove carbons, asphaltenes and other sulfur compounds by precipitation from the oil, and then to be refined by treatment with various bleaching clays (Bhushan, 2016). The major problem in the acid /clay process is the removal of high concentrations of acid and sülfür, asphaltenes, and carbons in sediment, as well as a highly contaminated bleaching clay. Since the disposal process is very expensive and costly, waste oil recycling plants which were established primarily to prevent environmental pollution, cause greater environmental problems. Low process efficiency (60-65%) is also a disadvantage.

The method used in this study consists of a series of physicochemical processes in which base oils are obtained from waste oils, which are less costly, without the need for high process cost distillation. In this study, carbon and metallic components in the waste oil were precipitated together with asphaltenes using coagulatory agents such as aluminum sulfate and sodium silicate instead of acid. Sulfur components, one of the biggest problems in waste oils, were removed from the oil by interacting with amine groups. Thus, acid-free sediment removed from the waste oil can be used in asphalt production, will not pose an environmental risk, and there will be no disposal problems. Active bentonite (acid active bentonite) was used as clay. The purpose of using clay is to remove polymeric materials, colloidal materials remaining in the oil phase by adsorbing with clay.

During the physicochemical refining, asphaltenes and other impurities were precipitated in waste oil with the help of coagulants at low temperatures, while the double bonds formed in the high molecular weight oxidation molecule interacted with amines to ensure oxidation stability. Thus, more stable base oils were obtained from the distillation methods without the need for hydrogenation. 85% base oil was recovered by the new method used in this study, and the acid-free precipitate amount was 10-15%. However, in the acid / clay method, the yield is as low as 60-65% and the amount of sediment is higher than 25-35%. The analysis results of the waste oil used in the experiments and the base oil obtained from the experiments are given in Table 1 and Table 2. The results were also compared with 20W50 oil.

Table 1. Physicochemical properties of waste oils, refined oil and original oil

Parameter	Waste Motor Oil	Refined Oil	20W50
Colour (ASTM D1500)	>8	3,5	4.5
Density 15 C (ASTM D1298)	0,9253	0,8870	0,8700
Viscosity 40 C (ASTM D445), CST	106,37	118	91,0
Viscosity 100 C (ASTM D445), CST	12,66	11,02	10,5
Flash Point (ASTM D97), C	210	225	230
TAN (ASTM D2896), mg KOH/g	2,74	0	0
TBN (ASTM D2896), mg KOH/g	4,66	0	0
Sulfur	>8	4	2,5

Table 2. Analysis of metals in waste oil, refined oil and the original oil

Parameter	Waste Motor Oil ppm	Refined Oil	20W50
Fe	58,6	0	0
Cr	3,2	0	0
Pb	2813	1,86	0
Cu	21,4	2,7	0
Ca	1570	9,56	543
Zn	566	4	0

As it can be seen from the results, the waste motor oils were refined in two stages without the need of hydrogenation and advanced distillation techniques and base oil was obtained again. As in the acid / clay process, it does not generate environmental waste, the processing time is much shorter, the amount of bleaching clay usage is much less, the yield is higher. In Table 3, waste mineral oil recycling methods are compared in terms of process time, recovery cost, efficiency and process setup cost.

Table 3. Comparison of waste mineral oil recycling processes

Regenerative Technologies	Energy requirement	Recycling rate (%)	Quality of regenerative oil	Economic costs	Acidic sludge	Residual oil sludge	Hazardous chemical materials
Acid/clay	Low	63	Good	Low	Much	Much	H_2SO_4
Distillation	High	50	Good	Low	Little	Much	H_2SO_4
Solvent de-asphalinting	High	70-65	API	High	Little	Much	$H_2SO_4$and Organic solvent
TFE with hydrofinishing	High	72	API	High	None	Little	None
TFE with clay finishing	High	72	API	High	None	Little	None
TFE with solvent finishing	High	72	API	High	None	Little	Orgsmic solvent
Solvent extraction hydrofinishing	High	74	API	High	None	Little	Oganic solvent
Thermal de-asphalting	High	74-77	API	High	None	Little	None
Physicochemical Regeneration	Very low	85	Good	Very low	None	Little	No

As can be seen from Table 3, chemical regeneration is the most ideal recycling method of waste mineral oil given the low process cost and high efficiency. In distillation methods, thermal cracking is inevitable because waste oils are processed at high temperatures. In recycling models containing distillation, hydrogenation is essential to produce base oil with high efficiency Otherwise, low quality base oils containing unsaturated oil molecules are obtained in distillation methods that do not contain hydrogenation. Since the unsaturated oil molecules are precipitated together with asphaltenes in chemical refining process, high quality base oils are obtained without hydrogenation.

Since the gasification rate will be increased as a result of thermal decomposition in distillation methods which do not contain hydrogenation, the base oil ratio obtained will be low. Therefore, chemical regeneration is the more preferable method if it is aimed to obtain base oil as a result of waste oil recovery. If it is desired to obtain fuel, known distillation methods by thermal decomposition at high temperature may be used. However, the law does not allow the production of fuel from waste oils.

In our country, hydrogenation-based recovery method is not available due to high process cost. In other distillation-based methods, not only base oil but also fuel-equivalent products are obtained. The Ministry of Environment emphasizes the production of base oil instead of fuel equivalent product with various regulations and measures. The way to prevent fuel production is by applying chemical regeneration, which may be an alternative to distillation methods involving thermal decomposition.

In the chemical regeneration process, it is not possible to obtain fuel, on the contrary, base oil is obtained with high efficiency. The Ministry of Environment should take steps to promote the production of base oils, which have a much higher economic value than fuel, by chemical regeneration. Products that can be produced from recovered base oils (such as grease) are included in the incentive scope and directing the recovery companies to this area will prevent the production of illegal fuel.

As a result, the consumption of lubricating oils produced from limited oil resources as fuel is a major disadvantage for the national economy and the production of base oil from waste oils is very advantageous both for the national economy and for the more conscious use of oil resources. The method determined as a result of the experiments is a method that can be preferred because of low investment costs and no environmental risk without the need for advanced technology processes.

REFERENCES

Abu-Elella, R., Ossman, M.E., Farouq, R., AbdElfatah, M. (2015), "Used motor oil treatment: turning waste oil into valuable products", International Journal of Chemical and Biochemical Sciences. Vol. 7, pp. 57-67.

Arner, R, (1992). "Used Oil Recycling Markets and Best Management Practice in the United States", Presented to the National Recycling Congress, Boston, USA.

Arpa, O., Yumrutas, R., Demirbas, A. (2010). "Production of diesel-like fuel from waste engine oil by pyrolytic distillation", Appl Energy, Vol. 87, pp. 122-127.

Bhushan, Z. K., Anil, S. M., Sainand, K., Shivkumar, H. (2016). "Comparison between Different Methods of Waste Oil Recovery", International Journal of Innovative Research in Science, Engineering and Technology. Vol. 5, No. 11, pp. 2001-2009.

Boadu, K. O., Joel, O. F., Essumang, D. K. and Evbuomwan, B. O., (2019). "A Review of Methods for Removal of Contaminants in Used Lubricating Oil", Chemical Science International Journal, Vol. 26, No. 4, pp. 1-11

Bridjanian, H., Sattarin, M. (2006). "Modern recovery methods in used oil rerefining", Petrol Coal Vol. 48, pp. 40–43.

Diphare, M. J., Muzenda, E., Pilusa, I. J., Mollagee, M., (2015). "A Comparison of Waste Lubricating Oil Treatment Techniques", 2nd International Conference on Environment, Agriculture and Food Sciences (ICEAFS'2013) August 25-26, Kuala Lumpur (Malaysia)

Diran, B. (1997). "The Little Adsorption Book: A Practical Guide for Engineers and Scientists". CRC Press, Boca Raton, FL, USA.

Durrani, H.A. (2014). "Re-Refining Recovery methods of used lubricating oil", International Journal of Engineering Sciences & Research Technology. Vol. 3, No. 3, pp. 1216-1220.

Giovanna, F. D., Khlebinskaia, O., Lodolo, A. and Miertus, S. (2003). "Compendium of Used Oil Regeneration Technologies", International Centre for Science and High Technology of the United Nations Industrial Development Organization (ICS-UNIDO), Trieste. 1-210

Hamad, A., Al-Zubaidya, E., Muhammad, E.F. (2005). "Used lubricating oil recycling using hydrocarbon solvents", Environ. Manage. Vol. 74, pp. 153–159.

Hamawand, I., Yusaf, T., Rafat, S. (2013), "Recycling of waste engine oils using a new washing agent", Energies. pp.1023-1049.

Hani, F. B., Al-Wedyan, H. (2011), "Regeneration of Base-Oil from Waste-Oil under Different Conditions and Variables", African Journal of Biotechnology", pp. 1150-1153.

Havemann, R. (1978), "The KTI used oil re-refining process". In Proceedings of the 3rd International Conference of Used Oil Recovery and Reuse, Houston, TX, USA, pp. 16–18.

Hegazi, S. E. F, Mohamd, Y. A., Hassan, M. I. (2017). "Recycling of waste engine oils using different acids as washing agents", International Journal of Oil, Gas and Coal Engineering, Vol(5), No.5, pp.69-74.

Kalnes, T., (1990). "Treatment and recycling of waste lubricants". A petroleum refinery integration study. In: AICHE National Meeting, San Diego, CA, pp. 19–22.

Kannan S. C., Mohan Kumar, K. S., Sakeer Hussain, M., Deepa Priya, N. K. (2014), "Studies on reuse of refined used automotive lubricant oil", Research Journal of Engineering Science. Vol. 3, No. 6, pp. 8-14.

Lam, S. S. And Chase, A. A. (2012). "A Review on Waste to Energy Processes Using Microwave Pyrolysis", Energies. Vol.5, pp. 4209-4232.

Lam, S.S., Liewa, K. K., Jusoh, A. A., Chong, C. T., Ani, F. N., Chase, H. A.(2016). "Progress in waste oil to sustainable energy, with emphasis on pyrolysis techniques". Renewable and Sustainable Energy Reviews. Vol. 53, pp. 714-753.

Oladimeji, T. E, Sonibare, J. A, Omoleye, J. A, Adegbola, A. A, Okagbue, H. I. (2018). "Data on the treatment of used lubricating oil from two different sources using solvent extraction and adsorption", Data in Brief. Vol. 19, pp. 2240- 2252.

Ouffoue, S. K, Oura, L., YAPO, K. D., Coffy A. A., (2013). "Physicochemical characterization of waste oils and analysis of the residues in contaminated soil", International Journal of Environmental Monitoring and Analysis, Vol. 1, No. 4, pp 162-166.

Puerto-Ferre, E., Kajdas, C. (1994). "Clean technology for recycling waste lubricating oils", In Proceedings of 9th International Colloquium, Ecological and Economic Aspects of Tribology, Esslingen, Germany, pp. 14–16.

Quang, D. V., Carriero, G., Schieppati, R., Comte, A., Andrews, J. W. (1974), "Propane purification of used lubricating oils". Hydrocarb. Process, Vol. 53, pp. 129–131.

Resmî gazete. (2008). "Atık yağların kontrolü yönetmeliği". Sayı: 26952.

Rincon, J., Canizares, P., Garcia, M. T. 2005), "Regeneration of used lubricating oil by polar solvent extraction". Ind. Eng. Chem. Res. Vol. 44: pp. 43-73.

Rincon, J., Canizares, P., Garcia, M. T., Gracia, I. (2003), "Regeneration of used lubricant oil by propane extraction". Ind. Eng. Chem. Res. Vol. 42, pp. 4867–4873.

Secretariat of the Stockholm Convention on Persistent Organic Pollutants, (2007). "Guidelines On Best Available Techniques And Provisional Guidance On Best Environmental Practices, Relevant to Article 5 and Annex C of the Stockholm Convention on Persistent Organic Pollutants", United Nations Environment Programme, International Environment House. Geneva, Switzerland

Udonne, J. D., Bakare, O. A. (2013),."Recycling of used lubricating oil using three samples of acids and clay as a method of treatment". International Archive of Applied Sciences and Technology. Vol. 4, No. 2, pp. 8–14.

US EPA (1996). "Managing Used Oil: Advice for Small Businesses". Report. 530EPA-F-96-004.
Web Map Tile Service, 1. http://www.cprac.org/docs/olis_eng.pdf (20.06.2019).

Zitte L. F., Awi-Waadu, G. D. B. and Okorodike, C. G, (2016). "Used-Oil Generation and Its Disposal along East-West Road, Port Harcourt Nigeria", International Journal of Waste Resources, Vol. 6, No. 1, 1-5.

Turkish Journal of Engineering

Turkish Journal of Engineering (TUJE)
Vol. 4, Issue 2, pp. 70-76, April 2020
ISSN 2587-1366, Turkey
DOI: 10.31127/tuje.596158
Research Article

DETERMINATION OF SOUND TRANSMISSION COEFFICIENT OF GYPSUM PARTITION WALLS INSULATED BY CELLUBOR™

Abdulkerim Ilgün [1] and Ahmad Javid Zia *[2]

[1] KTO Karatay University, Engineering Faculty, Civil Engineering Department, Konya, Turkey
ORCID ID 0000 – 0002 – 9784 – 460X
kerim.ilgun@karatay.edu.tr

[2] KTO Karatay University, Engineering Faculty, Civil Engineering Department, Konya, Turkey
ORCID ID 0000 – 0002 – 2808 – 6972
javid.zia@karatay.edu.tr

* Corresponding Author
Received: 24/07/2019 Accepted: 25/10/2019

ABSTRACT
One of the biggest problems of using public spaces for constructions, such as high-rise buildings, offices, hospitals, and hotels, is noise caused by sound transmission through the lightweight partition walls used to divide volumes. In this study, experiments were carried out to determine the sound transmission coefficient of lightweight gypsum partition walls insulated by CelluBor. Experiments were performed in an anechoic test chamber consists of two separate cells. One cell was used as the sound source, and the other one was used as the receiver cell. A total of 12 samples were used in the experimental studies, which were categorized into four separate groups. The main features that distinguished these groups from each other were the profile height used in the samples and the number of gypsum board layers used on each side of the profiles. In addition, one blank (no insulation) sample, one half filled, and one fully filled with insulation material were used for each test group. The test samples were placed between two cells. The sound volume of the sound source was measured separately in dB in both cells, and the sound transmission coefficients of 12 different samples were determined. It was observed that the most efficient results were obtained only when half of the profile height was filled with the CelluBor material. The use of a composite material consists of boron and waste materials such as CelluBor as sound insulation material in lightweight partition walls can affect the sound transmission coefficient greatly.

Keywords: *Gypsum Partition Walls, CelluBor, Sound, Transmission Coefficient, Structural Acoustic*

1. INTRODUCTION

In recent years, population is rapidly increasing, especially in cities. Big problems on residential areas are growing as well. One of the most practical solutions to these problems is to build multi-story structures in narrow spaces. Thus, high-rise buildings are built. Many people are allowed to live and work together. However, some problems still exist, which are caused by these common living spaces. One of them is the emergence of sound that is defined as disturbing noise. Different kinds of noise have many negative impacts on human health and performance (Ilgun *et al*., 2010). People living in common areas need to be protected from these adverse effects. One of the most basic solutions in solving this issue is to prevent sound transitions among volumes. According to the law of mass, partition walls must be rigid and heavy, causing undesired loads in addition to the loads of barrier elements of structures. Because the interactions of buildings from earthquake loads are directly proportional to their weight, buildings having heavy weight are impacted greatly by earthquake loads.

There are many valuable academic researches which investigates the sound transmission issue of lightweight partition walls. Researchers worked on both numerical and experimental solutions to solve the noise problem. One of the noteworthy works is to use the finite layer method as a numerical technique for modeling the acoustic behavior of walls (Díaz-Cereceda *et al*., 2012). Researchers also pointed out that, in addition to the mass and sound frequencies, some other parameters can affect acoustic insulation as well, such as the arrival angle of sound waves, weak points in insulation, hardness, and damping properties of the element (Tadeu and Santos, 2003). Moreover, investigations have also been done on the use of lightweight materials in different engineering fields because of their acoustic properties (Tadeu *et al*., 2004).

Experimental studies can be reviewed in different categories. Some researchers carried out experimental work on lightweight partition walls made of gypsum and some new materials, including mixtures of mushrooms, corn cobs, coconut shells, and cellulose with mineral additives. Meanwhile, researchers have also worked on the sound transmission of gypsum walls themselves (Senthilkumar, 2012; Hernández-Olivares *et al*., 1999; Carvalho, 1995; Faustino *et al*., 2012; Karaağaçlioğlu, 2012; Warnock and Quirt, 1997).

Other noteworthy works include determinations of the influence of slit size on sound transmission through a lightweight partition wall, measurements of the plumbing appliance noise using ISO 3822-(1999) test procedures, and determination of the sound insulation performance of suspended ceilings (Başbuğ, 2005; Uris *et al*., 2004; Thomalla, 2003). In addition, some researchers focus on issues such as experimental determination of the accuracy of methods that are used to approximately calculate the loss in sound transmission among walls and floors, analysis for noise control of conservatory buildings, comparison of computer programs used to design acoustic rooms, and noise problems of a building built of tunnel formwork systems (Cambridge, 2006; Çoşgun *et al*., 2008; Özkan, 2001; Ballagh, 2004).

In this study, an experimental work was carried out to find the sound transmission coefficient of CelluBor, which is used as a sound insulation material inside lightweight partition walls to solve the noise problem and to reduce unnecessary loads of these walls to a building. CelluBor is a material obtained from cellulose-based materials and contains boron salts, which is mostly used as the heat and fire insulation material. Because CelluBor can be produced directly from cellulose, it can be produced using recycled paper as well. In addition, the experiment also investigated the optimum thickness for both the partition wall and the insulation inside it.

2. EXPERIMENTAL STUDY

2.1. Materials

To produce the test specimens, 75 × 30 × 0.5 mm and 50 × 30 × 0.5 mm (height, width and thickness) U aluminum profiles, 1200 × 2500 × 12.5 mm (width, height and thickness) gypsum boards and CelluBor were used.

2.2. Preparation of Test Specimens

A total of 12 test specimens were produced in four groups having dimensions of 1500 × 1500 mm^2 to find the sound transmission coefficient of the lightweight gypsum partition walls insulated with CelluBor. As shown in Fig 1, the main structure of all 12 test specimens consisted of an aluminum U profile skeleton frame, gypsum boards at each side of the frame and CelluBor sprayed inside as sound insulation material. The test specimens were constructed according to infrastructures of lightweight partition walls that are very commonly used in Turkey.

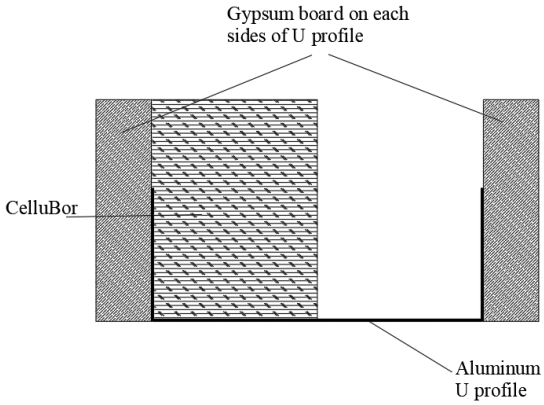

Fig. 1. Main structure of test specimens (The number of profiles, gypsum boards and the thickness of CelluBor differs in all test specimens).

The first group P[75]GB[I] was constructed using a 75 mm aluminum and one gypsum board attached on each side of the profile. Three different specimens were used in this group. One of them had no CelluBor insulation. The second one had half filled (37 mm) CelluBor insulation, and the third one had fully filled (75 mm) insulation. The three specimens in the second group P[75]GB[II] had the same insulation and aluminum profile. The two gypsum boards were placed on each side of the profile. The third and fourth groups had two 50 mm aluminum profiles attached with each other, with a total height of 100 mm, and the insulation materials (0, 50, and 100 mm) were placed inside the profiles.

Table 1. Materials used in all test specimens and cross section for every single test specimen.

No	Specimens	U Profile	Gypsum Board (Number)	CelluBor (Thickness)	U profile (Number)	Specimens Cross Section
1	P[75]GB[I]-00	42x74x42 mm	1	-	1	
2	P[75]GB[I]-37	42x74x42 mm	1	37 mm	1	
3	P[75]GB[I]-75	42x74x42 mm	1	75 mm	1	
4	P[75]GB[II]-00	42x74x42 mm	2	-	1	
5	P[75]GB[II]-37	42x74x42 mm	2	37 mm	1	
6	P[75]GB[II]-75	42x74x42 mm	2	75 mm	1	
7	P[100]GB[I]-00	2x42x49x42 mm	1	-	2	
8	P[100]GB[I]-50	2x42x49x42 mm	1	50 mm	2	
9	P[100]GB[I]-100	2x42x49x42 mm	1	100 mm	2	
10	P[100]GB[II]-00	2x42x49x42 mm	2	-	2	
11	P[100]GB[II]-50	2x42x49x42 mm	2	50 mm	2	
12	P[100]GB[II]-100	2x42x49x42 mm	2	100 mm	2	

The third and fourth groups had two 50 mm aluminum profiles attached with each other, with a total height of 100 mm, and the insulation materials (0, 50, and 100 mm) were placed inside the profiles. The only difference between the third and fourth groups is the number of gypsum boards attached on each side of the profiles, i.e., the third group P[100]GB[I] had one gypsum board, and the fourth group P[100]GB[II] had two. A summary of the materials used in all test specimens and the cross section for each single test specimen are listed in Table 1.

3. METHODOLOGY

To conduct transmission loss testing according to standardized method is to use two adjacent reverberant room with a gap between to put test specimen in (Phillips, 2014). Due to constraints, experiments were performed in an anechoic chamber built at the Construction Laboratory of KTO Karatay University in Konya, Turkey.

This anechoic chamber was constructed with almost same properties used by (Ilgun *et al*., 2010). The chamber consists of two adjacent rooms. Each room has a net volume of 2.28 m^3 and a surface area of 8.71 m^2. The interior dimension of each chamber was 1.35 × 1.3 × 1.33 m^3. A 0.15 × 1.50 × 1.50 m^3 gap between two chambers was designed for test specimens to be placed. This anechoic chamber with two cells was made in a suitable section of the laboratory. Rubber wedges were placed underneath the anechoic chamber to dampen possible vibrations from the ground.

The plan view and A-A section with all dimensions of this chamber is shown in Fig. 2. For entrance and exit purposes, two 70 × 70 cm^2 windows insulated with two layers of rock wool were constructed on both sides of the anechoic chamber.

In addition, the entire inner surface of the cells was also covered by two layers of rock wool having a thickness of 5 cm and a density of 150 kg/m^3. The aim was to prevent possible external noises and to prevent reflections in the cells where noise was produced and transmitted.

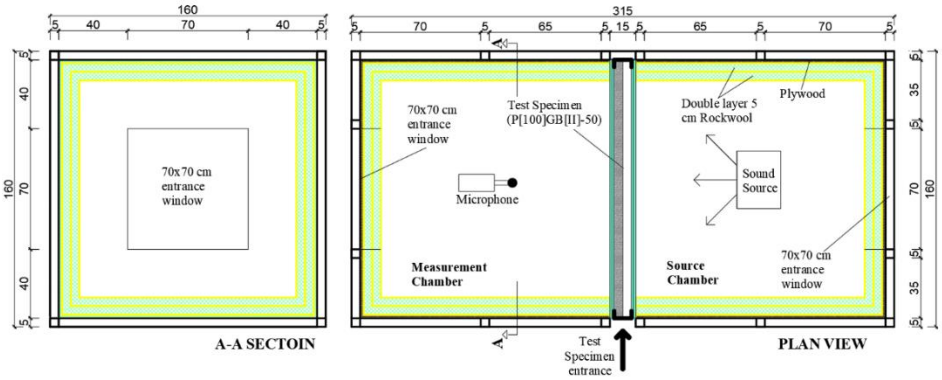

Fig. 2. The plan view and A-A section of anechoic.

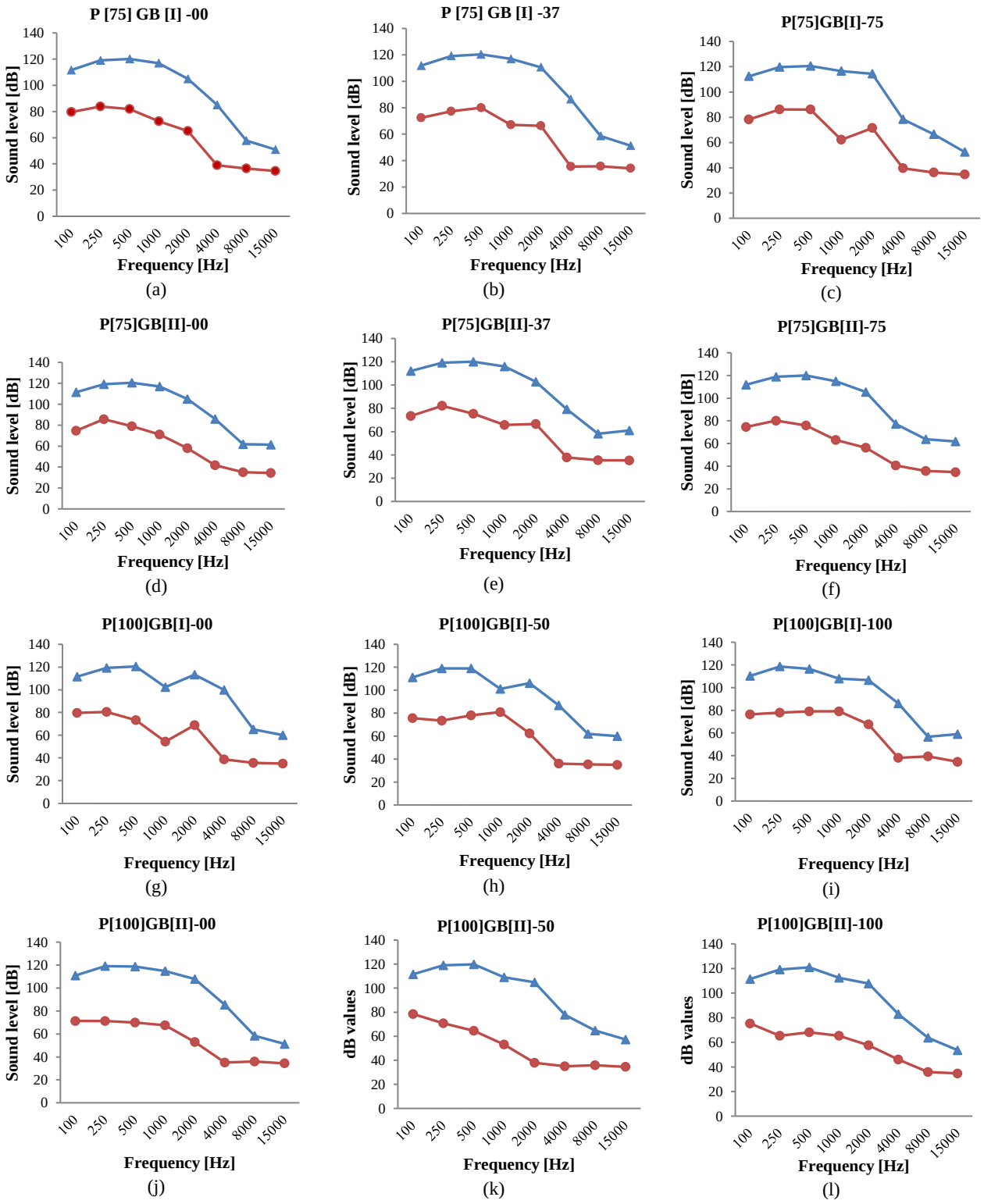

▲ Represent the source chamber's sound level as dB.
● Represent the transmitted sound level as dB measured in the receiver chamber.

Fig. 3. The transmission losses (TL) for all 12 test specimens (a-l).

Different frequencies were produced inside one of the cells at very high decibels using Tone Generator 100-15k Hz (*http://www.ringbell.co.uk/software/audio.htm accessed date: August 10, 2018*) and an amplifier loudspeaker. The generated frequencies are the central frequencies which human ears can hear at middle and

high levels of noises, including 100, 250, 500, 1000, 2000, 4000, 8000, and 15000 Hz. After placing the test specimen between two chambers, any gaps between test specimens remained open, and the chambers were filled and closed with rook wool.

Different frequencies were generated in the source chamber (Ilgun *et al*., 2010). The generated sound level was first measured in the source room before the same sound level was measured in the receiver room. The measurements were done on both rooms using an Extech HD600 sound meter.

The TL and α values of the test specimens were calculated using eq. (1) and (2) (Ilgun *et al*., 2010).

$$TL = IS - (RS + TR) \quad (1)$$

$$\alpha = \frac{TL}{IS} \quad (2)$$

Where TL stands for sound transmission, IS incoming sound, RS reflected sound and TR transmitted sound

4. EXPERIMENTAL RESULTS AND ANALYSIS

The transmission losses (TL) for all 12 test specimens are given between [a-l] in Fig. 3. In addition, Fig. 4 shows the incoming sound, reflected and observed sounds, and the transmitted one. The reflected sound was neglected because of the double layers of rook wool.

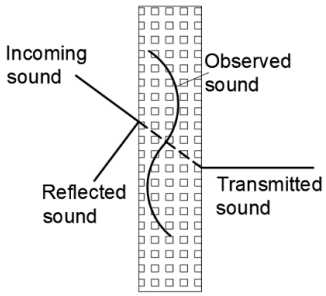

Fig. 4. Transmission losses (TL) for all 12 test specimens

12 different test specimens were divided into groups according to their size and types of insulation. According to their dimensions, the test specimens were divided into

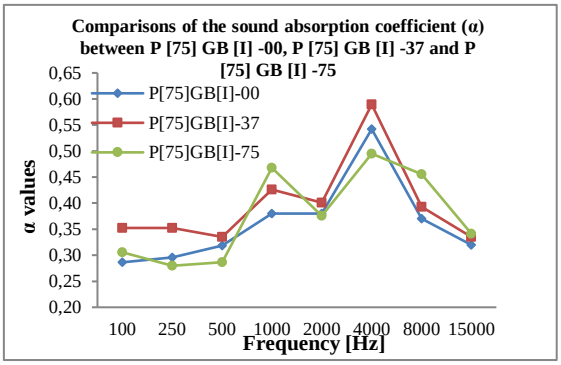

Fig. 5. Comparison of test specimens in group P[75]GB[I].

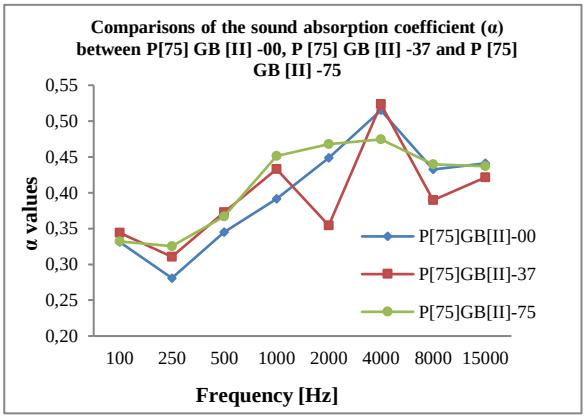

Fig. 6. Comparison of test specimens in group P[75]GB[II].

4 groups, i.e., P [75] GB [I], P [75] GB [II], P [100] GB [I] and P [100] GB [II]. According to the insulation types, each group above (P[75]GB[I], P[75]GB[II], P[100]GB[I], and P[100]GB[II]) was further divided into three different subgroups. These subgroups which contained 12 test specimens in total were examined with five different insulation thicknesses, i.e., uninsulated, 37 mm, 50 mm, 75 mm and 100 mm. First, the comparison among the three test specimens of each group is graphically represented. Then, the comparison among the best four test specimens in each group is demonstrated.

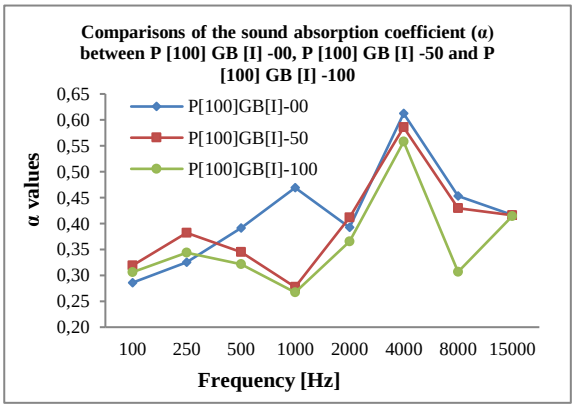

Fig. 7. Comparison of test specimens in group P[100]GB[I].

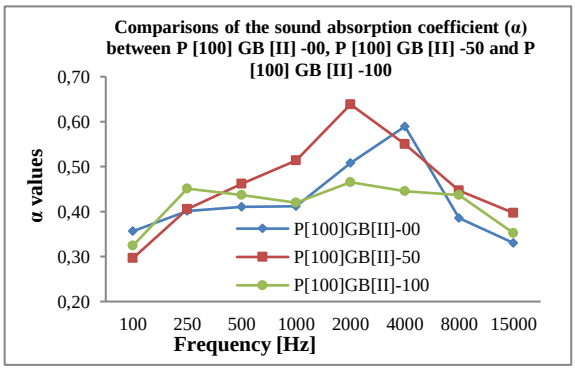

Fig. 8. Comparison of test specimens in group P[100]GB[II].

The comparisons of the test specimens in the four groups are shown in Fig. 5 to Fig. 8.

As shown in Fig. 5, the comparison of the three test specimens in the P[75]GB[I] group shows that the α values were between 0.28 and 0.58. The first reduction in α values occurred at 500 Hz. After an increase, the second reduction occurred at 2000 Hz. The maximum α values were at 4000 Hz, after which it decreased steadily. Fig. 6 shows the comparison of the three specimens in the P[75]GB[II] group. The first reduction in α values was at 250 Hz. Then, the α values increased until 4000 Hz. P[75]GB[II]-37, however, decreased at 2000 Hz. After a rapid reduction, the α value of P[75]GB[II]-37 was the highest at 4000 Hz. After that, the α values of all three specimens decreased.

As shown in Fig. 7 and Fig. 8, the α values of the P[100]GB[I] and P[100]GB[II] groups were between 0.26 and 0.62 and between 0.29 and 0.64 respectively. In the P[100]GB[I] group at 1000 Hz, the α values of all specimens decreased, except for P[100]GB[I]-00, which had a higher α value. The same specimen also had the highest α value at 4000 Hz. In the P[100]GB[II] group, the P[100]GB[II]-50 specimen had the best performance over the other specimens.

The best four test specimens in their groups can be easily observed, i.e., P[75]GB[I]-37, P[100]GB[I]-00, P[75]GB[II]-37, and P[100]GB[I]-50. Fig. 9 shows the four test specimens that had the highest α value at their own groups. The sound absorption performance of P[100]GB[II]-50 was much better than the other specimens till 2000 Hz. After a reduction, its performance was still at average.

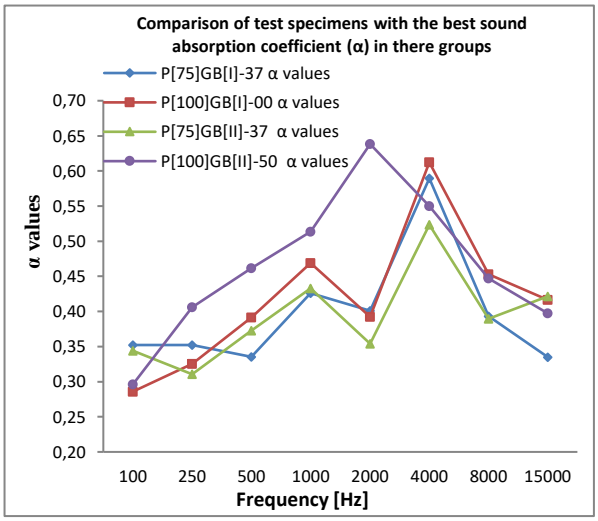

Fig. 9. Comparison of 4 different test specimens according to their α values.

5. CONCLUSION

The first aim of this study was to find out the sound transmission loss of lightweight partition walls insulated by CelluBor. The second aim was to find the optimum thickness of lightweight partition walls and the insulator inside them. To reach the goal, an experimental work carried out on lightweight partition walls with different sizes and insulated by CelluBor.

The results showed that the fully filled profile height with insulation did not give the best sound transmission loss. Half filling the profile would be the optimum choice because air can also work as a sound insulator. The number of gypsum boards on each side of the profile had a positive impact on the sound transmission coefficient.

It was understood from the results of this study that insulation should be made to reduce sound transmission when constructing lightweight partition walls. However, it is more economical and efficient to manufacture gypsum panels having insulation materials by half. As a result, it is recommended that the extension of such works and the development of lightweight partition walls insulated with different materials are noteworthy in terms of scarce resources.

ACKNOWLEDGEMENTS

This article is a part of Master Degree Thesis of Ahmad Javid Zia which is completed in Graduate School of Natural and Applied Sciences at Selcuk University (ZIA). I would also like to thank KTO Karatay University for their support in obtaining laboratory results in the paper.

REFERENCES

Ballagh, Keith O. “Accuracy of Prediction Methods for Sound Transmission Loss.” Inter-Noise, vol. 47, no. 1, 2004, pp. 1–8.

Başbuğ, Ercüment. Sound Transmission Through Suspended Ceilings. Boğaziçi University, 2005.
Cambridge, Jason Esan. An Evaluation of Various Sound Insulation Programs and Their Use in the Design of Silent Rooms. Chalmers University Of Technology, 2006.

Carvalho, António Pedro O. “Acoustical Behavior of a New Lightweight Partition Made with Gypsum Board and Cork.” The Journal of the Acoustical Society of America, vol. 98, no. 5, Presented at the 130th meeting of the Acoustical Society of America, St. Louis MO, Nov. 1995, 1995, p. 2879, doi:10.1121/1.413124.

Çoşgun, Turgay, *et al*. “A Research about the Noise Problems in Buildings Constructed with Tunnel Shuttering System.” Uygulamalı Yerbilimleri Sayı:1, 2008, pp. 65–72.

Díaz-Cereceda, Cristina, *et al*. “The Finite Layer Method for Modelling the Sound Transmission through Double Walls.” Journal of Sound and Vibration, vol. 331, no. 22, Journal of Sound and Vibration, 2012, pp. 4884–900, doi:10.1016/j.jsv.2012.06.001.

Faustino, Jorge, *et al*. “Impact Sound Insulation Technique Using Corn Cob Particleboard.” Construction and Building Materials, vol. 37, 2012, pp. 153–59, doi:10.1016/j.conbuildmat.2012.07.064.

Hernández-Olivares, F., *et al*. “Development of Cork-Gypsum Composites for Building Applications.” Construction and Building Materials, vol. 13, no. 4, 1999, pp. 179–86, doi:10.1016/S0950-0618(99)00021-5.

Ilgun, Abdulkerim, *et al*. “Determination of Sound Transfer Coefficient of Boron Added Waste Cellulosic

and Paper Mixture Panels." Scientific Research and Essays, vol. 5, no. 12, 2010, pp. 1530–35.

Karaağaçlioğlu, İbrahim Ethem. Bor ve Mineral Katkili Selülozik Yalitim Malzemesi Üretimi ve Karakterizasyonu. İstanbul Teknik Üniversitesi, 2012.

Özkan, Sadık. "Ses Yalitimi Uygulamalari." TMMOB Makina Mühendisleri Odası Yalıtım Kongresi 23-24-25 Mart 2001 Eskişehir - Türkiye, TMMOB Makina Mühendisleri Odası, 2001, pp. 114–19.

Phillips, Richard Michael. Investigation of Transmission Loss through Double Wall Structures with Varying Small Air Gaps Using Modal Analysis . University of Louisville, 2014.

Senthilkumar, P. "Studies on the Transmission of Sound in Lightweight Building Components." In Partial Fulfillment of the Requirements for the Degree of Doctor Of Philosophy, Srm University, Kattankulathur – 603 203, 2012.

Tadeu, A., and P. Santos. "Assessing the Effect of a Barrier between Two Rooms Subjected to Low Frequency Sound Using the Boundary Element Method." Applied Acoustics, vol. 64, 2003, pp. 287–310.

Tadeu, António, *et al*. "Sound Insulation Provided by Single and Double Panel Walls—a Comparison of Analytical Solutions versus Experimental Results." Applied Acoustics, vol. 65, no. 1, 2004, pp. 15–29, doi:10.1016/j.apacoust.2003.07.003.

Thomalla, Richard O. "Plumbing Appliance Noise-It Can Now Be Measured." Architectural Engineering, Architectural Engineering, 2003, p. 3.

Uris, Antonio, *et al*. "The Influence of Slits on Sound Transmission through a Lightweight Partition." Applied Acoustics, vol. 65, no. 4, 2004, pp. 421–30, doi:10.1016/j.apacoust.2003.11.006.

Warnock, A. C. C., and J. D. Quirt. "Control of Sound Gypsum Board Walls." Institute for Research in Construction, National Research Council of Canada., vol. 1, no. Construction Technology Updated No. 1, 1997, pp. 1–6, http://www.nrc-cnrc.gc.ca/ctusc/files/doc/ctu-sc/ctu-n1%0Aeng.pdf.

Zia, Ahmad Javid. Analysis of Experimentally Designed Soundproof Gypsum Partition Wall's Sections in Terms of Structural Engineering. Selçuk University, 2014.

Turkish Journal of Engineering

Turkish Journal of Engineering (TUJE)
Vol. 4, Issue 2, pp. 77-84, April 2020
ISSN 2587-1366, Turkey
DOI: 10.31127/tuje.626913
Research Article

DEVELOPMENT OF A NEW APPROACH TO MEMBRANE BIOREACTOR TECHNOLOGY: ENHANCED QUORUM QUENCHING ACTIVITY

Tülay Ergön-Can [1], Börte Köse-Mutlu [*2], Meltem Ağtaş [3], Chung-Hak Lee [4] and Ismail Koyuncu [5]

[1] Istanbul Technical University, National Research Center on Membrane Technologies, Istanbul, Turkey
ORCID ID 0000-0002-7553-7836
tulayergon@hotmail.com

[2] Istanbul Technical University, National Research Center on Membrane Technologies, Istanbul, Turkey
Yeditepe University, Faculty of Engineering, Civil Engineering Department, Istanbul, Turkey
ORCID ID 0000-0001-9747-5499
borte.kose@yeditepe.edu.tr

[3] Istanbul Technical University, National Research Center on Membrane Technologies, Istanbul, Turkey
Istanbul Technical University, Faculty of Civil Engineering, Environmental Engineering Department, Istanbul, Turkey
ORCID ID 0000-0002-8087-7827
agtas@itu.edu.tr

[4] Seoul National University, National Research Center on Membrane Technologies, Istanbul, Turkey
Yeditepe University, School of Chemical and Biological Engineering, Seoul, Republic of Korea,
ORCID ID 0000-0002-8131-5025
leech@snu.ac.kr

[5] Istanbul Technical University, National Research Center on Membrane Technologies, Istanbul, Turkey
Istanbul Technical University, Faculty of Civil Engineering, Environmental Engineering Department, Istanbul, Turkey
ORCID ID 0000-0001-8354-1889
koyuncu@itu.edu.tr

* Corresponding Author
Received: 30/09/2019 Accepted: 16/11/2019

ABSTRACT
Quorum Quenching (QQ) is a mechanism that prevents cell to cell communication and has recently used as an effective control method against biofouling in membrane bioreactors (MBRs). Rotary microbial carrier frame (RMCF) is an innovative application used in QQ-controlled MBRs that provides immobilization medium to QQ bacteria. However, it eventually caused to decrease in QQ activity as a result of a decline in the number of viable QQ cells in the immobilization media over time, especially during long-term MBR operations. In this study, the effect of regeneration of the QQ cells in the immobilization media on biofouling control in MBR was investigated. The growth kinetic of Rhodococcus sp. BH4 as model QQ bacteria was revealed and the bacteria regeneration time was obtained as 28.3 days. In the operation of the regenerated group, an additional QQ activity of 38.2% was achieved compared to control during a 14 day-duration of QQ-controlled MBR operation. It could be indicated that regenerated QQ bacteria reduced SMP and EPS by degrading the signal molecules, thus more efficient control of membrane fouling was achieved.

Keywords: *Wastewater Treatment; Membrane Processes; Biofouling; Quorum Quenching.*

1. INTRODUCTION

Membrane bioreactors (MBRs) have become an attractive process in advanced wastewater treatment. One of the major problems of MBRs is membrane biofouling which causes the flux decline and increases the unit cost of wastewater treatment (Drews, 2010; Lade *et al*., 2014; Wu and Fane, 2012). Various studies have considered the effect of membrane modification with nanoparticles (Koseoglu-Imer *et al*., 2013; Rahimi *et al*., 2015; Ergön-Can *et al*., 2016) and the effect of the varying operating conditions (Ahmed *et al*., 2007; Wu *et al*., 2011; Dvorak *et al*., 2011) in order to prevent and/or mitigate the biofouling. However, biological-based biofouling mitigation techniques have come forward due to the high costs and instability of the physical and chemical-based approaches. Bacteria detect the environment and communicate each-others to form biofilm via signaling molecules (Hammer and Bassler, 2003; Barrios *et al*., 2006; Dong and Zhang, 2005) which is known as quorum sensing (QS). On the other hand, biofilm formation can be inhibited by disrupting the signaling molecules. The inhibition of QS is commonly referred to as quorum quenching (QQ). Recently, the QQ mechanism for the inhibition of biofilm formation was adapted to MBR studies (Yeon *et al*., 2008; Oh *et al*., 2012; Kim *et al*., 2013; Köse-Mutlu *et al*., 2016).

Firstly, Yeon *et al*. (Yeon *et al*., 2009) used the QQ enzyme (acylase) by immobilizing on magnetic particles for effective biofouling control in MBR. Then QQ bacteria having QQ enzyme activity was used by immobilizing in a polymeric microbial vessel due to the instability and purification cost of the enzyme. Up to now, a number of studies have reported that investigate the effect of immobilization media with QQ bacteria such as alginate bead (Kim *et al*., 2013), ceramic microbial vessel (Cheong *et al*., 2014) on the sustainability of the QQ activity. However, QQ applications for biofouling control in the MBR can raise difficulties and carried studies presented that QQ alginate beads as an immobilization media are nondurable and QQ microbial vessels have a low food-to-microorganism ratio to could cause the growth inhibition of QQ bacteria. In our previous studies (Köse-Mutlu *et al*., 2016; Ergön-Can *et al*., 2017) a new approach on the immobilization media to overcome these drawbacks of QQ-controlled MBR has suggested. Rotary microbial carrier frame (RMCF) was manufactured from a polycarbonate multi-frame covered by microfiltration membrane. It was then filled with QQ bacteria and attached to an impeller shaft to allow rotating independently of the main membrane filtration module in the bioreactor. RMCF as an immobilization media provides a durable, renewable and refillable environment for QQ bacteria. However, a decrease in the QQ activity could occur in each cycle of the MBR operation over time. As our knowledge, bacteria can realize the QS and QQ in high levels during their exponential growth phases in which bacterial vital activities are at the highest point (Wagner *et al*., 2003).

This study aims to maintain a stable and sustainable QQ activity of *Rhodococcus sp.* BH4 as model QQ bacteria in order to prevent biofouling in MBR operation as this specie was preferred in the previous studies and the results can be comparable. It is possible to regenerate QQ bacteria in the RMCF to keep bacteria in the exponential growth phase. RMCF is made of an inert and non-dispersible material/structure and provides an opportunity for the regeneration of immobilized bacteria by using possible discharge/filling lines during the pilot- or full-scale MBR plant operation. Batch and continuous experiments were carried out for the determination of growth kinetics and QQ activity. The net biomass production rate (μ) and the endogeneous decay coefficient (k_d) of *Rhodococcus sp.* BH4 in the MBR conditions was used to calculate bacteria regeneration time. The efficiency of suggested operation conditions was evaluated by comparing the results with the un-regenerated group.

2. MATERIALS AND METHODS

2.1. Reagents

Spectinomycin and Tetracycline were supplied as powders (Sigma-Aldrich, USA), and the stock solutions were stored at 4 °C, in the dark and at -20 °C, respectively. Since it is the most common signal molecule in QS systems, commercial homoserine lactone (C8-HSL) that was supplied from Cayman (USA) was selected and used as the representative chemical for signal molecules. The stock solution stored at -20 °C. X-Gal (5-bromo-4-chloro-3-indolyl-β-D-galactopyranoside) from Sigma-Aldrich was used with its powder form. After the X-Gal solution was prepared using dimethylformamide (DMF), which was bought from Merck (Germany), it was kept at -20 °C and in the dark. Microfiltration membrane was a polyvinylidene fluoride (PVDF) membrane (Microdyn Nadir GmbH, Germany) and had a nominal pore size of 0.20 μm and thickness of 210–250 μm (Ergön-Can *et al*., 2017). All synthetic wastewater ingredients were also supplied from Sigma-Aldrich (USA).

2.2. Bacterial Strains and Growth Conditions

Agrobacterium tumafaciens A136 (Ti-)(pCF218)(pCF372) was preferred as a biosensor strain for the detection of N-acyl homoserine lactone (AHL) signal molecules (Yeon *et al*., 2008; Oh *et al*., 2012; Kawaguchi *et al*., 2008). A Luria-Bertani (LB) medium containing spectinomycin (50 mg/L) and tetracycline (4.5 mg/L) was used to culture *A. tumefaciens* A136 for the maintaining the two plasmids that provide the AHL response system. *Rhodococcus sp*. BH4, which was isolated from a real MBR plant by Oh *et al.* (2012), was tasked as the QQ bacterium. It was cultured on LB broth and incubated at 30 °C for 24 hours.

2.3. Batch Study on Mass Flux

The mass flux of the microfiltration membrane that is used for covering the RMCF surface was determined. Within this regard, an experimental setup was prepared. This experimental setup included a beaker, which contains synthetic wastewater with 150 mg/L chemical oxygen demand (COD), and a pocket made using an MF membrane, which is filled with distilled water (Fig. 1.A). The composition of the synthetic wastewater was as follows (mg/L): glucose, 133; yeast extract, 4.67;

bactopeptone, 38.3; $(NH_4)_2SO_4$, 34.9; KH_2PO_4, 7.25; $MgSO_4$, 5.21; $FeCl_3$, 0.025; $CaCl_2$, 0.817; $MnSO_4$, 0.6; and $NaHCO_3$, 85.17. Osmotic pressure and total organic matter (TOC) concentration in the synthetic wastewater (outside environment) and in the distilled water (inside environment) were routinely determined. Sampling had been continued until the osmotic pressures on the outside and on the inside were the same. Mass flux was calculated using the equation given below (Eq. 1).

$$J_m=(\Delta TOC)/(\Delta t*A_{mem}) \quad (1)$$

where J_m ($mg.m^{-2}h^{-1}$), ΔTOC (mg/L), and A_{mem} (m^2) are the mass flux through the membrane, the change in the TOC amount in time and the membrane area, respectively.

2.4. Batch Study on Growth Kinetic

After the mass flux was determined, the growth kinetics of *Rhodococcus sp.* BH4 in the reactor conditions was tried to be revealed by using a batch study. With this aim, a batch experimental setup was prepared. Inoculated BH4 bacteria were centrifuged and BH4 with the same amount used in the RMCF studies (Köse-Mutlu *et al*., 2019; Ergön-Can *et al*., 2017), which is approximately 25 mg dry weight of biomass per ml, added into the synthetic wastewater. The composition of the synthetic wastewater was the same as the recipe given in the section of the batch study. The determination of the elemental concentrations in synthetic wastewater was based on the calculations related to the dilution of the feed in the reactor caused by existing water in it. The measurements carried with the samples taken from the supernatant of the activated sludge (data not shown). During the 6 days-duration incubation of BH4 in this synthetic wastewater, the optical density (OD) of the bacterial solution was routinely measured by using an ultraviolet (UV) spectrophotometer (Hach Lange, DR 500, USA). Moreover, TOC concentrations were also measured in order to see the rate of organic matter removal by the microorganisms. According to the results of these measurements, μ and k_d coefficients were found out using Eq. 2 and Eq. 3 and minimum mean cell residence time (MCRT) (Equation 4) was calculated. μ and k_d coefficients were found out by using the slope of the exponential growth and exponential decay phases, respectively (Metcalf and Eddy, 1980). According to these values, the minimum MCRT was calculated and used as the regeneration time. All studies had carried out duplicated.

$$\mu_m=(\ln(OD_{t1})-\ln(OD_o))/\Delta t \quad (2)$$
$$k_d=-(\ln(OD_{t2})-\ln(OD_{t3}))/\Delta t \quad (3)$$
$$\mu = \mu_m - k_d \quad (4)$$
$$1/\Theta_{min} = \mu$$

where μ_m is the maximum specific bacterial growth rate (d^{-1}), ODt is optical density at time t, OD_o is optical density at the beginning, k_d is endogenous decay coefficient (d^{-1}), μ is the net biomass production rate (d^{-1}), and Θ_{min} is the minimum mean cell residence time (d).

2.5. Continuous Study on Quorum Quenching Activities

In the light of idea about the positive effect of bacteria regeneration on the quorum quenching activity, an experimental study was realized with a continuous feed. Sterilized synthetic wastewater, which is the same as the used one in the growth kinetic study, was used as inoculation media, and COD concentration was kept constant and at 150 mg/L according to the previously determined organic matter removal rates. 10 mg BH4 (dry weight) were inoculated on the first day. This study was carried with two groups: 1) control group and 2) regenerated group. While the control group was inoculated without an interception, a determined volume of the regenerated group was removed from the flask according to the sludge retention time calculations. The aim was this removal was to provide a constant QQ bacteria number and log phase for the regenerated group. Besides, a control group can carry on their routines like growing, divisions, aging and cannibalism in an interference-free environment. All studies had carried out duplicated.

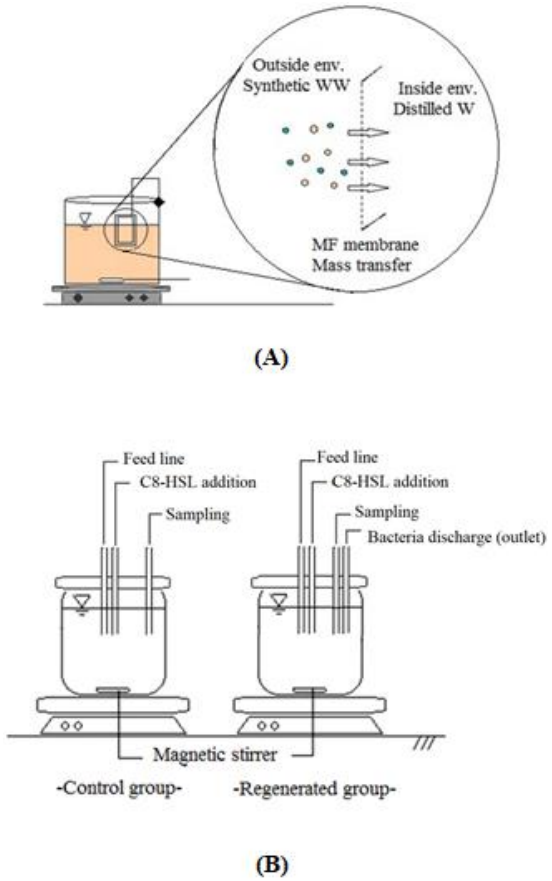

Fig. 1. (A) Experimental setup for mass flux determination (WW: wastewater, W: water, env.: environment) and (B) experimental setup of continuous study on the regeneration

This experiment was carried out under the aseptic conditions. The experimental setup can be seen in Fig. 1.B. QQ activities of these two groups were daily

determined by adding 200 nM C8-HSL and taking samples at 0^{th}, 10^{th} and 30^{th} minutes. AHL concentrations were determined with the indicating agar plate method from Park *et al.* (2003). Indicating agar plate was prepared as follows: 1) mixing (ratio of 9:1) LB-agar, 2) an overnight culture of *A. tumefaciens* A136 including spectinomycin (50 mg/L), tetracycline (4.5 mg/L), and X-gal (0.2 g/L), 3) AHL degradation by *Rhodococcus sp*. BH4 occurred in the reaction tube (the initial concentration of C8-HSL was 200 nM), and 4) reaction mixtures were added into the well of plates. The residual amounts of AHL were determined by the equations that were based on the color zone sizes.

2.6. MBR Operation

Three parallel MBRs were operated under the same operating conditions as MBR-A, MBR-B, and MBR-C. MBR-A was a conventional MBR. While MBR-B was operated with RMCF, MBR-C was a parallel operated MBR with RMCF having QQ bacteria regeneration lines. The scheme of the MBR system was depicted in Fig. 2. Activated sludge was supplied from an advanced biological wastewater treatment plant in Istanbul. The activated sludge was subjected to an acclimation before the operation. The composition of the synthetic wastewater was the same used in the batch study on the mass flux. The elemental concentrations in the MBR were the same ass the concentrations in the batch and the continuous studies by using this recipe taking the dilution into the consideration. MBRs were connected to a computer to control all operating parameters like water levels, pH, temperature, oxidation-reduction potential (ORP) values and dissolved oxygen concentrations (Table 1). All membrane bioreactors were operated under the steady-state conditions following the previous studies carried out during several months (Ergön-Can *et al*., 2017).

Table 1. MBR operation details

Parameter	Unit	Value or information
pH		6.8~7.2
Dissolved oxygen	mg/L	4.2-6.6
ORP	mV	170-210
Temperature	^oC	24±2
Membrane type		Hollow fiber (Philos MegaFluxI)
Membrane area	cm^2	100
Flux	$L/m^2/h$	60
COD removal efficiency	%	~ 96
MLSS	mg/L	12,000
Feed COD	mg/L	440
Seeding sludge		Paşaköy Advanced Biological WWTP (Istanbul/Turkey)
Reactor volume	L	4.75

MBR-A, MBR-B, and MBR-C were operated under the constant flux condition by using a microfiltration system consisting of the hollow fiber membrane module. Membrane module properties and dimensions were the same as in the previous study (Ergön-Can *et al*., 2017). While the effective area of the hollow fiber membranes in the module was around 100 cm^2, the hydraulic retention time (HRT) and sludge retention time (SRT) were kept as 13 h and 30 d, respectively. The mixed liquor suspended solids (MLSS) concentrations in MBRs were maintained within the range of 11000-12000 mg/L.

2.7. Analytical Methods

MLSS and COD were determined according to Standard Methods. TOC concentrations were measured using the TOC instrument (Shimadzu, Japan). Osmotic pressures were determined with a 3250 model instrument of Advanced Instruments Inc. (USA).

3. RESULTS AND DISCUSSION

3.1. Mass Flux

Firstly, the mass flux of the microfiltration membrane that is used for coverage of the RMCF and in which *Rhodococcus sp*. BH4 is immobilized was determined. The change of the osmotic pressures of the inside and of the outside environments in time was monitored. In addition to this, organic matter concentrations in these environments were determined and mass flux was calculated. Osmotic pressures in two environments were equal after a time and this result can mean that nutrients and minor elements could pass through the microfiltration membrane as expected. At the end of the 8^{th} hour, the microfiltration membrane totally soaked, and the osmotic pressures had started to change. The osmotic pressures in the two environments were nearly equal at the end of the 12^{th} hour. After 24 hours, the immobilized bacteria can achieve to get the total nutrient mass because of the total equalization. Moreover, the mass flux of total organic carbons throughout the microfiltration membrane was calculated as 2.26 $mg.m^{-2}h^{-1}$ using the data obtained from this side-study. Because there is no filtration process in which driving force is an applied pressure, the mass transfer was realized as a result of the osmotic pressure differences.

3.2. Growth Kinetics

After the mass flux was determined, a growth kinetic study was carried. The growth kinetic study was realized under the conditions which are seen in the membrane bioreactors operated in this study, and the result of the study was given in Fig. 3. As shown in the figure, bacteria can degrade the synthetic wastewater with 150 mg COD/L with 60% efficiency in their first 24 hours. At the end of the 48 hours, the rate of substrate degradation started to decrease. The reason can be explained as the beginning and the end of the log phase of the culture. Bacteria could easily reach the substrate and use for their rapid metabolism in the first 48 hours. According to the slope changes in the biomass graph, growth phases could be determined. As expected, the bacteria stayed in a stable situation in their first 23

hours. At the end of the 23rd hour, divisions immediately started and this was the siren of the start of the exponential growth phase. The exponential growth phase had continued until the end of the 50th hour. Because there was feed for once at the beginning, bacteria had been faced with the substrate limiting condition between 48th and 74th hours. At the end of the stationary phase, the culture started to show a decay situation which can get by looking at the high negative slope of the OD graph

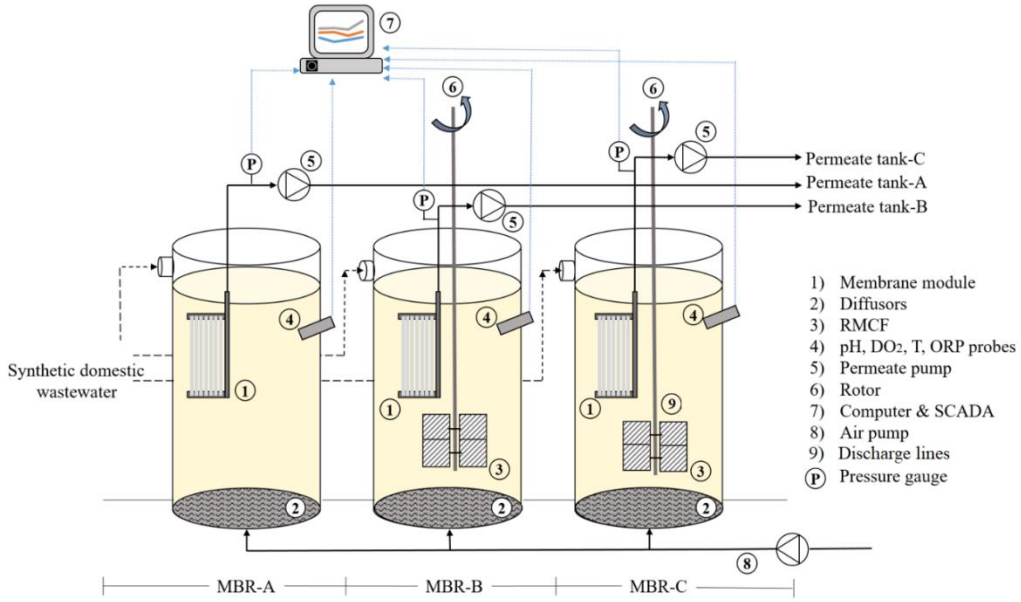

Fig. 2. Schematic description of the MBR set-up

At the end of the inoculation, the OD values were lower than the OD values at the beginning. This final term was the decay phase of the inoculated species. By using the slope values, the growth, and the decay rate constants can be determined. In this study, Eq. 2, Eq. 3 and Eq. 4, and data from Fig. 3 was used, and bacteria retention time of *Rhodococcus sp.* BH4 was determined as 28.3 days. This means that 3.5% of the total volume can be daily removed, all volume can be renewed at the end of this 28.3 days-duration.

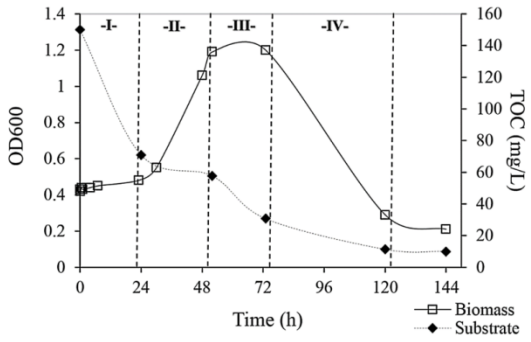

Fig. 3. Growth phases of BH4

This means that daily removal of 3.5% of the total immobilized bacteria amount from the medium may help the bacteria regeneration, constant bacteria OD, prevention of the bacterial aging, and increase of the QQ activity, which are closely related together. In this study, the application of the daily bacteria removal from the immobilization medium was tried to be explained by the means of the "regeneration of the immobilized culture" statement.

3.3. Effect of the Regeneration on the Quorum Quenching Activity

An experimental study with a control group was carried in order to check the possible effect of the bacterial regeneration on the quorum quenching activity. QQ activities of control and regenerated groups during the 4 days were daily determined. Daily removal of 3.5% of the total immobilized bacteria amount from the group, which is named as the regenerated group, was realized during this continuous study. AHL degradations were given in Fig. 4.A. The detailed results can be seen in the Appendix. Correlation coefficients were higher than 0.953 for each quorum quenching activity experiment, and the results can be used if the correlation coefficient should be higher than 0.95 for this type of bio-assay. The initial AHL concentration was 200 nmol/L for both groups at the beginning of each AHL degradation rate study carried daily. Because both groups include a high amount of *Rhodococcus sp*. BH4 in their environments, AHL degradation was realized dramatically. In 30 minutes *Rhodococcus sp*. BH4 could degrade the AHL up to 50 mg/L and lower concentrations. It is a known fact that *Rhodococcus sp*. BH4 is a highly effective QQ specie used before for biofouling control by the researchers (Dong and Zhang, 2005; Jahangir *et al*., 2012). It can be said that while the regenerated group could save its quorum quenching

activity, control group started to lose its quorum quenching activity after 24 hours. On the first day, the two groups showed the same quorum quenching activity (87% for the control group and 88% for the regenerated group), and they could rapidly degrade the AHL in their environment. 24 hours after the first bacteria removal application; the QQ activities were determined as 80% and 88% for the control group and regenerated group, respectively. It may be said that the control group had started to lose its activity because this group had lived in the stationary phase for that 24 hours-duration. After 48 hours, the time was the 72nd hour and the quorum quenching activities were 72% and 82% for the control group and regenerated group, respectively. The decrease in the QQ activity of the control group as 8% may result from the late stationary phase and the start of the decay phase. In the last day of the experiments; it was seen that the regenerated group could sustain its quorum quenching activity, the control group showed a quorum quenching activity with 65% efficiency. This means that quorum quenching bacteria can lose its AHL degradation efficiency with time in the environment because of the limiting factors and living population ratio in the suspension. In light of this study, it may be mentioned that bacteria removal from the cubbyholes of the RMCF can result in sustained quorum quenching activities.

3.4. Effect of Regeneration on Quorum Quenching Activites During the MBR Operation

In order to examine the effect of bacteria regeneration in QQ MBR operation, two parallel MBRs were operated for two weeks. Transmembrane Pressure (TMP) profiles obtained from operations were given in Fig. 4.B. In order to determine the TMP decreasing effect caused by the daily bacteria removal, the areas under the TMP graphs were calculated by taking integrals of the line equations having correlation coefficients higher than 0.997.

$$\text{Decreasing percentage (\%)} = \frac{(\int_0^t f\,control\,(t)\,dt - \int_0^t f\,regenerated\,(t)\,dt)}{\int_0^t f\,control\,(t)\,dt} * 100 \quad (5)$$

where $f_{control}$ is the equation of the TMP profile of MBR-A and $f_{regenerated}$ is the equation of the TMP profile of MBR-B. According to these TMP profiles, it can be said that the regeneration of bacteria resulted in an additive effect on biofouling prevention via quorum quenching. There is a slight difference between the TMP profile of MBR-A and the TMP profile of MBR-B. While TMP values reached 200 mbar in MBR-A, it was around 100 mbar in MBR-B. Because these both MBRs were operated as QQ MBRs, TMP values could not reach high values during these 14 days of operation. According to the decreasing percentage calculations, it can be mentioned that there was an additional 38.2% TMP decrease via daily bacteria removal from the cubbyholes of RMCF. The TMP decrease with RMCF usage against conventional MBR usage resulted in a 60% TMP decrease (Köse-Mutlu *et al*., 2016). Bacterial regeneration may create an increase in the quorum quenching effect of 15%, which means an additional decrease of 3.4% on the total MBR operation costs.

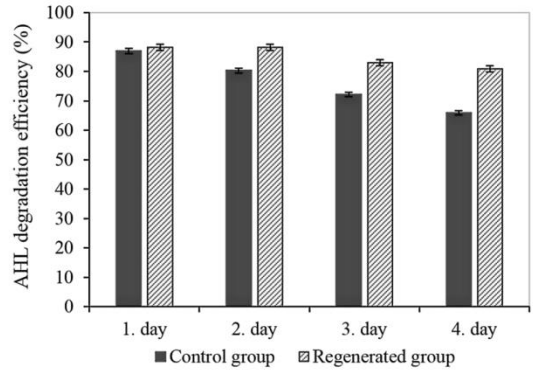

(A)

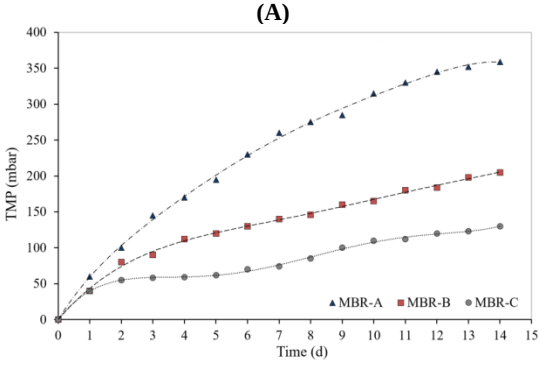

(B)

Fig. 4. (A) The effect of the regeneration on the QQ activity and (B) TMP profiles obtained from the parallel MBR operations

4. CONCLUSION

Within the scope of this study, the possible positive effect of bacterial regeneration on the quorum quenching activity was examined. The younger bacteria in their log phases results in the higher efficiencies of many vital activities. Because of this reason, it was thought that a definite percentage, which was decided according to the net biomass production rate which indicates the difference between growth rate and decay rate, of the *Rhodococcus sp.* BH4 solution in the RMCF can be removed, and this can be adapted to the MBR operation. The concluding remarks of this study can be listed as:

- The nutrient mass transfer throughout the microfiltration membrane used for the immobilization of *Rhodococcus sp.* BH4 in RMCF was totally achieved in 12 hours, and the mass flux was determined as 2.26 $mg.m^{-2}h^{-1}$.
- Over the first 23 hours, *Rhodococcus sp.* BH4 was in lag-phase and reached in the exponential growth-phase between 23rd and 50th hours. After a 23 hour-duration stationary-phase, specie had started to live its decay-phase. In light of the net growth rate calculations, it was found out that the regeneration of the immobilized culture may be realized by the means of a volumetric removal of 3.5%.
- According to the QQ activity tests, it was seen that while the QQ activity of the control group had decreased from 87% to 65%, the regenerated group could sustain its QQ activity.

- The sustainability of the QQ activity via bacteria regeneration was also tried to prove with QQ-MBR operations, and an additional QQ activity of 38.2% could be obtained during a 14 day-duration MBR operation.

This concept and the mechanism mentioned in this paper should be studied to enlighten all the effects of various parameters. Since it is an innovative idea, this study is the first for the researchers focused on the QQ MBR. Finally, it can be said that the application of this idea was successful during MBR operation, and it will be possible, especially for the pilot- and full-scale MBR plants with bacteria discharge lines.

ACKNOWLEDGMENTS

TUBITAK (The Scientific and Technological Research Council of Turkey), and KORANET (the Korean Scientific Cooperation Network with the European Research Area) supported this work financially under project no 112M739. In addition, Tülay Ergön-Can thanks to TUBITAK 2218-National Postdoctoral Research Fellowship Program.

REFERENCES

Ahmed Z, Cho J, Lim BR, Song KG, Ahn KH. (2007) "Effects of sludge retention time on membrane fouling and microbial community structure in a membrane bioreactor". *Journal of membrane science.* Jan 15; 287(2):211-8.

Barrios AF, Zuo R, Hashimoto Y, Yang L, Bentley WE, Wood TK. (2006) "Autoinducer 2 controls biofilm formation in Escherichia coli through a novel motility quorum-sensing regulator (MqsR, B3022)". *Journal of bacteriology.* Jan 1;188(1):305-16.

Cheong WS, Kim SR, Oh HS, Lee SH, Yeon KM, Lee CH, Lee JK. Design of quorum quenching microbial vessel to enhance cell viability for biofouling control in membrane bioreactor. J. Microbiol. Biotechnol. 2014 Jan 1;24(1):97-105.

Dong YH, Zhang LH. (2005) "Quorum sensing and quorum-quenching enzymes". *The Journal of Microbiology*. Feb;43(1):101-9.

Drews A. (2010) "Membrane fouling in membrane bioreactors—characterisation, contradictions, cause and cures". *Journal of membrane science*. Nov 1;363(1-2):1-28.

Dvořák L, Gómez M, Dvořáková M, Růžičková I, Wanner J. (2011) "The impact of different operating conditions on membrane fouling and EPS production". *Bioresource technology*. Jul 1;102(13):6870-5.

Ergön-Can T, Köse-Mutlu B, Koyuncu İ, Lee CH. (2017) "Biofouling control based on bacterial quorum quenching with a new application: rotary microbial carrier frame". *Journal of membrane science.* Mar 1;525:116-24.

Ergön-Can T, Köseoğlu-İmer DY, Algur ÖF, Koyuncu İ. (2016) "Effect of different nanomaterials on the metabolic activity and bacterial flora of activated sludge medium". *CLEAN–Soil, Air, Water.* Nov;44(11):1508-15.

Hammer BK, Bassler BL. (2003) "Quorum sensing controls biofilm formation in Vibrio cholerae". *Molecular microbiology*. Oct;50(1):101-4.

Jahangir D, Oh HS, Kim SR, Park PK, Lee CH, Lee JK. (2012) "Specific location of enca.psulated quorum quenching bacteria for biofouling control in an external submerged membrane bioreactor". *Journal of membrane science*. Sep 1;411:130-6.

Kawaguchi T, Chen YP, Norman RS, Decho AW. (2008) "Rapid screening of quorum-sensing signal N-acyl homoserine lactones by an in vitro cell-free assay". *Applied Environmental Microbiology.* Jun 15;74(12):3667-71.

Kim SR, Oh HS, Jo SJ, Yeon KM, Lee CH, Lim DJ, Lee CH, Lee JK. (2013) "Biofouling control with bead-entrapped quorum quenching bacteria in membrane bioreactors: physical and biological effects". *Environmental science & technology.* Jan 4;47(2):836-42.

Koseoglu-Imer DY, Kose B, Altinbas M, Koyuncu I. (2013) "The production of polysulfone (PS) membrane with silver nanoparticles (AgNP): physical properties, filtration performances, and biofouling resistances of membranes". *Journal of membrane science.* Feb 1;428:620-8.

Köse-Mutlu B, Ergön-Can T, Koyuncu İ, Lee CH. (2016) "Quorum quenching MBR operations for biofouling control under different operation conditions and using different immobilization media". *Desalination and Water Treatment.* Aug 14;57(38):17696-706.

Lade H, Paul D, Kweon JH. (2014) "Quorum quenching mediated approaches for control of membrane biofouling". *International Journal of Biological Sciences*. 10(5):550.

Metcalf & Eddy B, (1980). "Wastewater engineering: Treatment disposal reuse." Central Book Company. New york, USA.

Oh HS, Yeon KM, Yang CS, Kim SR, Lee CH, Park SY, Han JY, Lee JK. (2012) "Control of membrane biofouling in MBR for wastewater treatment by quorum quenching bacteria encapsulated in microporous membrane". *Environmental science & technology*. Apr 11;46(9):4877-84.

Park SY, Lee SJ, Oh TK, Oh JW, Koo BT, Yum DY, Lee JK. (2003) "AhlD, an N-acylhomoserine lactonase in Arthrobacter sp., and predicted homologues in other bacteria". *Microbiology.* Jun 1;149(6):1541-50.

Rahimi Z, Zinatizadeh AA, Zinadini S. (2015) "Preparation of high antibiofouling amino functionalized MWCNTs/PES nanocomposite ultrafiltration membrane

for application in membrane bioreactor". *Journal of Industrial and Engineering Chemistry*. Sep 25;29:366-74.

Wagner VE, Bushnell D, Passador L, Brooks AI, Iglewski BH. (2003) "Microarray analysis of Pseudomonas aeruginosa quorum-sensing regulons: effects of growth phase and environment". *Journal of bacteriology*. Apr 1;185(7):2080-95.

Wu B, Fane AG. (2012) "Microbial relevant fouling in membrane bioreactors: influencing factors, characterization, and fouling control". *Membranes.* Aug 15;2(3):565-84.

Wu B, Yi S, Fane AG. (2011) "Microbial community developments and biomass characteristics in membrane bioreactors under different organic loadings". *Bioresource technology.* Jul 1;102(13):6808-14.

Yeon KM, Cheong WS, Oh HS, Lee WN, Hwang BK, Lee CH, Beyenal H, Lewandowski Z. (2008) "Quorum sensing: a new biofouling control paradigm in a membrane bioreactor for advanced wastewater treatment". *Environmental science & technology.* Dec 18;43(2):380-5.

Yeon KM, Lee CH, Kim J. (2009) "Magnetic enzyme carrier for effective biofouling control in the membrane bioreactor based on enzymatic quorum quenching". *Environmental science & technology.* Sep 2;43(19):7403-9.

Turkish Journal of Engineering

Turkish Journal of Engineering (TUJE)
Vol. 4, Issue 2, pp. 85-91, April 2020
ISSN 2587-1366, Turkey
DOI: 10.31127/tuje.625475
Research Article

LOW-POWER DYNAMIC COMPARATOR WITH HIGH PRECISION FOR SAR ADC

Ersin Alaybeyoğlu *[1]

[1] Istanbul Technical University, Faculty of Department of Electrical and Electronics Engineering, Department of Electronics and Communication Engineering, İstanbul, Turkey
Bartın University, Faculty of Engineering Architecture and Design, Department of Electrical and Electronic Engineering, Bartın, Turkey
ORCID ID 0000-0002-8318-4081
ealaybeyoglu@bartin.edu.tr

* Corresponding Author
Received: 27/09/2019 Accepted: 02/12/2019

ABSTRACT
In this work, low-power dynamic comparator is presented with auto-zeroing technique for successive approximation register (SAR) analogue-to-digital converter (ADC). The comparator designed with DTMOS technique operates in sub-threshold region. The designed circuit consumes low power with high gain. The dynamic range of the comparator is increased with a new biasing technique for DTMOS transistors. The core design consumes 6.01µW power and overall design consumes 17.06µW. The design is realized with two different supply voltage with 600mV (core design) and 1.8V (biasing circuit). The comparator has been simulated with 0.18µm TSMC process in Cadence environment.

Keywords: *SAR ADC, Comparator, CMOS analog integrated circuits*

1. INTRODUCTION

Comparative circuits are indispensable interface elements between analog and digital world. Also, comparators play key roles in the design of analog-to-digital converters, memories, dynamic logic, and sense amplifiers as decision-making circuits (Cohen *et al*. 2005; Kim, Choi, and Lee 2015; Ming-Dou Ker and Jung-Sheng Chen 2008; Verma and Chandrakasan 2007). The input referred offset voltage in the design of comparator circuits is the biggest problem affecting the resolution of converters. Auto-zeroing and chopper methods are useful techniques to cancel offset and low-frequency noise (Cohen *et al*. 2005; Witte, Makinwa, and Huijsing 2006; Wu, Makinwa, and Huijsing 2009). Dynamic switches with auto-zeroing technique are the common and successful approach to cancel offset (Schinkel *et al*. 2007; Sepke *et al*. 2006).

Dynamic comparators are suitable for low-supply, low-power and high-speed applications (Zhong, Bermak, and Tsui 2017). Furthermore, various types of sensors to gather information are applied to everyday objects of Internet of Things (IoT). These sensor requirements oblige the need of analog-to-digital converters (ADCs) dissipated low power with high resolution and high linearity for use in an energy-constrained environment (Shim *et al*. 2018). Moreover, the power consumption of the dynamic comparators is called the dynamic power. The dynamic power is defined as the power of dissipated during the evaluation of signal in one period of clock. The successive approximation register (SAR) ADCs has the resolution of 12-14 bit level and are very energy-efficient (Yan *et al*. 2018).

Furthermore, in wide common mode range applications, for example, the speed and offset of CMOS designs in A / D converters depends on the common mode voltage of the input and this is a challenging situation for sub-micron CMOS technologies. However, a large voltage headroom, which is problematic, especially in circuits with transistor stacks and especially in low-voltage deep-micron CMOS technologies (Schinkel *et al*. 2007; Wicht, Nirschl, and Schmitt-Landsiedel 2004; Wong and Yang 2004).

In this work, offset cancelled low power dynamic comparator for successive approximation register (SAR) ADCs is designed. The CMOS implementation of the designed comparator is realized with standard 0.18μm CMOS technology with DTMOS technique. The designed circuit has mixed 0.6V-1.8V supply voltage. The biasing circuitries (current sources and current sinks) are designed with normal CMOS transistor to extend headroom. The core design is implemented with DTMOS transistors (Achigui *et al*. 2006; Ramírez-Angulo *et al*. 2001). DTMOS transistor is realized for only pMOS transistor by connecting its gate to the body without the need for another manufacturing process or step. As a result, the DTMOS transistors can be used in standard CMOS process. DTMOS offers the low power designs for especially biomedical applications and portable devices.

This paper is organized as follows. Section 2 explains the CMOS implementation and layout with analysis. Corner and Monte-Carlo analysis are also given in the same section. Finally, section 3 gives some conclusions.

2. COMPARATOR DESIGN

Due to the nature of analog signals, all IoT applications require both analog and digital system design for a high integration level with low cost. Although many analog designs can perform digitally, the analog-digital converters (ADCs) are still required as an interface between the analog domain and the digital (Lin, Wei, and Lee 2018). Many wireless sensor node (WSN) for IoT applications require low-power ADCs ranging in resolution (8 - 12 bit) and speed around (MS / s) (Ding *et al*. 2018). Comparators are the essential building block of the successive approximation register (SAR) ADCs. Comparators need extremely low offset, and very low input noise. The dynamic range of the comparator can be improved by cancelling the low-frequency noise and offset with auto-zeroing technique (Enz and Temes 1996).

Operational amplifiers have been used as basic circuit components in analog circuit design since the emergence of integrated circuits. After the emergence of new analog circuit applications, the performance characteristics of the voltage-mode operational amplifiers are not sufficient for analog signal processing requirements. The compensation capacitance, which ensures the stability of the OPAMP (operational amplifier), reduces the bandwidth of the operational amplifier due to the excessive voltage gain expected from OPAMP (Palmisano G. 1999). Therefore, OPAMPs are replaced by operational transconductance amplifiers (OTAs) whose output resistance is quite high (Maloberti 2006). At the same time, in a fully differential system not only rejects the common mode voltages but also eliminates the external noise. For the reasons mentioned above, the CMOS implementation of comparator is realized with fully differential operational transconductance amplifier in sub-threshold region.

Fig. 1 shows a block diagram of the comparator structure. The proposed implementation is developed based on the comparator proposed in (Allen and Holberg 2012). The structure of the comparator is made up of a fully differential operational transconductance amplifier, latch and switch. The gain of the overall design is 142.8dB. The overall design consists of three cells. Each cell has the gain of 35.7dB. The input referred offset is $V_{OS1} + V_{OS2} \,/\, A_{V1} + V_{OS3}/A_{V1}A_{V2}$. V_{OS1} and A_{V1} is the first cell's offset voltage and gain, respectively. V_{OS2} and A_{V1} define the second cell's offset voltage and gain while the third stage offset and gain is defined as V_{OS3} and A_{V3}, respectively.

OTAs and dynamic latch operate in sub-threshold region and the supply voltage is 0.6V. The biasing circuit operates with 1.8V supply voltage. pMOS transistor of core design are designed with DTMOS technique to decrease the power dissipation and to increase the gain and dynamic range of the design.

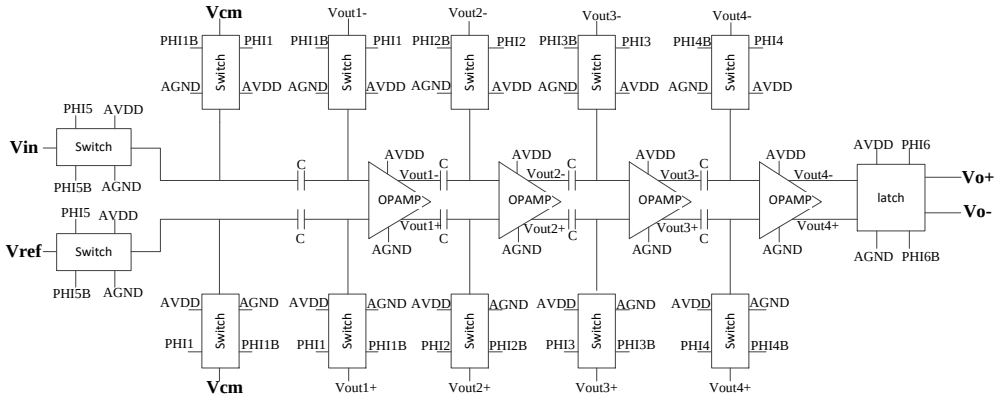

Fig. 1 Block diagram of the designed comparator

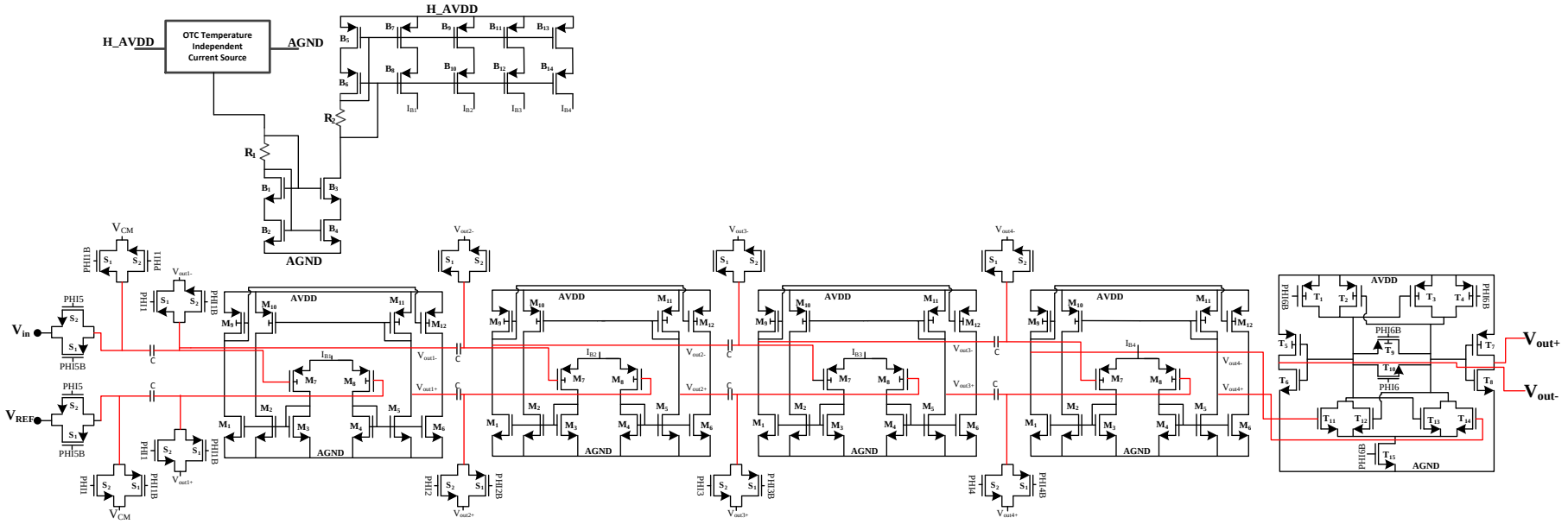

Fig. 2 CMOS implementation of overall comparator

(1) shows the transistor current in sub-threshold region. I_0 and m are technology dependent parameters, $V_T = kT/q$ is thermal voltage.

$$I = I_0 \frac{W}{L} e^{\frac{V_{GS}-V_{th}}{mV_T}} (1 - e^{-(V_{DS}/V_T)}) \quad (1)$$

The sub-threshold current-voltage relationship of the MOS transistor is very similar to the bipolar transistor, but still the gain effect of the threshold voltage is clearly visible as in (1). The threshold voltage of the transistor is decreased dynamically by connecting the device gate and body, seen as the relationship given in (2).

The DTMOS transistor under the same V_{GS} voltage has a higher g_m than the MOS transistor. (3) gives the relationship of g_m under sub-threshold region. As a result, DTMOS transistor has higher gain than the standards under same conditions.

Only pMOS transistors can be selected as DTMOS because of the single well process of used 0.18µm CMOS process. The biasing circuit is designed with standard CMOS transistor with 1.8V supply voltage to increase the swing and gain of amplifier. Table 1 gives the size of the transistors.

Table 1. The size of the transistors

		Transistors	***W/L***
Supply Voltage (1.8V)	**Biasing Transistors**	B_1, B_2, B_3, B_4, B_5, B_6, B_7	10µm/2µm
		B_8, B_9, B_{10}, B_{11}, B_{12}, B_{13}, B_{14}	10µm/2µm
Supply Voltage (0.6V)	**Switch**	S_1	100µm/180nm
		S_2	100µm/180nm
Operational Transconductance Amplifier	Supply Voltage (0.6V) DTMOS Technique	M_1, M_2	8µm/360nm
		M_3, M_4	4µm/360nm
		M_5, M_6	8µm/360nm
		M_7, M_8	10µm/360nm
		M_9, M_{10}, M_{11}, M_{12}	8µm/360nm
Latch		T_1, T_4	6µm/180nm
		T_2, T_3	1.3µm/180nm
		T_5, T_7	6.6µm/180nm
		T_6, T_8	6.6µm/180nm
		T_9	4µm/180nm
		T_{11}, T_{14}	3µm/180nm
		T_{12}, T_{13}	1µm/180nm

The CMOS implementation of the comparator is given in Fig. 2. The implementation of temperature independent current generator is designed based on (Alaybeyoğlu and Kuntman 2016). Layout of the comparator is given in Fig. 3. The core occupation area of the designed circuit is 61.5µmx115.4µm; 0.007mm^2.

$$|V_{th,p}| = |V_{th0,p}| + \gamma_p(\sqrt{|2\Phi_F| + V_{SB}} - \sqrt{|2\Phi_F|}) \quad (2)$$

$$g_m = \frac{\partial I_D}{\partial v_{GS}} = \frac{I_D}{nV_T} \quad (3)$$

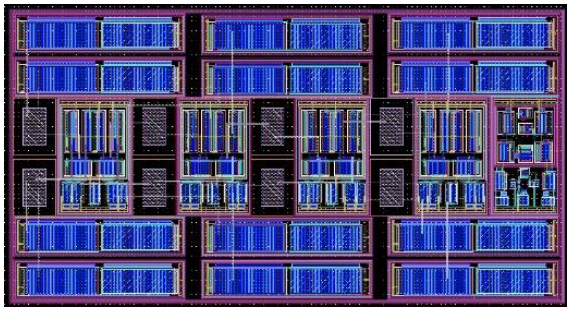

Fig. 3 The layout of overall comparator

Fig. 4 shows the DC gain of single cell. The gain of the overall circuit is 142.8dB for four cascaded OPAMPs. The timing diagram of comparator is given in Fig. 5. Reset and Comparison phased of the comparator are two operation duration. The evaluation of the comparison is realized after the offset cancellation in reset time.

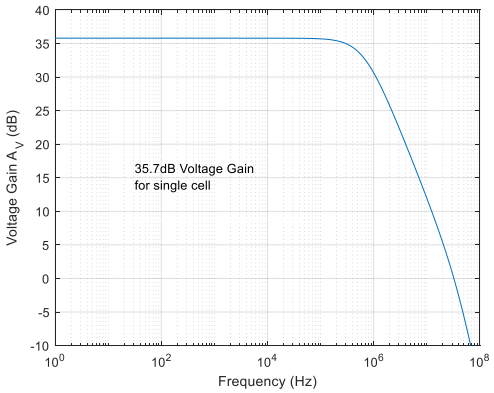

Fig. 4 DC gain of single cell.

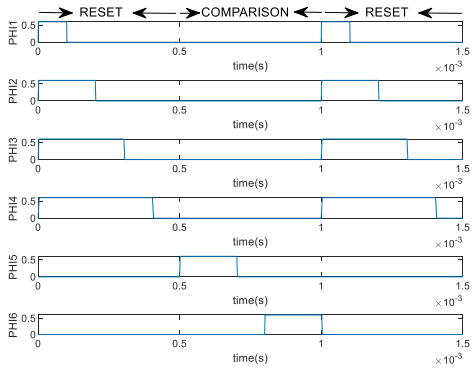

Fig. 5 Timing diagram of comparator.

Offset analysis under the variation of process (ss, tt, ff, sf, fs), power supplies (AVDD [0.54V, 0.66V]) and temperatures (−40ºC, 85ºC) is given in Fig. 6. The solution in Fig. 6 is realized without offset cancellation. Table 2 gives the offset value for each corners. Offset coming from fourth stage is suppressed by the 1st, 2nd and 3th stage gain. Furthermore, offset coming from third stage is suppressed by the 1st and 2nd stage gain. As a result, the most dominant offset contributed by M_7, M_8 is 1st- stage offset (Zhong, Bermak, and Tsui 2017).

The 1st- stage offset is cancelled out with auto-zeroing capacitances (50fF). Fig. 7 shows the Monte Carlo analysis of offset without offset cancellation (OC) Histograms of offset with OC technique given in Fig. 1. is shown in Fig. 8.

Table 2 The offset values according to the each corner

Temperature	-40º					27º					85º				
Process Variations	ss	tt	ff	sf	fs	ss	tt	ff	sf	fs	ss	tt	ff	sf	fs
AVDD=0.54V	22.9m	5.1m	3.3m	23.1m	3.6m	25.9m	5.3m	3.0m	26.0m	3.3m	28.6m	5.9m	3.6m	28.7m	3.1m
AVDD=0.60V	4.9m	3.2m	5.1m	3.5m	3.5m	5.2m	2.8m	5.4m	3.9m	3.1m	5.8m	2.6m	6.0m	2.0m	2.9m
AVDD=0.66V	5.1m	3.5m	2.3m	5.1m	3.4m	5.4m	3.1m	2.6m	5.4m	3.1m	6.0m	2.9m	2.8m	6.0m	2.9m
Offset Voltage is 5.4mV at nominal (for AVDD=0.6V, 27º and tt-process variation)															

Table 3 Comparison with the State of Art comparator designs

Parameters	(Cohen *et al.* 2005)	(Pipino *et al.* 2016)	(Belloni *et al.* 2010)	(Lu and Holleman 2013)	***This Work***
Technology	0.35µm	28nm	0.18-0.5µm	0.5µm	0.18 µm
Supply Voltage	3.3/4.5V	0.9V	1.8/5V	5V	0.6/1.8V
DC Gain	55.7dB	106dB	168dB	118.1dB	142.8dB
GBW	-	329kHz	260kHz	-	33.3MHz
Input Referred Offset Standard Deviation	413µV	2.2µV	1.94µV	50.57µV	6.5 µV
Supply Current	40µA	60µA	14.4µA	0.93µA	10.01µA
Power	160µW	54µW	26/72µW	4.62µW	6.01/17.06 µW
Area	0.0024mm^2	0.014mm^2	1.14mm^2	0.062mm^2	0.007mm^2

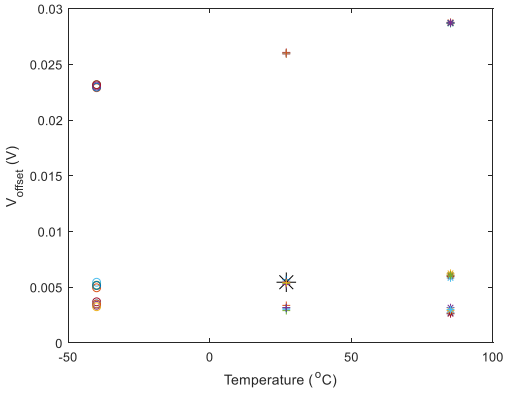

Fig. 6 Offset analysis {under the variation of process (ss, tt, ff, sf, fs), power supplies (AVDD [0.54V, 0.66V]) and temperatures (−40ºC, 85ºC)}.

Table 3 shows the comparison with state of art. The performances of designed comparator is higher than the previous works in terms of gain, GBW (gain bandwidth product) and core occupation area. GBW of the designed comparator is 33.3MHz while the core occupation area is 0.007mm^2 without Electrostatic Discharge Protection.

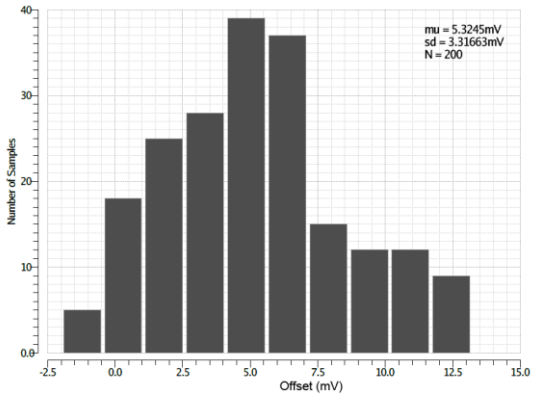

Fig. 7 Monte Carlo analysis of Offset without Offset Cancellation.

Fig. 9 shows the dynamic range of a single amplifier. The dynamic range of the comparator is increased with a new biasing technique for the positive rail. The positive rail of 0.56V approximately approaches to the positive supply voltage of 0.6V with the proposed biasing technique.

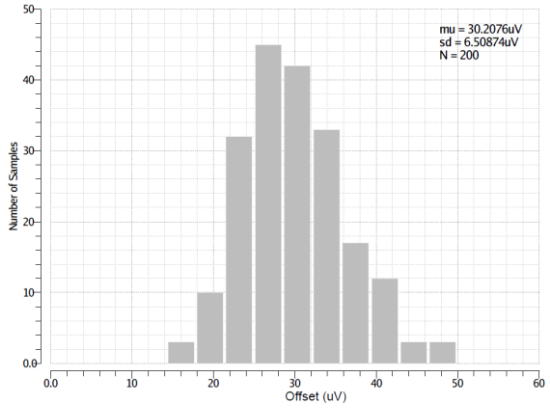

Fig. 8 Monte Carlo analysis of Offset with Offset Cancellation.

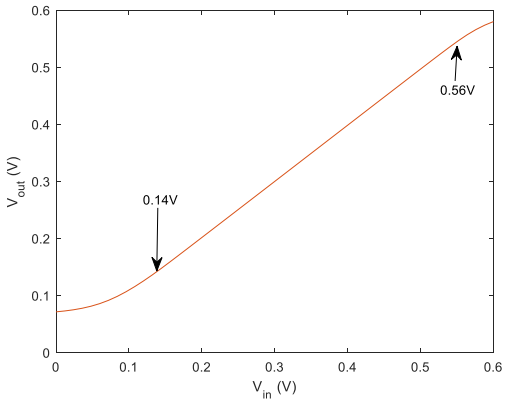

Fig. 9 Dynamic range of a single amplifier.

3. CONCLUSION

In this work, the design of a low power high precision comparator with 142.8dB gain is presented. The sub-circuits (OTA, latch) of the comparator is designed with DTMOS technique. The standard deviation of offset voltage is reduced from 3.31mV to 30.2µV. The core occupation of the designed circuit is 0.007mm^2. The comparator designed with offset cancellation can operate up to 30MHz with energy consumption per comparison of 20pJ. The designed comparator is implemented with TSMC 0.18µm process in Cadence environment.

REFERENCES

Achigui, Hervé Facpong, Christian Jésus B Fayomi, Mohamad Sawan, and PMC-Sierra. 2006. "1-V DTMOS-Based Class-AB Operational Amplifier: Implementation and Experimental Results." *IEEE Journal of Solid-State Circuits* 41(11): 2440–48.

Alaybeyoğlu, Ersin, and Hakan Kuntman. 2016. "CMOS Implementations of VDTA Based Frequency Agile Filters for Encrypted Communications." *Analog Integrated Circuits and Signal Processing* 89(3): 675–84.

Allen, P. E., and D. R. Holberg. 2012. *CMOS Analog Circuit Design*. Oxford uni.

Belloni, Massimiliano, Edoardo Bonizzoni, Andrea Fornasari, and Franco Maloberti. 2010. "A Micropower Chopper - CDS Operational Amplifier." *IEEE Journal of Solid-State Circuits* 45(12): 2521–29.

Cohen, M H *et al*. 2005. "A Floating-Gate Comparator with Automatic Offset Adaptation for 10-Bit Data Conversion A 750MHz 6b Adaptive Floating Gate Quantizer In." 52(August): 1316–26.

Ding, Ming *et al*. 2018. "A Hybrid Design Automation Tool for SAR ADCs in IoT." *IEEE Transactions on Very Large Scale Integration (VLSI) Systems* 26(12): 2853–62.

Enz, C., and Gabor Temes. 1996. "Circuit Techniques for Reducing the Effects of Op-Amp Imperfections: Autozeroing, Correlated Double Sampling, and Chopper Stabilization." *Proc. of the IEEE* 84(1): 1584–1614.

Kim, Kichan, Keun Yeong Choi, and Hojin Lee. 2015. "A-InGaZnO Thin-Film Transistor-Based Operational Amplifier for an Adaptive DC-DC Converter in Display Driving Systems." *IEEE Transactions on Electron Devices* 62(4): 1189–94.

Lin, Chin Yu, Yen Hsin Wei, and Tai Cheng Lee. 2018. "A 10-Bit 2.6-GS/s Time-Interleaved SAR ADC with a Digital-Mixing Timing-Skew Calibration Technique." *IEEE Journal of Solid-State Circuits* 53(5): 1508–17.

Lu, Junjie, and Jeremy Holleman. 2013. "A Low-Power High-Precision Comparator with Time-Domain Bulk-Tuned Offset Cancellation." *IEEE Transactions on Circuits and Systems I: Regular Papers* 60(5): 1158–67.

Maloberti, F. 2006. *Analog Design for CMOS VLSI Systems*. Springer S.

Ming-Dou Ker, and Jung-Sheng Chen. 2008. "Impact of MOSFET Gate-Oxide Reliability on CMOS Operational Amplifier in a 130-Nm Low-Voltage Process." *IEEE Transactions on Device and Materials Reliability* 8(2): 394–405.

Palmisano G., Palumbo G. and Pennisi S. 1999. *CMOS Current Amplifiers*. Boston MA: Kluwer Academic Publishers.

Pipino, A *et al*. 2016. "A Rail-to-Rail-Input Chopper Instrumentation Amplifier in 28nm CMOS." *Proceedings of the IEEE International Conference on Electronics, Circuits, and Systems* 2016-March: 73–76.

Ramírez-Angulo, J, R G Carvajal, J Tombs, and A Torralba. 2001. "Low-Voltage CMOS Op-Amp with Rail-to-Rail Input and Output Signal Swing for Continuous-Time Signal Processing Using Multiple-Input Floating-Gate Transistors." *IEEE Transactions on Circuits and Systems II: Analog and Digital Signal Processing* 48(1): 111–15.

Schinkel, Daniël *et al*. 2007. "A Double-Tail Latch-Type Voltage Sense Amplifier with 18ps Setup+hold Time." *Digest of Technical Papers - IEEE International Solid-State Circuits Conference*: 314–16.

Sepke, Todd *et al*. 2006. "Switched-Capacitor Circuits for Scaled CMOS Technologies." *ISSCC Dig. Tech. Papers* 41(12): 2658–68.

Shim, Junbo, Min Kyu Kim, Seong Kwan Hong, and Oh Kyong Kwon. 2018. "An Ultra-Low-Power 16-Bit Second-Order Incremental ADC with SAR-Based Integrator for IoT Sensor Applications." *IEEE Transactions on Circuits and Systems II: Express Briefs* 65(12): 1899–1903.

Verma, Naveen, and Anantha P. Chandrakasan. 2007. "An Ultra Low Energy 12-Bit Rate-Resolution Scalable SAR ADC for Wireless Sensor Nodes." *IEEE Journal of Solid-State Circuits* 42(6): 1196–1205.

Wicht, Bernhard, Thomas Nirschl, and Doris Schmitt-Landsiedel. 2004. "Yield and Speed Optimization of a Latch-Type Voltage Sense Amplifier." *IEEE Journal of Solid-State Circuits* 39(7): 1148–58.

Witte, Johan F., Kofi A.A. Makinwa, and Johan H. Huijsing. 2006. "A CMOS Chopper Offset-Stabilized Opamp." *ESSCIRC 2006 - Proceedings of the 32nd European Solid-State Circuits Conference* 42(7): 360–63.

Wong, K. L J, and C. K K Yang. 2004. "Offset Compensation in Comparators with Minimum Input-Referred Supply Noise." *IEEE Journal of Solid-State Circuits* 39(5): 837–40.

Wu, Rong, Kofi A. A. Makinwa, and Johan H. Huijsing. 2009. "A Chopper Current-Feedback Instrumentation Amplifier With a 1 MHz 1/f Noise Corner and an AC-Coupled Ripple Reduction Loop." *IEEE Journal of Solid-State Circuits* 44(12): 3232–43.

Yan, Na *et al*. 2018. "A 10-Bit 16-MS/s Ultra Low Power SAR ADC for IoT Applications." *2018 14th IEEE International Conference on Solid-State and Integrated Circuit Technology, ICSICT 2018 - Proceedings*: 1–3.

Zhong, Xiaopeng, Amine Bermak, and Chi Ying Tsui. 2017. "A Low-Offset Dynamic Comparator with Area-Efficient and Low-Power Offset Cancellation." *IEEE/IFIP International Conference on VLSI and System-on-Chip, VLSI-SoC.*

Turkish Journal of Engineering

Turkish Journal of Engineering (TUJE)
Vol. 4, Issue 2, pp. 92-96, April 2020
ISSN 2587-1366, Turkey
DOI: 10.31127/tuje.623785
Research Article

ANALYSIS OF THE TRACE ELEMENT CONTENT OF GRAPE MOLASSES PRODUCED BY TRADITIONAL MEANS

Hacer Sibel Karapınar *[1] and Fevzi Kılıçel [2]

[1] Scientific and Technological Research & Application Center, Karamanoğlu Mehmetbey University, Karaman, Turkey
ORCID ID 0000-0002-0123-3901
sibelkarapinar@kmu.edu.tr

[2] Karamanoğlu Mehmetbey University, Kamil Özdağ Science Faculty, Department of Chemistry, Karaman, Turkey
ORCID ID 0000-0002-5454-5597
fevzi@kmu.edu.tr

*Corresponding Author
Received: 24/09/2019 Accepted: 13/12/2019

ABSTRACT
Molasses, sugar and other food additives, such as without adding any substance, concentrated by boiling and shelf life is a long concentrated product. Molasses is an important food for humans in terms of mineral content and high energy content. Grape fruit is considered as a rich food source with strong health effects. Grape fruit generally contains 70-80% water, 15-25% carbohydrate and small amount of minerals, amino acids, phenolic compounds. Heavy metals are highly toxic elements, which can severely influence plants and animals and have been involved in causing a large number of afflictions. Heavy metals in the environment are non-biodegradable and ubiquitous, it can cause serious human health hazards and momentous ecological effects through food chain's bioaccumulation. Inorganic micro-pollutants are of important concern because they are non-biodegradable, highly toxic and have a probable carcinogenic influence. In this study, it was aimed to determine the heavy metal levels in grape molasses collected from the villages of Karaman and to emphasize the importance of nutrition in carob molasses. The samples were prepared to be 2 parallel for each sample and were solutioned by wet burning method. The concentrations of the determined elements were determined by Flame Atomic Absorption Spectrometry (FAAS). Traditional produced grape molasses are determined by comparing metal contents with each other and with standard values.

Keywords: *Molasses, Grape, Trace element, FAAS*

1. INTRODUCTION

Molasses is a traditional sweets prepared in many Mediterranean countries commonly known as 'pekmez' in Turkey. Molasses can be produced from various fruits such as grape, mulberry, apple and carob (Petkova *et al*., 2017). Since molasses contain carbohydrates in the form of monosaccharides such as glucose and fructose, they can easily pass into the blood without being digested. This is especially important for infants, children, athletes and those who need urgent energy (Tosun & Ustun, 2003). It is also a dark viscous liquid containing sugar, amino acids, vitamins and a group of minerals (Zhang *et al*., 2015, Xia *et al*., 2016). Grape has an important place in molasses production. Grape is grown in our country, especially in rural areas and is consumed as molasses after being concentrated and kept in the sun and brought to consistency due to its limited consumption as fresh (Viran *et al*., 2003). There are micro and macro elements in the grape (K, Ca, Mg, Na, Zn, Mn, Fe and Cu). The presence of elements such as As, Cr, Pb and Cd which show toxic properties are caused by anthropogenic activities such as industrial processes, agricultural applications, use of minerals discharge of toxic residues or soil composition (Segura-Muñoz, 2006). Chromium can be considered essential or toxic to living organisms depending on the oxidation state (Quináia & Nóbrega, 1999). The elements Pb and Cd do not have a biological function and are extremely toxic to living organisms. These elements cause various damages to the body (kidney, neurological, hepatic, inter alia cardiovascular) and can also cause various types of cancer such as lung, prostate, and testis. Recently developed analytical methods for the determination of minerals in foodstuffs have features such as high precision, easy to apply, low cost, robustness, selectivity, speed, and environmental friendliness. Analytical techniques that can be used for this purpose are inductively coupled plasma atomic emission spectroscopy (ICP-OES and ICP-MS) (Ohki *et al*., 2016), flame atomic absorption spectrometry (FAAS) (Yıldız *et al*., 2016). In this work, trace element levels of Zn, Pb, Ni, Cu, Cr, Mg, Mn, Ca and Fe in grape molasses produced in 12 different villages of Karaman province were investigated. Samples were prepared according to wet burning method and mineral analysis were performed with FAAS method.

2. MATERIALS AND METHODS

2.1. Study Area

Grape molasses were collected from 12 different places which were produced by traditional. Samples were gathered from Manyan, Burhan, Pınarbaşı, Başkışla, Morcalı, Bozkandak, Aygan, Bostanözü, Bucakışla, Kızılyaka, villages, Ermenek and Karaman center. Fig. 1 shows the sampling locations on the map. In this study, samples of molasses prepared by using freshly harvested grape fruits from 12 different producers without waiting were taken and analyzes were carried out on these samples.

Fig. 1. Map of sampling locations

2.2. Methods

Molasses were produced on the same day without waiting from the harvested grape fruits. In the molasses made by traditional methods, grape molasses are first squeezed in various ways and juice is obtained. The grape juice collected is boiled at 50-60 ° C for 10-15 minutes and molasses soil is added. After resting for 4-5 hours, the substance formed is molasses by removing the sediment from the bottom of the container and boiling again. The samples were brought to the laboratory by placing them in 200 ml bottles of molasses made from newly harvested grapes in 2017. Weighed 2 g each of the samples which were made ready for weighing with precision scales and placed them in 100 ml beakers. 16 ml of HNO_3 (65%, w/w, Merck) was added and allowed to stand for 8-10 hours. Then, 4 ml of $HClO_4$ (70-72%, w/w, Merck) were added and the solutions were heated slowly in the fume hood for 5-6 hours. Heating was stopped near the end of the acids, and after cooling the solutions, 5 ml of H_2O_2 (30%, w/w, Merck) were added. Heating was carried out until clear liquid was obtained. The cooled samples were filtered through blue band filter paper and filled to 20 ml with distilled water and stored in a refrigerator at 4 °C until analysis. Flame atomic absorption spectrometry (FAAS) (Perkin Elmer 900T) was used for elemental analysis of the samples.

2.3. Evaluation of Instrumental and Method Performance

The method and instrumental performance were evaluated by determining the detection limit (LOD) and the quantification limit (LOQ). LOD and LOQ were calculated as 3xSD/b and 10xSD/b, respectively, where SD is the standard deviation of 10 consecutive measures of the analytical blank and b is the slope of the analytical curve (ICH, 1996). Table 1 presents the linear ranges used for calibration and the coefficients of determination (R^2) used to assess the linearity (R^2>0.99). LOD, LOQ and precision are given in Table 2.

3. Results and Discussion

Each molasses sample was prepared for analysis in 2 parallel and 3 replicate measurements were taken from each sample. The concentrations of trace elements in molasses samples are given in Table 3, 4. Pb, Mn, Cr element concentrations of molasses samples taken from 12 different places are shown in Fig. 2, 3, 4. Perkin Elmer 900T series FAAS was used for this work. Instrument operating conditions were given Table 5.

Table 1. Linear range ($mgkg^{-1}$), regression, correlation coefficient (R^2), for the elements analyzed

Element	Linear Range	Regression	R^2
Cu	0.5 - 5	y=0.020x + 0.002	0.992
Cr	0.5 - 5	y=0.014x - 0.003	0.995
Fe	1 - 10	y=0.042x - 0.023	0.997
Ca	0.1- 10	y=15.20x - 0.111	0.998
Ni	0.1 - 5	y=0.034x - 0.019	0.999
Mg	0.1 - 5	y=2.124x - 0.123	0.999
Mn	0.1 - 5	y=0.054x + 0.005	0.998
Zn	0.1 - 5	y=0.156x + 0.003	0.994
Pb	0.5 - 5	y=0.121x - 0.045	0.998

Table 2. LOD, LOQ and precision (RSD%) for the elemental analyzed

Element	LOD ($mgkg^{-1}$)	LOQ ($mgkg^{-1}$)	Precision (RSD%)
Cu	1.543	5.138	0.565
Cr	2.457	8.181	0.721
Fe	1.451	4.831	0.733
Ca	0.049	0.163	0.119
Ni	2.232	7.432	0.223
Mg	0.124	0.413	0.721
Mn	1.192	3.969	0.869
Zn	0.765	2.547	0.348
Pb	1.487	4.952	0.712

Table 3. Trace element concentrations in molasses samples ($mgkg^{-1}$)

	Average±SD				
	Zn	**Pb**	**Ni**	**Cu**	**Cr**
1	2.887 ±0.028	1.516 ±0.042	1.576 ±0.066	9.985 ±0.167	0.130 ±0.038
2	1.466 ±0.073	1.397 ±0.167	0.399 ±0.099	2.102 ±0.080	0.069 ±0.047
3	1.417 ±0.349	5.993 ±0.131	0.274 ±0.091	1.580 ±0.155	0.002
4	1.407 ±0.021	2.151 ±0.188	0.226 ±0.032	2.063 ±0.172	0.009
5	1.319 ±0.101	2.349 ±0.764	0.050 ±0.034	1.122 ±0.094	0.050 ±0.008
6	1.521 ±0.058	1.150 ±0.140	0.112 ±0.090	4.607 ±0.224	0.019 ±0.005
7	1.518 ±0.057	1.203 ±0.202	0.145 ±0.064	1.397 ±0.053	0.102
8	3.390 ±0.289	0.745 ±0.184	0.052 ±0.029	0.769 ±0.107	0.018
9	1.158 ±0.060	1.072 ±0.188	0.187 ±0.053	2.300 ±0.111	0.067 ±0.005
10	1.053 ±0.074	1.120 ±0.117	0.341 ±0.014	1.422 ±0.084	0.093 ±0.003
11	1.029 ±0.021	1.274 ±0.145	0.396 ±0.022	1.378 ±0.049	0.014
12	11.13 ±0.193	1.971 ±0.181	0.274 ±0.055	1.226 ±0.061	0.092 ±0.025

SD: Standard Deviation

Table 4. Trace concentrations in molasses samples ($mgkg^{-1}$)

	Average±SD			
	Mg	**Mn**	**Ca**	**Fe**
1	203.1 ±2.447	10.52 ±0.149	231.6 ±3.535	20.72 ±2.581
2	203.4 ±2.688	1.547 ±0.027	163.3 ±6.793	11.62 ±1.540
3	218.0 ±3.102	0.508 ±0.020	190.9 ±2.486	12.27 ±0.383
4	201.2 ±2.413	1.241 ±0.015	232.7 ±1.484	11.58 ±0.756
5	139.3 ±1.532	0.528 ±0.014	214.6 ±2.547	10.21 ±0.560
6	186.5 ±3.758	0.752 ±0.011	221.9 ±4.768	21.73 ±0.627
7	215.5 ±2.819	6.341 ±0.152	152.7 ±1.290	33.89 ±0.442
8	184.7 ±3.366	5.303 ±0.100	233.6 ±1.092	21.68 ±0.460
9	179.8 ±2.375	2.057 ±0.031	214.8 ±3.282	17.78 ±0.417
10	211.8 ±2.972	4.829 ±0.070	228.1 ±1.301	20.83 ±0.203
11	202.4 ±2.598	4.552 ±0.078	229.6 ±1.380	20.90 ±0.706
12	183.3 ±2.709	4.336 ±0.081	197.7 ±1.186	29.59 ±1.126

Table 5. Instrument Operating Conditions

Element	Wavelength (nm)	Current intensity (mA)	Slit width (nm)
Cu	324.8	15	0.7
Cr	357.9	25	0.7
Fe	248.0	30	0.2
Ca	422.7	20	0.7
Ni	232.0	25	0.2
Mg	285.2	20	0.7
Mn	279.5	20	0.2
Zn	213.9	15	0.7
Pb	283.31	440	0.7

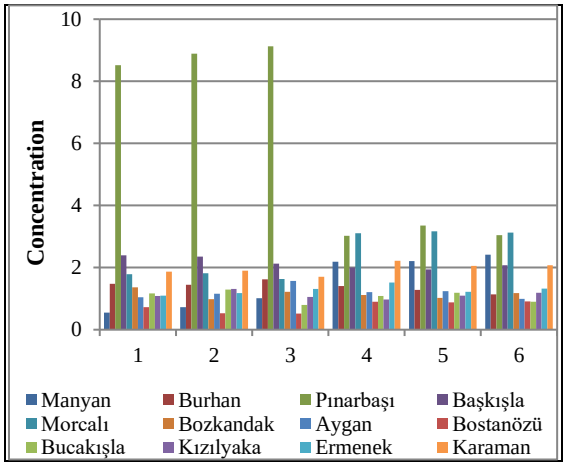

Fig. 2. Pb element concentrations of molasses samples taken from 12 different places ($mgkg^{-1}$)

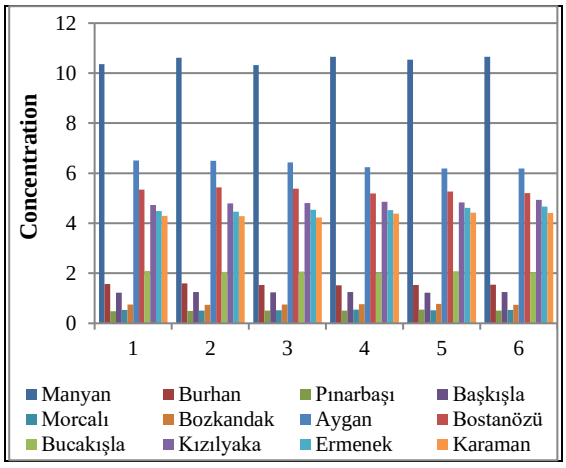

Fig. 3. Mn element concentrations of molasses samples taken from 12 different places (mgkg^{-1})

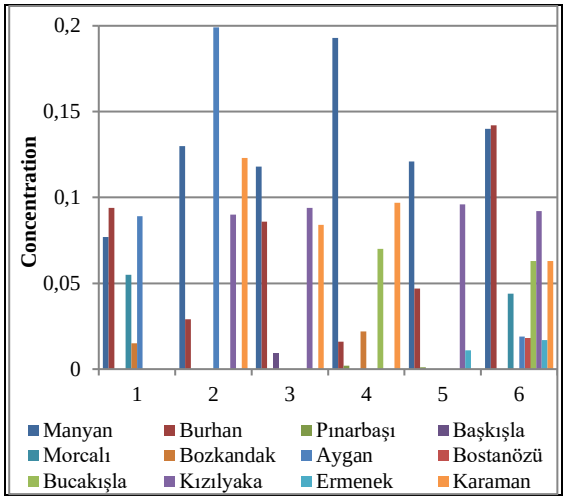

Fig. 4. Cr element concentrations of molasses samples taken from 12 different places (mgkg^{-1})

Food products contaminated with various types of heavy metals threaten human health. Cr and Pb heavy metals are toxic and carcinogenic, especially Pb causes stomach cancers (Zahao *et al*., 2014). Chatterjee (2000), found that Cu is toxic in terms of its negative effects on physiological activities. The concentration of heavy metals and evaluation are given Table 6. In this study, according to the literature values given in Table 6, Ni (0.050-1.576 mgkg^{-1}), Fe (17.78-33.89 mgkg^{-1}), Cu (0.769-9.985 mgkg^{-1}), Mn (0.508-10.52 mgkg^{-1}), Pb (0.745-5.993 mgkg^{-1}), Ca (152.7-231.6 mgkg^{-1}) high amounts; Mg (139.3-218 mgkg^{-1}) at low levels; Cr (0.002-0.130 mgkg^{-1}) and Zn (1.029-3.390 mgkg^{-1}) elements were determined at normal concentrations in molasses samples.

Tosun and Ustun, (2003) found iron content ranging from 26.2 to 163.0 mgkg^{-1} in molasses samples. Artık and Velioğlu, (1993) in their study stated that the iron content in molasses is 100 mgkg^{-1}. According to these studies, iron content remained low in our study. However, it was found to be higher than Table 6. Demirci, (2006) determined that ingredient of calcium in traditional method was 1051.6 mgkg^{-1} in grape molasses. In this study, Ca content was found to be low levels according to the literature. Copper is found in the structure of some polyphenolase enzymes. Excess copper has a toxic effect on the body. Tosun and Ustun, (2003) studied 11 molasses samples and found that the copper level ranged from 2.9 to 9.4 mgkg^{-1}. Our values are consistent with these values. However, it was observed that it was higher than the literature values given in Table 6. Zinc is found in the composition of certain enzymes and hormones and influence their work. It is also involved in the regeneration of cells and tissues by taking part in DNA and RNA synthesis, but high amounts of zinc have toxic effects on the body (Tarakçı & Küçüköner, 2003). Pb is an element with multiple effects. The absorbed lead passes into the blood and reaches equilibrium in a short time and is distributed to various organs through blood circulation (Assis *et al*., 2008). Zinc values found in our study were consistent with the literature, but lead levels were found to be high.

Table 6. The concentration of heavy metals and evaluation (Demiröz*ü et al*., 2002; Karababa & Develi, 2005; Akbulut & Özcan, 2008; TFC, 2017)

Element	Founded value (mgkg^{-1})	Accepted value	Evaluation
Cr	0.002-0.130	0.20-45 (µgg^{-1})	Normal
Zn	1.029-3.390	< 5 (µgg^{-1})	Normal
Mn	0.508-10.52	6.2 (µgg^{-1})	High
Mg	139.3-218	730 (µgg^{-1})	Low
Ni	0.050-1.576	0.5 (mgkg^{-1})	High
Fe	17.78-33.89	< 25 (mgkg^{-1})	High
Cu	0.769-9.985	< 5 (mgkg^{-1})	High
Pb	0.745-5.993	< 0.30 (mgkg^{-1})	High
Ca	152.7-231.6	130-144 (mgkg^{-1})	High

4. CONCLUSIONS

Environmental pollutants, food safety and human health are inextricably linked. Sources of heavy metals in food products are changing in developing countries. Heavy metals can be managed by reducing the use of treated waste material or by properly treating sewage before it can be used for irrigation (Cherfi *et al*.. 2015). Optimization of land use improves food safety. Roadside food products tend to accumulate metal on plant leaves and fruit (Nabulo *et al*.. 2006). There may be heavy metal pollution from soil where grapes are grown. In the molasses produced in the traditional way soil is used in the production stage and metal pollution from this can occur in molasses. In addition, Pb, Cd, Cr, Zn and Mn pollution can come from fertilizers used for fruit production (Fan *et al*.. 2017). In order to avoid health risks the available remediation options should focus on reducing the concentration of heavy metals in the soil and food chain. It is necessary to prevent the transfer of metal pollutants to the food chain and formulate appropriate healing strategies.

REFERENCES

Akbulut. M.. & Özcan. M. M. (2008). "Some physical. chemical. and rheological properties of sweet sorghum (Sorghum Bicolor (L) Moench) Pekmez (Molasses)." *International Journal of Food Properties*. *11*(1). 79-91.

Artık, N., & Velioğlu, S. (1993). Research on Determining the Compliance of Some Molasses Samples to the Standard.. *Standard*, *32*, 51-54.

Assis, R.A.D., Küchler, I.L., Miekeley, N., & Silveira, C.L.P.D. (2008). Trace elements and sodium in grape juice: nutritional and toxicological aspects. *Quimica Nova*, *31*(8), 1948-1952.

Chatterjee. J.. & Chatterjee. C. (2000). "Phytotoxicity of cobalt. chromium and copper in cauliflower." *Environmental pollution*. *109*(1). 69-74.

Cherfi. A.. Achour. M.. Cherfi. M.. Otmani. S.. & Morsli. A. (2015). "Health risk assessment of heavy metals through consumption of vegetables irrigated with reclaimed urban wastewater in Algeria." *Process safety and environmental protection*. *98*. 245-252.

Demirci, S.K.M. (2006). Effects of storage time and condition on mineral contents of grape pekmez produced by vacuum and classical methods. *Tekirdağ Ziraat Fakültesi Dergisi*, *3*(1), 1-7.

Demirözü. B.. Sökmen. M.. Uçak. A.. Yilmaz. H.. & Gülderen. Ş. (2002). "Variation of copper. iron. and zinc levels in pekmez products." *Bulletin of environmental contamination and toxicology*. *69*(3). 330-334.

Fan. Y.. Li. H.. Xue. Z.. Zhang. Q.. & Cheng. F. (2017). "Accumulation characteristics and potential risk of heavy metals in soil-vegetable system under greenhouse cultivation condition in Northern China." *Ecological engineering*. *102*. 367-373.

ICH. (1996). Guidance for Industry: Validation of Analytical Procedures: Definitions and Terminology. Q2A. Geneva Switzerland.

Karababa. E.. & Develi Isikli. N. (2005). "Pekmez: A traditional concentrated fruit product." *Food reviews international*. *21*(4). 357-366.

Nabulo. G.. Oryem-Origa. H.. & Diamond. M. (2006). "Assessment of lead. cadmium. and zinc contamination of roadside soils. surface films. and vegetables in Kampala City. Uganda." *Environmental Research*. *101*(1). 42-52.

Ohki. A.. Nakajima. T.. Hirakawa. S.. Hayashi. K.. & Takanashi. H. (2016). "A simple method of the recovery of selenium from food samples for the determination by ICP-MS." *Microchemical Journal*. *124*. 693-698.

Petkova. N.. Petrova. I.. Ivanov. I.. Mihov. R.. Hadjikinova. R.. Ognyanov. M.. & Nikolova. V. (2017). "Nutritional and antioxidant potential of carob (Ceratonia siliqua) flour and evaluation of functional properties of its polysaccharide fraction." *Journal of Pharmaceutical Sciences and Research*. *9*(11). 2189-2195.

Quinaia. S.P.. & Nobrega. J.A. (1999). "Direct determination of chromium in gelatine by graphite furnace atomic absorption spectrophotometry." *Food chemistry*. *64*(3). 429-433.

Segura-Muñoz. S.I.. da Silva Oliveira. A.. Nikaido. M.. Trevilato. T.M.B.. Bocio. A.. Takayanagui. A.M.M.. & Domingo. J.L. (2006). "Metal levels in sugar cane (Saccharum spp.) samples from an area under the influence of a municipal landfill and a medical waste treatment system in Brazil." *Environment International*. *32*(1). 52-57.

Tarakçı, Z., & Küçüköner, E. (2003). Investigation of Some Mineral and Heavy Metal Content of Various Herbal Additive Dairy Products. *III. Food Engineering Congress*, (2-3 October), Ankara, 448-449.

Tosun. I.. & Ustun. N.S. (2003). "Nonenzymic browning during storage of white hard grape pekmez (Zile pekmezi)." *Food Chemistry*. *80*(4). 441-443.

TFC. (2017). Turkish Food Codex Communiqué on Grape Molasses (Communiqué No: 2017/8).

Viran. R.. Erkoç. F.Ü.. Polat. H.. & Koçak. O. (2003). "Investigation of acute toxicity of deltamethrin on guppies (Poecilia reticulata)." *Ecotoxicology and environmental safety*. *55*(1). 82-85.

Xia. J.. Xu. J.. Hu. L.. & Liu. X. (2016). "Enhanced poly (L-malic acid) production from pretreated cane molasses by Aureobasidium pullulans in fed-batch fermentation." *Preparative Biochemistry and Biotechnology*. *46*(8). 798-802.

Yıldız. E.. Saçmacı. Ş.. Kartal. Ş.. & Saçmacı. M. (2016). "A new chelating reagent and application for coprecipitation of some metals in food samples by FAAS." *Food chemistry*. *194*. 143-148.

Zhao. Q.. Wang. Y.. Cao. Y.. Chen. A.. Ren. M.. Ge. Y.. ... & Ruan. L. (2014). "Potential health risks of heavy metals in cultivated topsoil and grain. including correlations with human primary liver. lung and gastric cancer. in Anhui province. Eastern China." *Science of the Total Environment*. *470*. 340-347.

Zhang. Y.Y.. Bu. Y.F.. & Liu. J.Z. (2015). "Production of L-ornithine from sucrose and molasses by recombinant Corynebacterium glutamicum." *Folia microbiologica*. *60*(5). 393-398.

Zhang. Y.. Ji. X.. Ku. T.. Li. G.. & Sang. N. (2016). "Heavy metals bound to fine particulate matter from northern China induce season-dependent health risks: a study based on myocardial toxicity." *Environmental pollution*. *216*. 380-390.

Turkish Journal of Engineering

Turkish Journal of Engineering (TUJE)
Vol. 4, Issue 2, pp. 97-103, April 2020
ISSN 2587-1366, Turkey
DOI: 10.31127/tuje.636350
Research Article

A NEW METHOD FOR THE MEASUREMENT OF SOFT MATERIAL THICKNESS

Mustafa Tahsin Guler *[1] and İsmail Bilican [2]

[1] Kirikkale University, Art and Sciences Faculty, Physics Department, Kirikkale, Turkey
ORCID ID 0000-0002-0478-3183
gulermt@gmail.com

[2] Aksaray University, Science and Technology Application and Research Center, Aksaray, Turkey
ORCID ID 0000-0002-4415-6803
ismailbilican@aksaray.edu.tr

* Corresponding Author
Received: 22/10/2019 Accepted: 13/12/2019

ABSTRACT
Thickness measurement is very critical especially in fabrication of micro and nano devices to determine the thickness of the layers. Stylus measurement is the easiest and most common technique that is being employed among the other thickness measurement methods. Micro-nano fabrication processes requires the usage of both rigid and soft materials. While thickness of a rigid material can be easily detected, thickness measurement of the soft materials presents some difficulties for standard stylus thickness measurement devices. Since the soft materials are deformed by the stylus due to the applied pressure, correct thickness measurement cannot be realized. Here, PDMS (Polydimethylsiloxane) is used as soft material for thickness measurement. By taking the replica of the soft material with liquid plastic which becomes rigid after curing, the depth can be measured easily via conventional stylus thickness measurement devices.

Keywords: *Casting, PDMS, Thickness Measurement, Soft Materials, Stylus Thickness Measurement.*

1. INTRODUCTION

Soft materials are widely used in research and manufacturing (Marcali *et al.* 2016; Guner *et al.* 2017; Tavakoli *et al.* 2017; Bakan *et al.* 2018). Microfluidics community is one of the biggest users of the soft materials since PDMS has been the primary supply in fabrication of the microchannels after the invention of the soft lithography (Duffy *et al.* 1998) which changed the microfluidics research dramatically. Soft lithography introduced a very useful fabrication way for microchannels. In soft lithography, following the fabrication of the molds from SU8, PDMS is poured on the mold and cured. This process enables the replication of the mold with PDMS and saves the mold providing multiple replications. It removes the requirement of cleanroom fabrication every time for the acquisition of the microchannel.

There are also other fabrication methods for the microchannels which decrease the fabrication cost and complexity providing more access to microfluidics for the research community. These methods include xurography (Bartholomeusz *et al.* 2005; de Santana *et al.* 2013), micromilling (Lopes *et al.* 2015; Singhal *et al.* 2015) and laser machining (Romoli *et al.* 2011; Mohammed *et al.* 2016; Prakash *et al.* 2018; Benton *et al.* 2019). These methods proved themselves in several lab-on-a-chip applications. For example, a micro milled chip is employed in ESR (erythrocyte sedimentation rate) measurement (Isiksacan *et al.* 2017; Isiksacan *et al.* 2018) and laser machined PMMA chip is employed in PT (prothrombin time) measurement (Guler *et al.* 2018). Some of these methods realize microchannel fabrication by machining a bulk PMMA material while some of the fabrication methods require machining of PDMS after the spin coating (Isiksacan *et al.* 2016). Machining of spin coated PDMS endows controlling the channel thickness through the speed of spin coating process.

Soft materials like PDMS is also used for other applications like flexible devices (Kudo *et al.* 2006; Lei *et al.* 2012) and wearable devices (Moon *et al.* 2010; Gao *et al.* 2017). PDMS is also used for coating the surface of other materials for changing the specific properties such as turning a conductive metallic surface into an insulator (Isgor *et al.* 2015). Coating the electrode surface with PDMS to eliminate the conductivity in order to make a total capacitive sensor is a very precise process. Because a thick PDMS may kill the sensor totally or a thin PDMS may not be enough to disable resistive effects, measurement of PDMS thickness is very critical.

Another advantage of the PDMS is that it can be plasma bonded to the glass. Since many kind of clean room fabrication methods can be realized on glass, like the fabrication of microelectrodes (Bilican *et al.* 2016; Guler *et al.* 2018), PDMS becomes more crucial for lab-on-chip (LOC) community. In addition, it is also easy to cut and punch the PDMS that enables easy integration of LOC environmental elements like valves (Guler *et al.* 2017).

Thickness is also important for machining of the PDMS layer aiming channel production (Gitlin *et al.* 2009; Li *et al.* 2012; Isiksacan, Guler, Aydogdu, Bilican and Elbuken 2016) as mentioned before. This method depends on to cut out a thin line from the PDMS layer which is followed by sealing of the layer from both sides. Thus, the layer thickness becomes equivalent to the channel height and the width of the line becomes equivalent to channel width. Examples can be verified addressing the significance of the thickness measurement of soft materials like PDMS.

We mention PDMS so much due to our microfluidics background where we encountered the problem of measuring the thickness of spin coated PDMS. Therefore, in this study, PDMS thickness is measured as an example of soft material which is one of the most basic material of the research in several fields thanks to its transparency (Isgor, Marcali, Keser and Elbuken 2015; Marcali and Elbuken 2016; Serhatlioglu *et al.* 2019) and biocompatibility (Sun *et al.* 2019). However, PDMS deforms under the pressure of the stylus which make it impossible to realize a correct measurement with devices employing the stylus method. While its flexibility has some benefits in fabrication (Guler *et al.* 2015) and in application (Kudo, Sawada, Kazawa, Yoshida, Iwasaki and Mitsubayashi 2006; Moon, Baek, Choi, Lee, Kim and Lee 2010; Lei, Lee and Lee 2012; Zhu *et al.* 2014; Gao, Ota, Schaler, Chen, Zhao, Gao, Fahad, Leng, Zheng and Xiong 2017), it also puts a challenge in measuring the thickness.

There are other methods for thickness measurement such as optical profilometer and SEM but they are very expensive devices limiting the accessibility for numerous researchers. There are also some other and less known alternatives to SEM and optical profilometer for measuring the thickness of soft tissues which are laser displacement sensors (Lee *et al.* 1988) and Vernier capillaries (Delgadillo *et al.* 2010). Unfortunately, these measurement setups are complex and expensive limiting their accessibility for standard labs.

In this study, a new methodology is developed for the thickness measurement of the soft materials. Here the method is tested on PDMS yet it is also applicable for other materials. For measurement of the thickness, first, a little part of the spin coated PDMS is cut with a razor blade. This part might be in shape of a line, a square or anything else. Afterward, liquid plastic is poured on the PDMS following the removal of the cut piece. After the hardening of the liquid plastic, it becomes a rigid material. The hard plastic enables the measurement of the thickness as it is a non-deformable material to stylus pressure. Since it is the negative replica of the PDMS, the difference of the two points, where one point is taken from the removed part and the other point is taken from the anywhere else on the surface, gives the thickness of the PDMS. A representative drawing for soft and hard material thickness measurement with stylus is shown in Fig. 1.

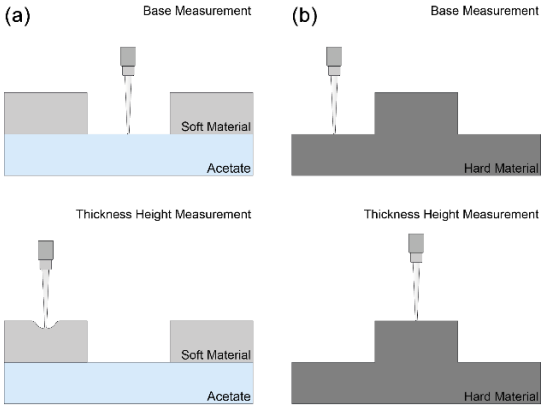

Fig. 1. Measurement of the thickness with stylus from a) soft and b) hard material

2. MATERIALS AND METHODS

PDMS is prepared by mixing 1/10 w/w ratio with its curing agents. For providing better mixing, the two additives are harshly mixed. The mixture quality can be evaluated by the naked eye. When the bubbles are all over the mixture, it means a good mixing quality. Hence the two additives are mixed until the bubbles cover all over the mixture. Then the mixture is put under the vacuum for degassing which removes the air bubbles. This process takes nearly 45 minutes to make the mixture totally bubble free. Hence the PDMS becomes ready for spin coating. Since the PDMS by itself is very viscous, it is not possible to have a thickness less than 10 µm by spin coating. Yet there is a little trick to thin the PDMS adding some toluene into the PDMS which reduce the viscosity and enables thickness down to 1 µm by spin coating. However, this is out of scope of this study.

Glass slides used in spin coating are first covered with an acetate sheath via a double sided tape. After putting the glass slide in the spin coating chamber, the PDMS is poured over it from a cup directly and the spinning process is started. The spinning is done at different rates from 1000 rpm to 5000 rpm for 2 minutes. The spin coated slides are left on a hot plate at 100 °C for 2 hours long. The heath treatment provides curing of the PDMS. Then a rectangular piece is cut with a razor blade from the PDMS layer. Plasma treatment is applied to a previously produced PDMS slab and the PDMS layer. The plasma enables the chemical bonding of PDMS. Thus, spin coated PDMS layer is bond to PDMS slab and it is easily peeled off from the acetate when the slab is removed.

Liquid plastic (Smooth-On, Smooth-Cast), which consists of two parts, is prepared at the same volume ratios. Both the PDMS slab and the liquid plastic solutions are put in the vacuum chamber for 15 minutes long. Due to its porous structure (Zhou *et al.* 2007), cured PDMS has gas molecules trapped inside. During the casting process, some of the trapped gas molecules escape which causes bubble formation on the interface between the liquid plastic and PDMS. Hence, it is a must to degas PDMS before the casting. After taking the PDMS and the liquid plastic from the vacuum chamber, the two parts of smooth on are mixed. It is very critical to pour the two parts into the same cup simultaneously. Afterward, the solution is mixed slowly. It needs to be done very gently avoiding bubble formation in the Smooth-On mixture.

PDMS is put in a container and the liquid plastic is poured over slowly. Pouring needs to be very gentle and slow to prevent bubble formation on the PDMS-liquid plastic interface. Waiting overnight ensures the hardening of the plastic however a few hours like 2-3 h is also enough. Hence PDMS can be separated from the hard plastic. Thickness measurements can be done on the hard plastic. As it is a negative replica of the PDMS, it would give the correct thickness for the mother mold. A representation of our method is shown in Fig. 2.

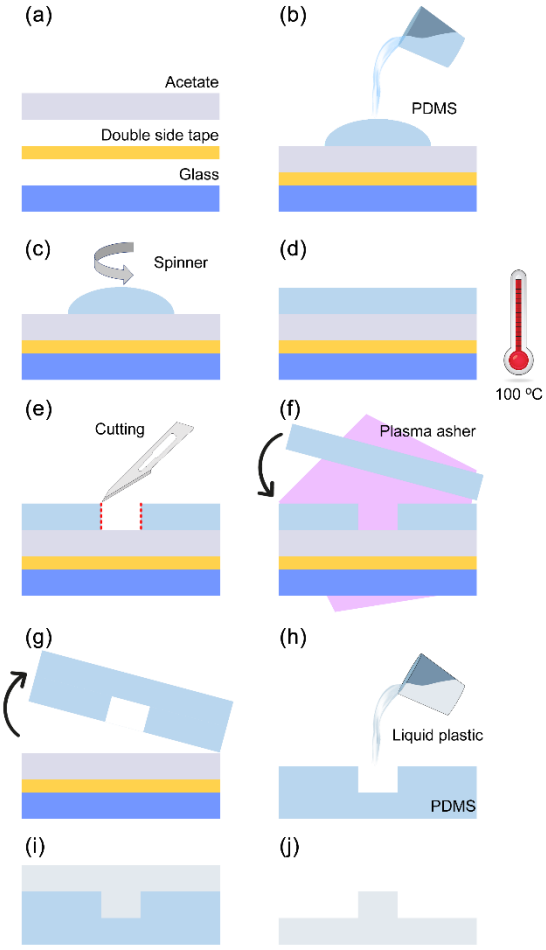

Fig. 2. Liquid plastic casting. a) An acetate sheet is stuck to glass slide with double sided tape b) PDMS is poured c) PDMS is spin coated d) It is put in hot plate at 100oC e) a little piece is cut out with a razor blade f) Plasma treatment is applied to PDMS slab and spin coated PDMS. g) PDMS slab and spin coated PDMS is peeled off from the surface following the plasma bonding h) liquid plastic is cast-over the PDMS i) after 3 hours of waiting hardened plastic is taken from the PDMS.

Thickness measurements are done with a precision stylus digital micrometer (Mitutoyo). The device realizes the measurement by pushing down on the substrate with the stylus. Displacement of the stylus is detected giving the thickness result. The measurement is done as follows: First, the stylus is put on the base area and the number on the screen is set to zero by pushing the yellow button shown in Fig. 3. And then the stylus is moved upward by pushing the metal arm over the digital head placed at the

right side of the head. The substrate is moved and the stylus is put on the protrusion or the intrusion on the sample. The thickness corresponds to the number that is shown on the screen of the device.

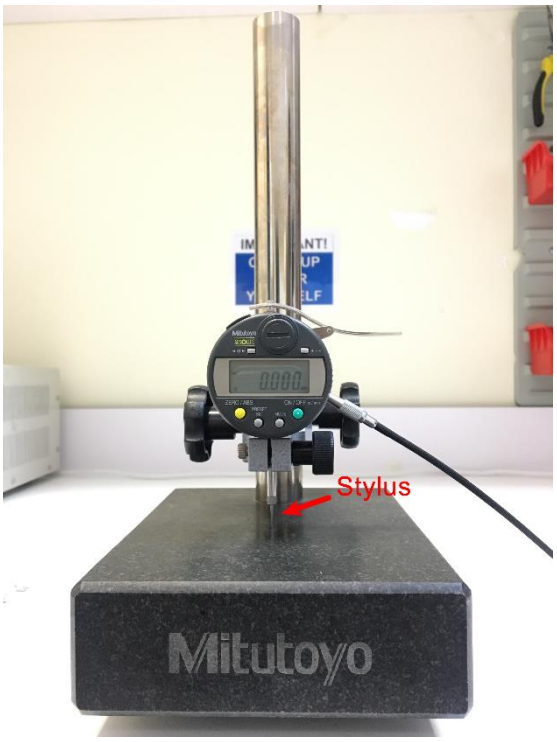

Fig. 3. Picture of thickness measurement device.

Smooth-On consists of two parts which are written on the yellow and blue bottle as part A and part B. These are yellowish and whitish liquids and they can be kept in their own air proof bottles for years without any decay according to our experience. Before dispensing the liquids, the two bottles should be mixed harshly. Then, two parts are put into different cups at the same volume. The precision of the naked eye is sufficient in preparation of liquids at the same volume. Two cups need to be degassed at the vacuum chamber at least for 15 mins. Degassing remove all the bubbles inside the liquids. Then, the two parts are poured in another cup simultaneously and gently. Afterwards, the mixture is stirred slowly and gently to make sure that the two parts are mixed well. Here, the last two steps are critical in terms of avoiding bubble formation, if bubbles form at these steps, it is not possible to get rid of them and the bubble shapes remain in the mold after the hardening of the plastic as well. Degassing the liquids after mixing is not possible since a chemical reaction between each part towards hardening is already started off after the first contact of each liquid. After hardening, the plastic takes the shape of the material to which it is in contact when it was in liquid form. For better seeing, a demonstration example is done in a plastic cup as shown in Fig. 4.

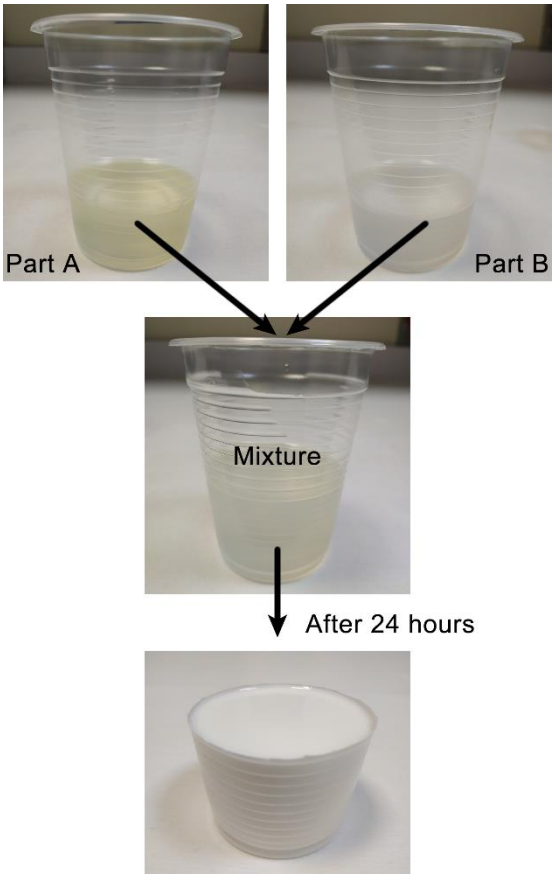

Fig. 4. Preparation of Smooth-On: first Part A and Part B is taken to different cups, after degassing, the two parts are mixed gently in the same cup at the same time. After waiting a few hours, the liquid plastic hardens taking the shape of whatever it is in.

3. RESULTS AND DISCUSSION

Measurements are carried out with three different tips of the thickness measurement device. Pink points in Fig. 5 shows the results of those tips for spin coated PDMS layers. According to the results, tip 3 gives the least while tip 2 and tip 3 nearly give the same height for PDMS in soft material measurement experiments.

After casting with smooth on from the PDMS slab, the same measurement is realized for the hard plastic. The thickness measurement results are shown in Fig. 5 with the blue points for the hard plastic. The tip type does not make any difference for the measurements which are done from the hard plastic.

Here, the same thicknesses are measured from the soft PDMS and the hard smooth on which gives totally different results. When the tip pushes to the PDMS, deformation takes place at the material and it gives less height then normally the PDMS layer has. However, the same fact does not arise for the hard material since the tip cannot cause deformation at the hard material. It proves that the soft materials are not suitable for stylus type thickness measurements due to deformation.

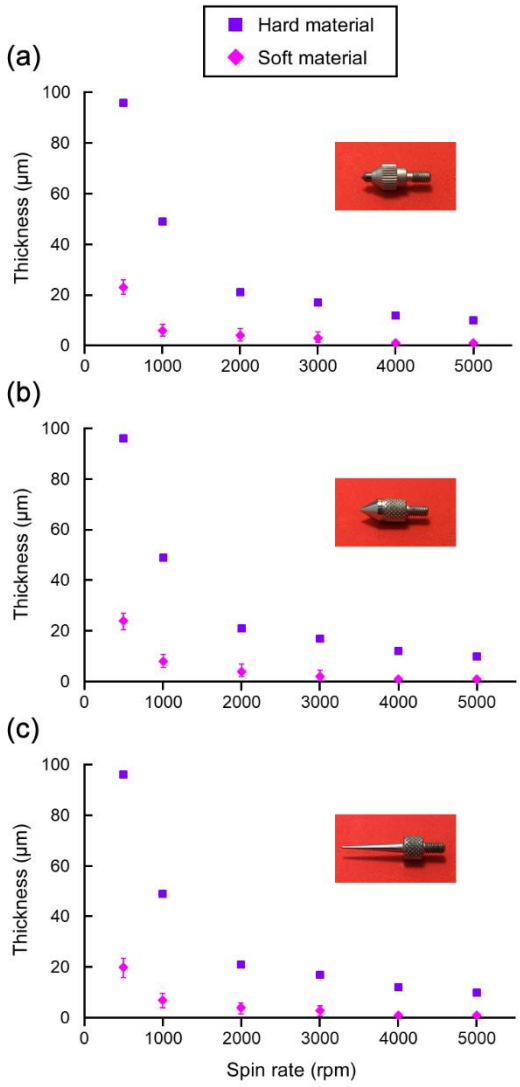

Fig. 5. Result of thickness measurement from PDMS and cast hard plastic for 3 different stylus types. Measurements are done directly from the spin coated PDMS layer at several rpm's and the hard plastic which was cast on the same PDMS layers.

To make sure that our results are correct, PDMS pieces that are cut from the original spin coated layer, as shown in Fig 2e, are sent to the SEM for inspection. The SEM images are shown in Fig. 6. The SEM images prove that the measurements which are done from the smooth on are accurate.

We accept the SEM results as the most valid since it shows every detail without any unclarity. It shows that the 500 rpm spin coated PDMS has 96.8 µm thickness which is the same with the result achieved by the stylus thickness measurement over the hard plastic. However stylus device gives nearly 21 µm thickness on the PDMS which is too different than the correct thickness. In 1000 rpm, PDMS has 49.8 µm thickness according to the SEM photo. Stylus thickness measurement gives 50 µm thickness over the hard plastic which is consistent with SEM image. However, stylus thickness measurement gives nearly 5 µm thickness when the measurement is realized over the PDMS directly. The trend goes on the same overall PDMS samples. When the stylus measurement is done over hard plastic, the results are consistent with SEM. When the stylus measurement is done from PDMS directly, it is far away to be consistent with the SEM. Besides, tip type does not make any difference when the measurement is realized from the hard plastic while it affects the results when it is done over the PDMS directly. Since PDMS is a soft material, sharper tips cause more deformation than the flat tips. In addition to giving wrong results at stylus measurement, soft material thickness measurement is also dependent on stylus type. Hence stylus measurement loses its reliability for soft materials.

Our method removes the disadvantages of the stylus measurement method for soft material. By casting the soft material with liquid plastic, it can be measured with a stylus after hardening. Since the liquid plastic hardens taking the shape of the PDMS, stylus cannot make any deformation by pushing the material. In addition, it totally takes the shape of the PDMS without any significant shrinkage enabling correct thickness. We prove our thickness results coming from the hard plastic by comparing with SEM images of the PDMS.

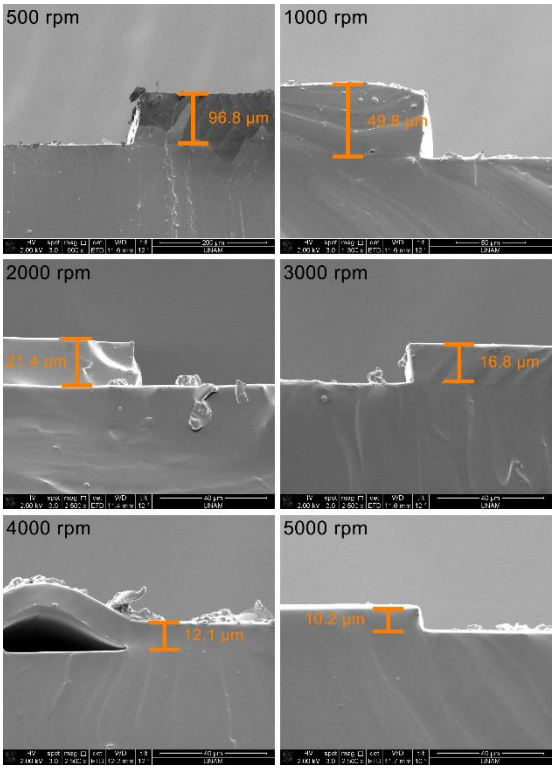

Fig 6. SEM pictures of PDMS pieces which are cut from the original spin coated PDMS layer with razor blade. Spin coating rpm is written on the upside of the left corner of every photo.

For clarity, we cut and inspected the hard plastic with SEM. The SEM picture of the smooth on cast over the PDMS is shown in Fig. 7 from the top view and side view. Here the hard plastic is a negative copy of PDMS. Thus, the protrusion and intrusion at the PDMS surface are found at trans located positions in smooth on. Hence the stylus is placed over the base area and the monitor is set

to zero and then the stylus is placed over the protrusion to measure the thickness. Since the material is hard, stylus cannot make any deformation so the device gives the correct thickness result.

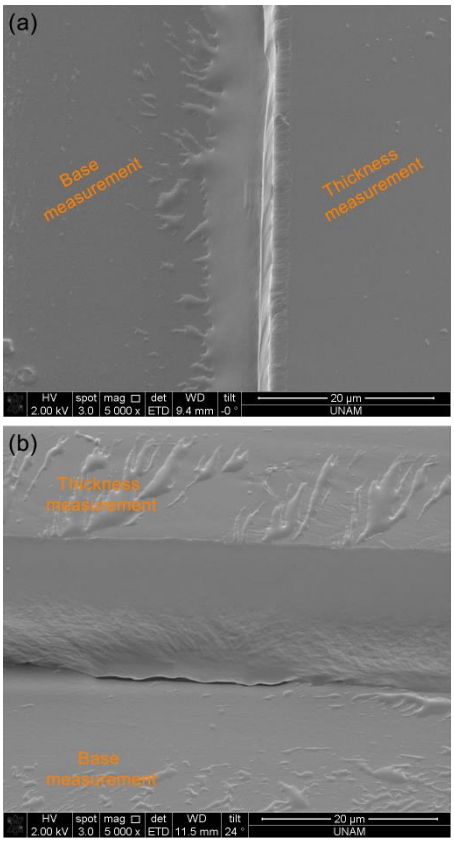

Fig. 7. SEM picture of smooth on casted over the PDMS a) Top view of the hard plastic b) side view of the hard plastic.

5. CONCLUSION

We show that stylus thickness measurement is not a suitable way for soft materials with serial experiments. Those experiments proves that, when the stylus pushes down on the soft material, a deformation takes place disabling accurate measurement of the thickness. Here, PDMS is chosen to carry out the experiments as soft material. A new method is offered to measure the thickness of soft material overcoming the deformation problem. In this new method, first, the soft material is cast by liquid plastic. After a few hours, the liquid plastic hardens and takes the shape of the soft material. Hence stylus can push the surface of the hard plastic without any deformation enabling correct measurement of the thickness. To make sure that our results are correct, PDMS pieces, which are cut from the original spin coated layer, are investigated with SEM microscopy. SEM images show that the thickness measured from the hard plastic is the same with the real thickness of PDMS.

REFERENCES

Bakan, G., S. Ayas, M. Serhatlioglu, C. Elbuken and A. Dana (2018). "Invisible Thin-Film Patterns with Strong Infrared Emission as an Optical Security Feature." *Advanced Optical Materials*, Vol. 6, No. 21, pp. 1800613.

Bartholomeusz, D. A., R. W. Boutté and J. D. Andrade (2005). "Xurography: rapid prototyping of microstructures using a cutting plotter." *Journal of Microelectromechanical systems*, Vol. 14, No. 6, pp. 1364-1374.

Benton, M., M. R. Hossan, P. R. Konari and S. Gamagedara (2019). "Effect of process parameters and material properties on laser micromachining of microchannels." *Micromachines*, Vol. 10, No. 2, pp. 123.

Bilican, I., M. T. Guler, N. Gulener, M. Yuksel and S. Agan (2016). "Capacitive solvent sensing with interdigitated microelectrodes." *Microsystem Technologies*, Vol. 22, No. 3, pp. 659-668.

de Santana, P. P., T. P. Segato, E. Carrilho, R. S. Lima, N. Dossi, M. Y. Kamogawa, A. L. Gobbi, M. H. Piazzeta and E. Piccin (2013). "Fabrication of glass microchannels by xurography for electrophoresis applications." *Analyst*, Vol. 138, No. 6, pp. 1660-1664.

Delgadillo, J. O. V., S. Delorme, R. El-Ayoubi, R. DiRaddo and S. G. Hatzikiriakos (2010). "Effect of freezing on the passive mechanical properties of arterial samples." *Journal of Biomedical Science and Engineering*, Vol. 3, No. 07, pp. 645.

Duffy, D. C., J. C. McDonald, O. J. Schueller and G. M. Whitesides (1998). "Rapid prototyping of microfluidic systems in poly (dimethylsiloxane)." *Analytical chemistry*, Vol. 70, No. 23, pp. 4974-4984.

Gao, Y., H. Ota, E. W. Schaler, K. Chen, A. Zhao, W. Gao, H. M. Fahad, Y. Leng, A. Zheng and F. Xiong (2017). "Wearable microfluidic diaphragm pressure sensor for health and tactile touch monitoring." *Advanced Materials*, Vol. 29, No. 39, pp. 1701985.

Gitlin, L., P. Schulze and D. Belder (2009). "Rapid replication of master structures by double casting with PDMS." *Lab on a Chip*, Vol. 9, No. 20, pp. 3000-3002.

Guler, M. T., P. Beyazkilic and C. Elbuken (2017). "A versatile plug microvalve for microfluidic applications." *Sensors and Actuators A: Physical*, Vol. 265, No., pp. 224-230.

Guler, M. T. and I. Bilican (2018). "Capacitive detection of single bacterium from drinking water with a detailed investigation of electrical flow cytometry." *Sensors and Actuators A: Physical*, Vol. 269, No., pp. 454-463.

Guler, M. T., I. Bilican, S. Agan and C. Elbuken (2015). "A simple approach for the fabrication of 3D microelectrodes for impedimetric sensing." *Journal of Micromechanics and Microengineering*, Vol. 25, No. 9, pp. 095019.

Guler, M. T., Z. Isiksacan, M. Serhatlioglu and C. Elbuken (2018). "Self-powered disposable prothrombin time measurement device with an integrated effervescent

pump." *Sensors and Actuators B: Chemical*, Vol. 273, No., pp. 350-357.

Guner, H., E. Ozgur, G. Kokturk, M. Celik, E. Esen, A. E. Topal, S. Ayas, Y. Uludag, C. Elbuken and A. Dana (2017). "A smartphone based surface plasmon resonance imaging (SPRi) platform for on-site biodetection." *Sensors and Actuators B: Chemical*, Vol. 239, No., pp. 571-577.

Isgor, P. K., M. Marcali, M. Keser and C. Elbuken (2015). "Microfluidic droplet content detection using integrated capacitive sensors." *Sensors and Actuators B: Chemical*, Vol. 210, No., pp. 669-675.

Isiksacan, Z., M. Asghari and C. Elbuken (2017). "A microfluidic erythrocyte sedimentation rate analyzer using rouleaux formation kinetics." *Microfluidics and Nanofluidics*, Vol. 21, No. 3, pp. 44.

Isiksacan, Z., M. T. Guler, B. Aydogdu, I. Bilican and C. Elbuken (2016). "Rapid fabrication of microfluidic PDMS devices from reusable PDMS molds using laser ablation." *Journal of Micromechanics and Microengineering*, Vol. 26, No. 3, pp. 035008.

Isiksacan, Z., N. Hastar, O. Erel and C. Elbuken (2018). "An optofluidic point-of-care device for quantitative investigation of erythrocyte aggregation during coagulation." *Sensors and Actuators A: Physical*, Vol. 281, No., pp. 24-30.

Kudo, H., T. Sawada, E. Kazawa, H. Yoshida, Y. Iwasaki and K. Mitsubayashi (2006). "A flexible and wearable glucose sensor based on functional polymers with Soft-MEMS techniques." *Biosensors and Bioelectronics*, Vol. 22, No. 4, pp. 558-562.

Lee, T. Q. and S. L. Woo (1988). "A new method for determining cross-sectional shape and area of soft tissues." *Journal of Biomechanical Engineering*, Vol. 110, No. 2, pp. 110-114.

Lei, K. F., K.-F. Lee and M.-Y. Lee (2012). "Development of a flexible PDMS capacitive pressure sensor for plantar pressure measurement." *Microelectronic Engineering*, Vol. 99, No., pp. 1-5.

Li, M., S. Li, J. Wu, W. Wen, W. Li and G. Alici (2012). "A simple and cost-effective method for fabrication of integrated electronic-microfluidic devices using a laser-patterned PDMS layer." *Microfluidics and nanofluidics*, Vol. 12, No. 5, pp. 751-760.

Lopes, R., R. O. Rodrigues, D. Pinho, V. Garcia, H. Schütte, R. Lima and S. Gassmann (2015). "Low cost microfluidic device for partial cell separation: Micromilling approach." *2015 IEEE International Conference on Industrial Technology (ICIT)*, pp.3347-3350.

Marcali, M. and C. Elbuken (2016). "Impedimetric detection and lumped element modelling of a hemagglutination assay in microdroplets." *Lab on a Chip*, Vol. 16, No. 13, pp. 2494-2503.

Mohammed, M. I., M. N. H. Z. Alam, A. Kouzani and I. Gibson (2016). "Fabrication of microfluidic devices: improvement of surface quality of CO2 laser machined poly (methylmethacrylate) polymer." *Journal of Micromechanics and Microengineering*, Vol. 27, No. 1, pp. 015021.

Moon, J.-H., D. H. Baek, Y. Y. Choi, K. H. Lee, H. C. Kim and S.-H. Lee (2010). "Wearable polyimide–PDMS electrodes for intrabody communication." *Journal of Micromechanics and Microengineering*, Vol. 20, No. 2, pp. 025032.

Prakash, S. and S. Kumar (2018). "Pulse smearing and profile generation in CO2 laser micromachining on PMMA via raster scanning." *Journal of Manufacturing Processes*, Vol. 31, No., pp. 116-123.

Romoli, L., G. Tantussi and G. Dini (2011). "Experimental approach to the laser machining of PMMA substrates for the fabrication of microfluidic devices." *Optics and Lasers in Engineering*, Vol. 49, No. 3, pp. 419-427.

Serhatlioglu, M., M. Asghari, M. Tahsin Guler and C. Elbuken (2019). "Impedance-based viscoelastic flow cytometry." *Electrophoresis*, Vol. 40, No. 6, pp. 906-913.

Singhal, J., D. Pinho, R. Lopes, P. C Sousa, V. Garcia, H. Schütte, R. Lima and S. Gassmann (2015). "Blood flow visualization and measurements in microfluidic devices fabricated by a micromilling technique." *Micro and Nanosystems*, Vol. 7, No. 3, pp. 148-153.

Sun, Z., C. Yang, M. Eggersdorfer, J. Cui, Y. Li, M. Hai, D. Chen and D. A. Weitz (2019). "A general strategy for one-step fabrication of biocompatible microcapsules with controlled active release." *Chinese Chemical Letters*, Vol., No.

Tavakoli, M., R. Rocha, L. Osorio, M. Almeida, A. De Almeida, V. Ramachandran, A. Tabatabai, T. Lu and C. Majidi (2017). "Carbon doped PDMS: Conductance stability over time and implications for additive manufacturing of stretchable electronics." *Journal of Micromechanics and Microengineering*, Vol. 27, No. 3, pp. 035010.

Zhou, X., L. Lau, W. W. L. Lam, S. W. N. Au and B. Zheng (2007). "Nanoliter dispensing method by degassed poly (dimethylsiloxane) microchannels and its application in protein crystallization." *Analytical chemistry*, Vol. 79, No. 13, pp. 4924-4930.

Zhu, B., Z. Niu, H. Wang, W. R. Leow, H. Wang, Y. Li, L. Zheng, J. Wei, F. Huo and X. Chen (2014). "Microstructured graphene arrays for highly sensitive flexible tactile sensors." *Small*, Vol. 10, No. 18, pp. 3625-3631.

CONTENTS

ISSN 2587-1366

TURKISH JOURNAL OF ENGINEERING

VOLUME 4 ISSUE 2 APRIL 2020